REGULATORS OF G PROTEIN SIGNALING MODULATE PLATELET FUNCTION TO IMPACT NORMAL PHYSIOLOGY AND THE HEMOSTATIC RESPONSE

Daniel DeHelian

A DISSERTATION

in

Biochemistry and Molecular Biophysics

Presented to the Faculties of the University of Pennsylvania

in

Partial Fulfillment of the Requirements for the

Degree of Doctor of Philosophy

2020

Supervisor of Dissertation

_____

Lawrence “Skip” F. Brass

Professor, Department of Medicine

Graduate Group Chairperson

_____

Kim A. Sharp, Associate Professor, Department of Biochemistry and Biophysics

Dissertation Committee

Joel S. Bennett, Professor, Department of Medicine

Scott L. Diamond, Professor, Department of Chemical and Biomolecular Engineering

David R. Manning, Professor, Department of Pharmacology

Sriram Krishnaswamy, Professor, Departments of Pediatrics and Biochemistry and Biophysics

DEDICATION

This dissertation is dedicated to family, whose support and encouragement have spurred my success since day one, and my loving fiancé, Heidi Jensen, without whom I never would have survived the grueling rigors of a graduate education.

ACKNOWLEDGMENT

I would like to thank my undergraduate PI and mentor, Dr. Julia Koeppe, for fostering a love for research that led to my pursuit of a PhD. I would also like to thank Dr. Peisong Ma and Dr. Shuchi Gupta, for their mentorship and support throughout my graduate career at Penn. Additionally, I'd like to acknowledge other past and present members of the Brass lab, Dr. Timothy Stalker, Dr. Maurizio Tomaiuolo, Dr. Tanya Marar, Dr. Jie Wu and Izmarie Poventud-Fuentes, Kelly Litts and Matthew Cooper, whose questions, comments, critiques, and scientific expertise were invaluable to developing and realizing my scientific ideas. Furthermore, I'd like to express gratitude to my thesis committee members, Dr. Joel Bennett, Dr. Sriram Krishnaswamy, Dr. Scott Diamond, and Dr. David Manning, for keeping me focused and on track as my research progressed. Moreover, I would like to specifically thank Chelsea Thorsheim, for performing our immunohistochemistry studies, Joe Park, for his help identifying RGS variants in the Penn Medicine Biobank, and Brian Estevez, for generating the *in vitro* megakaryocyte data. Finally, I would like to sincerely thank my teacher, mentor and PI, Dr. Skip Brass, whose unwavering support, keen scrutiny, and continued encouragement helped me not only survive, but thrive, throughout my PhD journey.

ABSTRACT

REGULATORS OF G PROTEIN SIGNALING MODULATE PLATELET FUNCTION TO IMPACT NORMAL PHYSIOLOGY AND THE HEMOSTATIC RESPONSE

Daniel John DeHelian

Lawrence “Skip” F. Brass, MD PhD

G protein-coupled receptors (GPCRs) are critical mediators of platelet activation whose signaling is limited in part by members of the regulator of G protein signaling (RGS) family. To better understand how individual RGS proteins impact the optimal balance between activation and inhibition, the most abundant RGS in platelets, RGS10 and RGS18, were deleted both individually and simultaneously in mice. Loss of RGS10 causes increased platelet activation and accumulation following hemostatic injury, due to an expansion of the P-selectin$^{(-)}$ shell, driven by thromboxane A_2 and ADP, rather than the P-selectin$^{(+)}$ core, driven by thrombin. Loss of RGS18 results in milder increases in GPCR signaling, primarily thrombin-dependent, and causes moderate thrombocytopenia, due to decreased platelet production. Loss of both RGS10 and RGS18 results in dramatically increased platelet activation and accumulation *in vivo*, with an expansion of both the P-selectin$^{(+)}$ core and the P-selectin$^{(-)}$ shell, and uninhibited growth that increases the occurrence of vascular occlusion. Furthermore, dual deletion of RGS10 and RGS18 results in reduced platelet survival due to premature activation in circulation and subsequent clearance. Additionally, in efforts to explore RGS-mediated regulation of G_q signaling in platelets, we induced a homozygous RGS-insensitive G188S mutation in mouse $G_q\alpha$ ($G_q\alpha$ G188S). Unexpectedly, $G_q\alpha$ G188S mice had dramatically reduced platelet accumulation *in vivo*, which was due to decreased G_q signaling via disrupted PLCβ interactions. Structural and computational analyses revealed substantial overlap between RGS and effector binding interfaces, but provided candidate mutations predicted to specifically disrupt RGS interactions. Finally, to corroborate our results with mouse models, we sought to identify predicted loss-of-function RGS10 and RGS18 variants in human patients and analyze their platelet function. We identified 16 variants in 101 patients and have plans to recall them to analyze platelet reactivity and RGS expression levels. Viable candidates will also

be selected for *in vivo* hemostatic analysis using iPSC-derived megakaryocytes and a humanized mouse model. Overall, these studies demonstrate how RGS-mediated regulation of platelet GPCRs is important for platelet production, survival and hemostatic reactivity. Furthermore, it suggests that a delicate equilibrium between negative and positive platelet activation regulators is necessary to promote rapid responsivity while restraining unwarranted signaling.

TABLE OF CONTENTS

LIST OF TABLES

LIST OF ILLUSTRATIONS

CHAPTER 1: Regulation of Platelet Activation

1.1 Platelets in Hemostasis and Thrombosis

Under normal conditions, the blood vessel endothelium maintains platelets in an inactive state by 1) physically separating them from subendothelial collagen and tissue factor (TF), 2) expressing CD39, a surface ecto-apyrase, and 3) producing nitric oxide (NO) and prostaglandin I_2 (PGI_2) (Figure 1-1A) [1-3]. If the endothelium is injured, however, a rapid response to stem bleeding and reduce blood loss (known as hemostasis) is triggered. The initial phase of this process involves adhesion of platelets to the subendothelial matrix and initiation of the coagulation cascade (Figure 1-1B). Initial platelet interactions via transmembrane receptors induce intracellular signaling cascades that ultimately result in platelet activation.[4] Platelet activation stimulates aggregation via inside-out activation of surface integrins, in particular $\alpha_{IIb}\beta_3$, thus increasing affinity for extracellular substrates to mediate platelet-platelet adhesion.[5] Furthermore, activated platelets release secondary agonists, such as TxA_2 and ADP, to activate additionally recruited platelets (Figure 1-1C).[6] Simultaneously, the coagulation cascade, initiated when circulating factors encounter tissue factor in the adventitia, generates thrombin, which has two major roles in hemostasis: 1) further activation of platelets by cleaving surface receptors[7] and 2) conversion of soluble fibrinogen to insoluble fibrin, which is then polymerized into networks that help stabilize the growing clot (Figure 1-1C)[8]. Defects in either the coagulation cascade (such as hemophilia)[9] or platelet adhesion/aggregation (such as Glanzmann's thrombasthenia)[10] can result in a bleeding diathesis, highlighting the importance of these interrelated phenomena to hemostasis.

In contrast, conditions such as cardiovascular disease (CVD) can create an environment that favors unwarranted platelet activation and excessive clot growth, known as thrombosis.[11] Under these circumstances, particularly in arterial thrombosis, rupture of TF-rich atherosclerotic plaques can result in excessive thrombin production and occlusive platelet-rich clot formation (Figure 1-1D)[12]. Complications (such as myocardial infarction or stroke) arising from CVD are the leading cause of death world-wide[13].

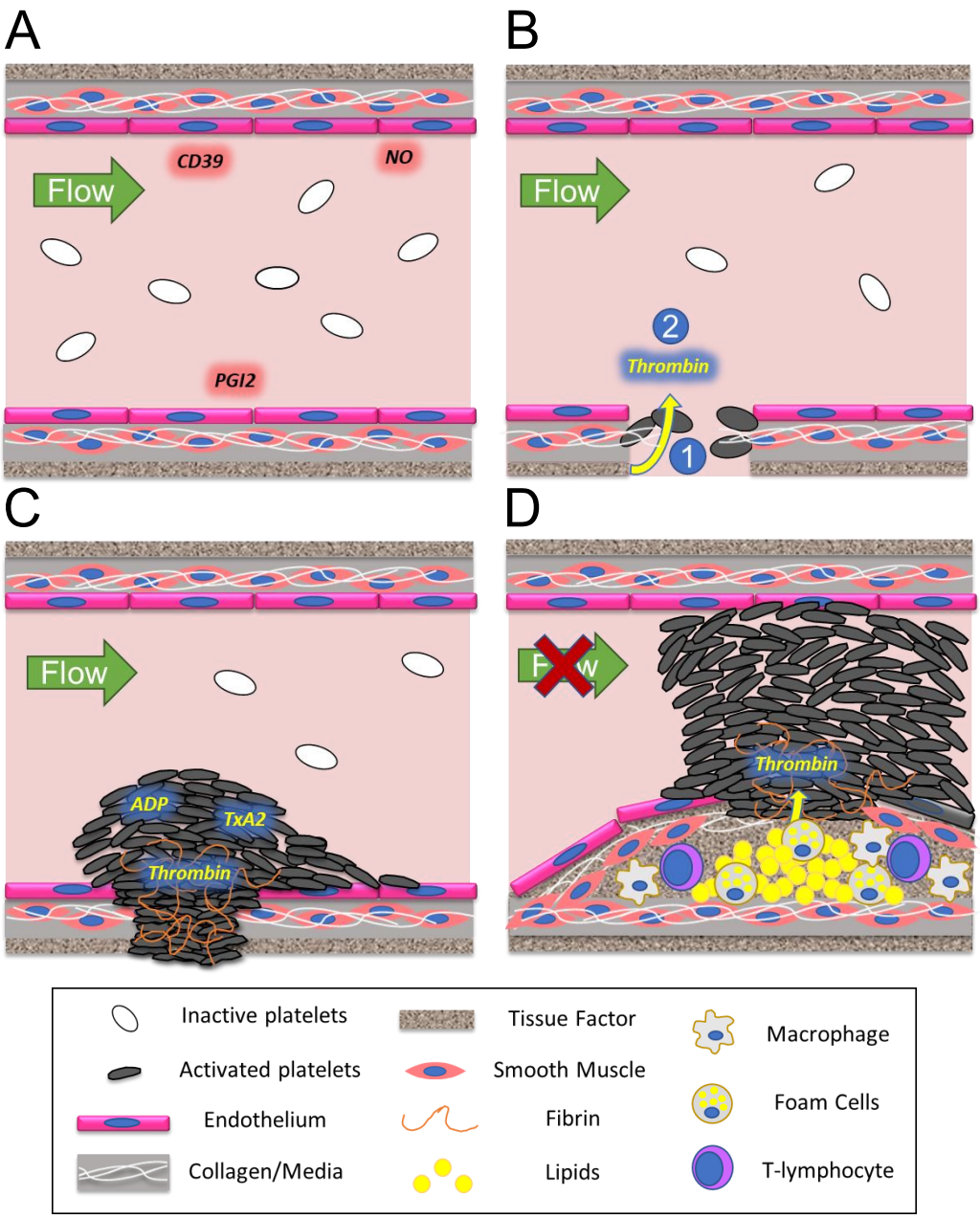

Figure 1-1. Platelet activation under physiological and pathological settings. (A) Under normal conditions, the endothelium provides several mechanisms (red) to prevent platelet activation. (B) Upon injury to the endothelium, (1) platelets begin adhering to the subendothelial matrix and undergoing activation, and (2) the coagulation cascade, mediated by exposure of tissue factor, begins generating thrombin (C) Activated platelets at the site of injury release secondary signaling agonists ADP and TxA_2. Additionally, thrombin plays dual roles by further activating platelets and converting soluble fibrinogen to insoluble fibrin, that then polymerizes into a network to stabilize the growing clot. (D) In contrast, atherosclerotic plaque rupture and aberrant thrombin generation can result in excessive platelet activation such that the clot blocks blood flow in the vessel, which results in tissue ischemia-related dysfunction, such as heart attack or stroke.

1.2 Positive and Negative Regulation of Platelet Activation

"Platelet activation" is a term used to describe the morphological and biochemical transformations that a platelet undergoes during a hemostatic response to injury or the pathological response to an insult such as atherosclerotic plaque rupture. These transformations include cytoskeletal rearrangements (that result in shape change, from a discoid to spherical shape), exocytosis of dense and α granules (that release markers of platelet activation, such as P-selectin, and secondary mediators of platelet activation, such as ADP, respectively), production of TxA_2 (another secondary mediator of platelet activation), and inside-out activation of integrin $\alpha_{IIb}\beta_3$ (that forms platelet-platelet contacts via fibrinogen).[6] Platelet activation is mediated, in large part, by the transduction of extracellular signals through transmembrane receptors.

GPVI, an immunoglobulin superfamily receptor, is stimulated by binding to collagen in the subendothelial matrix. It is constitutively associated with the immunoreceptor tyrosine-activating motif (ITAM)-containing Fc receptor γ-chain (Fc$R\gamma$).[14] Upon binding to collagen, Src family tyrosine kinases, Lyn and Fyn, constitutively associated with the proline-rich domain in GPVI, phosphorylate tyrosine residues within consensus ITAM sequences in Fc$R\gamma$.[15] Once phosphorylated, these consensus sequences serve as recruitment sites for the SH2 domains of Syk, another tyrosine kinase. Bound Syk becomes activated, initiating a phosphorylation cascade that results in formation of the linker of activated T cells (LAT) signalosome and activation of phospholipase C (PLC) γ (Figure 1-2).[15] PLCγ cleaves phosphatidylinositol 4,5-bisphosphate (PIP_2) into diacyl glycerol (DAG) and inositol 1,4,5-trisphosphate (IP_3). DAG is an important activator of conventional and novel isoforms of protein kinase C (PKC) while IP_3 stimulates the release of intracellular Ca^{2+} from stores in the dense tubular system (Figure 1-2).[16] Finally, PKCs (primarily conventional isoforms) phosphorylate downstream effectors involved in platelet activation,[17] while intracellular Ca^{2+} acts as a potent secondary messenger.[18] Together, these mechanisms combine to initiate activation-dependent events like granule secretion, integrin $\alpha_{IIb}\beta_3$ activation, TxA_2 generation and cytoskeletal rearrangement.[6]

The G protein-coupled receptor (GPCR) superfamily is involved in both platelet activation and inhibition. As the name implies, each GPCR is coupled to a heterotrimeric complex of G proteins composed of α, β, and γ subunits and can be subdivided into one of four families: G_s, G_i, G_q, and G_{12}, based upon the characteristics of their coupled α subunit. At rest, the α subunit of the complex is bound to GDP and its effector-binding interface is occupied by the tightly associated $\beta\gamma$ dimer (Figure 1-3A). Upon agonist stimulation of the coupled GPCR, the α subunit releases GDP and it is rapidly replaced with more abundant GTP.[19] In this GTP-bound state, the α subunit dissociates from the $\beta\gamma$ dimer, allowing both to bind to downstream effectors (Figure 1-3B). The diverse functions of individual GPCRs and their downstream effects are dependent upon the nature of the individual subunits within the associated heterotrimeric complex.[20]

Three of the four major GPCR families, G_i, G_q, and G_{12}, are involved in platelet activation. The platelet $P2Y_{12}$ receptor, activated by its agonist adenosine diphosphate (ADP), is the predominant G_i-coupled family member in platelets, and has a major role in relieving inhibitory pathways. It couples to $G_{i2}\alpha$, which antagonizes the effects of G_s by inhibiting adenylyl cyclase (AC) to promote platelet activation (Figure 1-2). Furthermore, its associated $\beta\gamma$ subunits stimulate phosphoinositide-3-kinase (PI3K), which inhibits RASA3, a GTPase activating protein (GAP) for the small GTPase RAP1. As RAP1 is only active in its GTP-bound form, inhibiting its GAP promotes integrin $\alpha_{IIb}\beta_3$ activation and platelet aggregation.[21]

Multiple platelet GPCRs couple to G_q subunits, including the protease activated receptors (PARs), the thromboxane A_2 (TxA_2) receptor (TP), and the ADP-activated $P2Y_1$ receptor. Activated $G\alpha_q$ stimulates β isoforms of phospholipase C (PLCβ), which in turn generates DAG and IP_3 by cleaving PIP_2.[22] At this point, GPVI and G_q-coupled GPCR signaling pathways converge, and the resulting downstream signaling effects of these secondary molecules are virtually indistinguishable, activating PKCs and stimulating the release of intracellular Ca^{2+}, respectively (Figure 1-2).

The predominant G_{12} isoform in platelets, G_{13}, couples to both PARs and TP receptors. Activated $G\alpha_{13}$ stimulates guanine nucleotide exchange factors (GEFs), including p115RhoGEF, that in turn leads to the exchange of GDP for GTP on the small GTPase, Rho (Figure 1-2).[23] GTP-bound Rho activates p160ROCK, a Rho-dependent kinase, which phosphorylates downstream effectors that mediate reorganization of the actin cytoskeleton.[24]

In addition, to those transmembrane receptors that promote platelet activation, there are also numerous mechanisms that restrain activation. The prostaglandin I2 (PGI_2) receptor (IP) represents the predominant G_s-coupled GPCR present in platelets. The active α_s subunit binds to and activates AC, which converts adenosine triphosphate (ATP) to cyclic adenosine monophosphate (cAMP). cAMP, in turn, binds to and activates protein kinase A (PKA), a serine/threonine kinase that phosphorylates multiple substrates. The net effect of this signaling cascade is inhibition of platelet activation (Figure 1-2).[25] Similarly, NO produced by endothelial cells can directly bypass the platelet membrane to activate soluble guanylyl cyclase (sGC), produce cyclic guanosine monophosphate (cGMP), and stimulate protein kinase G (PKG), another serine/threonine kinase involved in inhibition of platelet activation signaling pathways.[26] Finally, the endothelial ecto-apyrase, CD39, converts ATP and ADP in the circulation to AMP.[1] As ADP stimulates platelet activating G_q-coupled $P2Y_1$ and G_{i2}-coupled $P2Y_{12}$ receptors, CD39 limits unnecessary signaling and aberrant activation under basal conditions.

The presence of such a variety of mechanisms that both promote and restrain platelet signaling networks suggests the importance of maintaining a delicate balance between activation and inhibition. Moreover, it implies potential redundancy if a pathway were to be rendered inoperable. Of particular interest to our lab are the regulators of G protein signaling (RGS), negative intrinsic regulators of platelet activation, and their relative contributions to this optimal equilibrium.

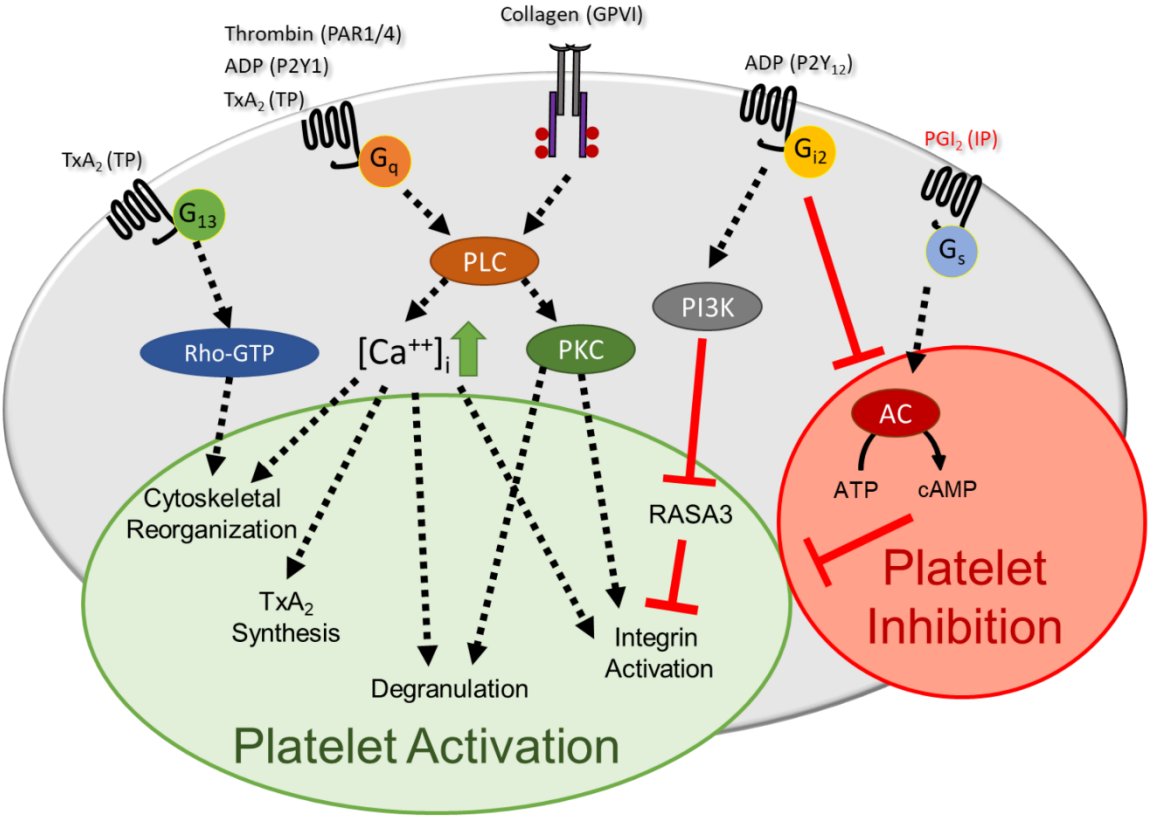

Figure 1-2. Signal transduction and platelet activation. Overview of signal transduction mechanisms that promote or inhibit platelet activation. Endogenous agonists are labelled above each G protein-coupled receptor with the receptor name in parentheses. Black indicates activating while red indicates inhibitory pathways. AC, adenylyl cyclase; ATP, adenosine triphosphate; $[Ca^{++}]_i$, intracellular cytosolic calcium; cAMP, cyclic adenosine monophosphate; GTP, guanosine 5'-triphosphate; PI3K, phosphatidylinositol 3-kinase; PLC, phospholipase C; PKC, protein kinase C.

1.3 Regulators of G protein Signaling

The magnitude of a GPCR-mediated response is proportional, at least in part, to the duration of the signaling via GTP-bound Gα and, in some cases, unbound βγ. Gα possesses intrinsic GTPase activity with which it can hydrolyze the terminal phosphate of GTP to generate GDP, resulting in reassociation with βγ subunits and termination of signaling via their effectors (Figure 1-3C).[27] However, this intrinsic GTPase activity is quite slow and its function alone is insufficient to adequately explain how rapidly certain GPCR signaling pathways, such as those regulating photoreceptor activity in the retina, are terminated.[28] Members of the regulator of G protein signaling (RGS) family solve this apparent problem. RGS proteins bind to active α subunits following GPCR stimulation and stabilize the GTP-to-GDP transition state to enhance hydrolysis and accelerate signal termination (Figure 1-3D).[29] As such, they belong to the GTPase activating protein (GAP) family, which includes GAPs for small GTPases such as Ras and Rho.[30] This GAP function is dependent upon the highly conserved RGS domain: an ~120 amino acid bundle of α helices periodically interrupted by variable linker regions.[29]

To date, at least 20 canonical RGS proteins (with described GAP activity towards $G_q\alpha$ and/or $G_i\alpha$ subunits) and many more RGS-like proteins (with GAP-deficient or more distantly related RGS homology domains) have been discovered.[31] Canonical RGS proteins have been classified into four major subfamilies based on sequence homology within the RGS domain: A/RZ, B/R4, C/R7 and D/R12.[32] A/RZ and B/R4 subfamilies are the most closely related and have relatively simple RGS domain-flanking regions. Their only putative domains consist of an N-terminal poly-cysteine region, which can be reversibly palmitoylated, and/or an amphipathic helix, both of which are thought to promote membrane anchoring.[33,34] C/R7 subfamily members possess Gγ-like (GGL) domains, that interact with Gβ5 subunits, as well as N-terminal Disheveled/EGL-10/Pleckstrin homology (DEP) domains, archetypically involved in plasma membrane anchoring.[35,36] D/R12 family members are more diverse in their domain structure. RGS12 and RGS14 share C-terminal tandem Rap-binding domain (RBD) motifs, that provide scaffolding for

mitogen-activated protein kinase (MAPK) proteins, and GoLoco motifs, that act as guanine nucleotide dissociation inhibitors (GDIs) towards G_i family α subunits.[37,38] Additionally, RGS12 has an N-terminal PSD-95/Discs-large/ZO-1 homology (PDZ) domain, mediating interactions with certain GPCRs, and a phosphotyrosine-binding (PTB) domain, whose phosphorylation promotes association with a transmembrane calcium channel.[39,40] RGS proteins have many diverse biological functions, which are distinguished, in large part, by the specificity of tissue expression.

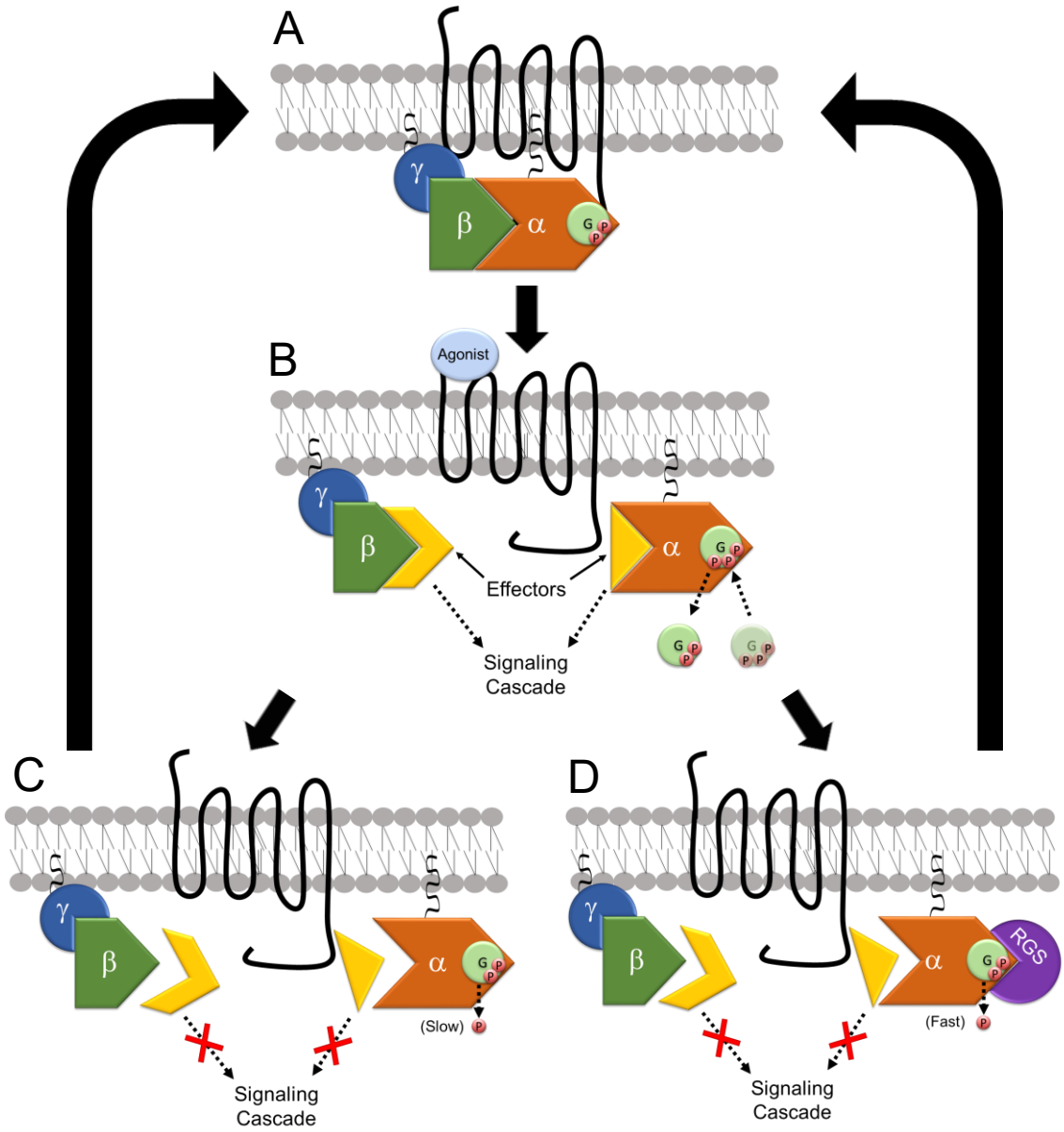

Figure 1-3. GPCR signaling and RGS proteins. (A) At rest, GDP-bound α and βγ subunits are associated in a heterotrimeric complex and interact with their G protein-coupled receptor. (B) Upon activation of the GPCR, classically via a bound agonist, GDP is exchanged for GTP, and the α and βγ subunits dissociate. This exposes binding sites for downstream effectors (yellow), which can initiate the resulting signaling cascades. (C) α subunits have intrinsic GTPase activity and hydrolyze GTP back to GDP to cause reassociation of the heterotrimeric complex which terminates signaling. However, this process is relatively slow ($t_{1/2}$ ≈ s). (D) RGS proteins (purple) bind to the α subunit to enhance GTPase activity and accelerate signal termination ($t_{1/2}$ ≈ ms). GDP, guanosine 5'-diphosphate; GTP, guanosine 5'-triphosphate; RGS, regulator of G-protein signaling

1.4 RGS in Platelets

Rapid activation of platelets is a crucial step in the hemostatic response to injury to prevent unnecessary bleeding and GPCRs are the predominant means by which this is accomplished. While these signaling networks have been well-described, less is known about the mechanisms that regulate these networks to prevent unnecessary or excessive platelet activation. RGS proteins represent one such mode of regulation and two are commonly and predominantly expressed in both human and mouse platelets: RGS10 and RGS18.[41-43]

RGS18, a member of the B/R4 RGS subfamily, is limited in expression to hematopoietic cells, including platelet progenitor megakaryocytes and osteoclasts.[44-46] RGS18 is slightly larger than RGS10 at ~28 kDa, but is still amongst the smallest and simplest of RGS proteins with a single putative amphipathic helix N-terminally flanking the RGS domain core (Figure 1-4).[45] Studies suggest that RGS18 binds with a similar affinity to both G_i and G_q α subunits, but not G_z, G_{12}, or G_s.[46,47]

RGS10, a member of the D/R12 subfamily, is widely expressed in a variety of tissues and cell types including ovaries, bones, T-cells, neurons, heart, and platelets.[48-52] While its functions are diverse depending on the cell type, they are mostly consistent with its canonical role as a regulator of GPCR signaling. RGS10 is amongst the smallest and simplest of the RGS proteins at ~20 kDa, and does not appear to possess any putative functional domains outside of its RGS domain (Figure 1-4).[53] RGS10 has been shown to selectively interact with G_i family α subunits, with only very weak binding reported for G_q and none for G_s.[47,54] And in cells other than platelets, various mechanisms, including transcriptional regulation, palmitoylation and phosphorylation, have been shown to modulate RGS10 activity (Figure 1-4).[55-58] Furthermore, at least two reports suggest non-canonical functions for RGS10 independent of GAP activity, although the precise mechanisms involved are unclear.[57,59]

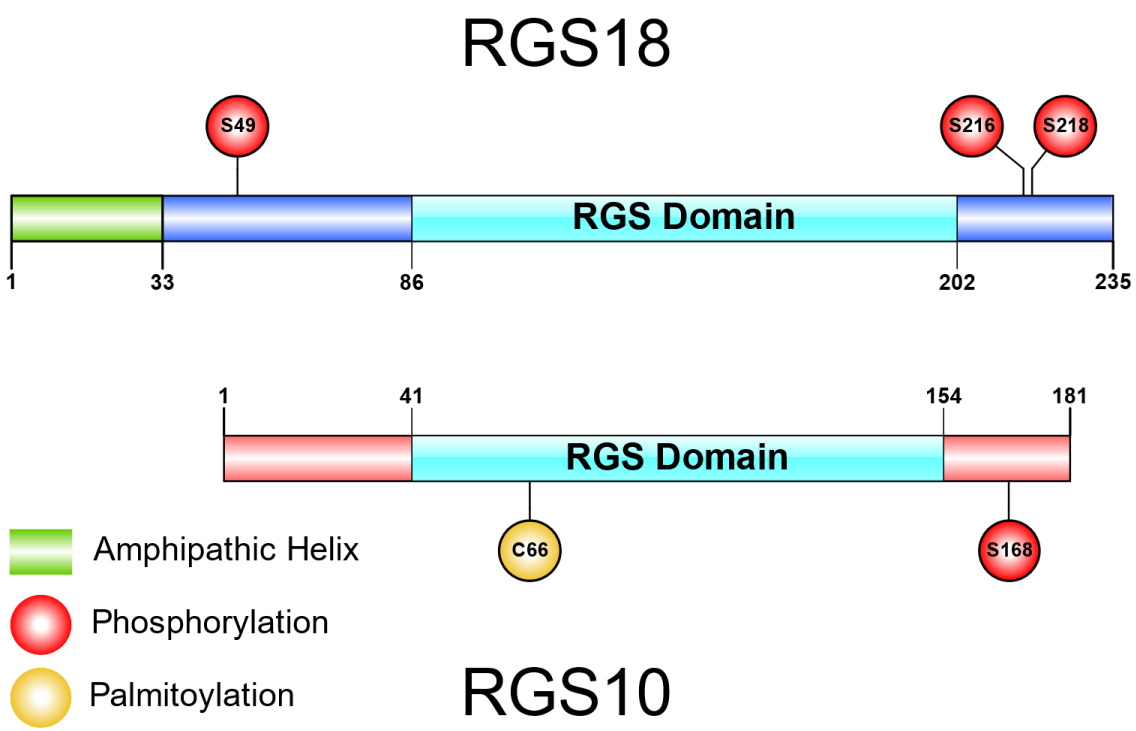

Figure 1-4. RGS10 and RGS18 protein sequence features. Graphical depiction of amino acid sequences for human RGS18 (Q9NS28-1) and RGS10 isoform 3 (O43665-3). Phosphorylation sites (red) and palmitoylation sites (yellow) were empirically determined. The putative amphipathic helix (green) has been predicted from the sequence and is not resolved in the available NMR structure. The RGS domain (cyan) is both necessary and sufficient to provide GTPase activity towards α subunits. Graphic was prepared using the Illustrator for Biological Sequences (Liu et al, 2015, Bioinformatics)

1.4.1 RGS deletion

In order to more precisely understand the physiological impacts of RGS10 and RGS18 in the context of platelets, researchers have relied upon genetically modified mouse models deficient in expression of these proteins, or knockouts (KOs; $RGS^{-/-}$). Comparing these KO mouse models to their genetically identical wild type counterparts has become one of the most widely used methods for investigating protein function in a context relevant to human biology and disease.[60]

Deletion of RGS18 results in a mild thrombocytopenia, which is reportedly due, in part, to a decrease in the number of mature megakaryocytes as well as their platelet producing potential. Furthermore, the same study suggests that $RGS18^{-/-}$ renders platelets sufficiently hyperactive in circulation to result in spontaneous aggregation, which appears to be mediated by its canonical function regulating GPCR signaling, primarily G_q. It is suggested that this may be another mechanism that leads to the mild thrombocytopenia observed.[61] Later reports confirm the GPCR-mediated hyperactive phenotype of $RGS18^{-/-}$ platelets *in vitro* and *in vivo*, using aggregometry, tail clip hemostasis assays, and a ferric chloride thrombosis model.[62]

Results from our work and that of others suggest that deletion of $RGS10^{-/-}$ has no effect on platelet counts, but it does result in similarly hyperactive platelets. Using aggregometry and flow cytometry, Hensch *et al* showed an increase in platelet activation in response to GPCR-stimulating agonists.[63] However, the authors present evidence suggesting that effects of these agonists, which include G_q-stimulating thrombin, and $G_{q/13}$ stimulating TxA_2 analogue (U46619), are due primarily to secondary signaling via ADP stimulation of $P2Y_{12}$ receptors.[63] Because $P2Y_{12}$ couples to G_{i2}, this suggests that RGS10 preferentially interacts with these α subunits, which is consistent with previous reports *in vitro*.[47,54] Lastly, the authors show a hyperactive platelet phenotype *in vivo* that is strikingly similar to $RGS18^{-/-}$ mice, using the same tail clip hemostasis assay, and ferric chloride thrombosis model. While our results are largely consistent (presented in detail in Chapter 2), we expand upon the phenotypic analysis to explore the architecture of hemostatic plugs *in vivo* and present data suggesting that both G_q and G_{i2} are impacted by RGS10 deletion. Furthermore, we

show that RGS10 is phosphorylated and binds to both spinophilin and 14-3-3γ in an agonist-selective manner, which may regulate its function *in vivo*.[64]

In summary, these KO studies suggest overlapping yet divergent roles for RGS10 and RGS18 in platelet biology, which may be a result of their specificities towards individual α subunits, interactions with regulatory adapters, post-translational modifications or intracellular localization. However, it is still unclear the extent to which both proteins cooperate with (or possibly counteract) one another to regulate platelet activation in the context of hemostasis.

1.4.2 RGS-insensitive mutations in Gα subunits

While RGS KOs provide valuable information about the individual role of each protein, most cells express multiple RGS that may have partially redundant functions. To circumvent this problem, investigators have turned to α subunits harboring RGS-insensitive substitutions: point mutations that disrupt RGS binding without impacting downstream effector interactions required for signaling. This allows one to probe the effects of *all* RGS proteins on individual α subunit-mediated signaling networks.[65]

Shortly after the discovery of these types of mutations, mouse models were generated to determine their physiological impacts. One such model was a glycine to serine substitution at position 184 (G184S) of the G_{i2} α subunit.[66] Investigators from our lab used this model to probe the platelet-dependent effects of RGS-insensitive G_{i2}, coupled to the primary ADP receptor in platelets, $P2Y_{12}$. By aggregometry, intravital microscopy, and microfluidics assays, they showed that heterozygous mice (G184S/+) had platelets that were hyperactive in response to GPCR agonists but not ITAM agonists, such as collagen. Furthermore, they demonstrated increased G_{i2}-mediated signaling via cAMP and Akt phosphorylation assays, but no increase in G_q-mediated signaling assessed by calcium mobilization.[67]

A similar discovery made for $G_q\alpha$ was first demonstrated in yeast and followed by Chinese hamster ovary cells exogenously expressing recombinant human proteins. Analogous to the

mutation described for $G_{i2}\alpha$, a glycine to serine substitution at position 188 (G188S) of human $G_q\alpha$ rendered the protein insensitive to RGS-dependent GAP activity and subsequent signal attenuation. And similarly, in these simplified models, the mutation did not appear to have any impact on interactions with downstream effectors required for signal transduction.[68] To explore the impact of RGS-mediated regulation of G_q in platelet activation and hemostasis, our lab used CRISPR-Cas9 and homology directed repair to create this substitution in mice (described in detail in Chapter 4). Unexpectedly, our phenotypic, biochemical and structural analyses of this model suggested that the G188S mutation does indeed disrupt other downstream effectors, like PLCβ, in addition to RGS proteins. The resulting platelets almost completely phenocopy a $G_q^{-/-}$, further supporting this notion. Why this phenomenon is not observed in yeast or a mammalian cell-based model but is observed in mice remains incompletely understood.

Overall, these results suggest that RGS-insensitive mutations are a useful tool to probe the effects of RGS proteins on individual α subunits. However, caution and diligence must be observed when attempting to translate results observed *in vitro* to an *in vivo* model.

1.4.3 Regulators of RGS function

While improving our understanding of how RGS proteins impact GPCR signaling networks remains important, equally as important is understanding how RGS proteins themselves are regulated within platelets.

Phosphorylation of RGS10 and RGS18 in platelets in response to agonist stimulation was first reported by Garcia *et al* in 2004 following a differential platelet proteomic analysis. And while serine 49 (S49) was identified as a site for RGS18, they did not determine the site(s) of RGS10 phosphorylation.[69] A later study by Gegenbauer *et al* used immunoblotting, transfected variants, and immunoprecipitation to identify the adapter protein 14-3-3γ as a phosphorylation-dependent regulator of RGS18. Their results identified two additional sites of phosphorylation on RGS18, serine 216 (S216) and serine 218 (S218) (Figure 1-4). Their proposed model, based on the data presented, suggests that RGS18 is basally phosphorylated on S218 at rest and weakly or

transiently associated with 14-3-3γ. Stimulation with a G_q-activating agonist results in phosphorylation at S49, which enhances interactions with 14-3-3γ, inhibiting RGS18 function to enhance G_q-mediated signaling. In contrast, inhibiting platelets with PGI_2 or nitric oxide (NO) stimulates cyclic nucleotide-dependent kinases to phosphorylate S216, causing dissociation of RGS18 and 14-3-3γ, and enhancing its ability to attenuate G_q-signaling.[70,71] These results are consistent with the role of RGS18 as a negative regulator of platelet activation and suggest that its activity is modified depending upon the biological context. Additional studies described phosphorylation of RGS10 at serine 168 (S168) via a PKA-dependent mechanism in nucleated cells (Figure 1-4). This results in nuclear translocation, thereby inhibiting its ability to act upon plasma membrane-associated α subunits, but had no apparent impact on GAP activity *in vitro*.[56] However, phosphorylation of RGS10 and its potential role in anucleate platelets has yet to be fully investigated. RGS10 can also be reversibly palmitoylated at cysteine 66 (C66), and this reportedly enhances GAP activity during receptor-stimulated, steady-state GTP hydrolysis.[55]

Studies from our lab have revealed another regulator of RGS function in platelets: spinophilin. First discovered in rat brain as a protein phosphatase 1 (PP1)-inhibiting scaffold protein,[72] spinophilin was later shown to interact with a subset of RGS proteins and specifically regulate activity of RGS2.[73] Investigators from our lab later demonstrated expression of spinophilin in both human and mouse platelets, its ability to bind both RGS10 and RGS18, and a phosphorylation-dependent, agonist-specific mechanism by which its interactions with RGS proteins in platelets are modulated (described in detail in Chapter 2).[74] Furthermore, data from KOs and a binding-deficient variant suggest that spinophilin interacting with RGS in the context of platelets inhibits GAP function.[74,75] This is in contrast to reports in nucleated cells suggesting that binding of RGS2 to spinophilin enhanced its function by localizing it to the α-adrenergic receptor,[73] but the reasons behind this phenomenon remain unclear.

CHAPTER 2: Hemostatic Role and Regulation of RGS10 in Platelets

2.1 Introduction

Human RGS10 was first discovered and characterized in 1996 as a GAP for G_i α subunits,[54] and its subsequent exogenous expression in cultured cell models was consistent with this analysis.[55,56] In 2004, Garcia *et al* presented evidence that RGS10 (in addition to RGS18) was expressed in human platelets,[69] but it was not until 2008 that the first RGS10$^{-/-}$ mouse model, generated using mouse embryonic stem cells and a randomized gene trapping method, was reported to explore its function in dopaminergic neurons.[76,77] However, it was still unclear how this protein affected platelet signaling and responses within a physiological context.

Our lab was the first to present evidence that RGS proteins negatively regulate platelet signaling and activation, using the RGS-insensitive $G_{i2}\alpha$ G184S mouse model (described in 1.4.2). And since RGS10 is the most abundant RGS in both human and mouse platelets and purported to be selective for G_i α subunits, we relied upon the RGS10$^{-/-}$ mouse model to explore the specific function of RGS10 with respect to hemostatic platelet reactivity.

Overall, our findings show that, while similar in some respects, the $G_{i2}\alpha$ G184S model is not identical to the RGS10$^{-/-}$ model. This suggests that the RGS10 must be exerting its effects on other α subunits in addition to $G_{i2}\alpha$. In support of this notion, we show that both G_q and G_{i2} signaling are impacted by RGS10 deletion, and that the nature of its impact depends upon specific receptors. Additionally, we provide evidence that RGS10 binds to both spinophilin and 14-3-3γ at rest and dissociates in an agonist-selective manner, suggesting that both adapter proteins may provide potential modes of regulation. Lastly, we show that RGS10 is phosphorylated in platelets in an activation-dependent manner downstream of PKC activation, which may regulate its *in vivo* function.

2.2 Materials and Methods

2.2.1. RGS10$^{-/-}$ mouse model

RGS10$^{-/-}$ mice and wild type (WT) littermate controls were produced by crossing heterozygotes obtained from the Mutant Mouse Regional Resource Center (MMRRC, Chapel Hill, NC). The mice were obtained on a mixed 129/C57BL/6 background. Studies were performed using sex-matched littermates and carried out with Institutional Animal Care and Use Committee approved protocols. We genotyped the mice using a strategy developed by the MMRRC. The following primers were used in PCR reaction. Forward primer: 5'-CCTTCCTGAGCACTGGACAACTGAT-3'; Reverse primer 1: 5'-ATAAACCCTCTTGCAGTTGCATC-3'; Reverse primer 2: 5'-AGGTGCTATGAAGCCTGGTTTGC-3'. We performed PCR with the following conditions: denaturation at 95°C for 7 minutes; 35 cycles of (96°C for10 seconds, 60°C for 30 seconds, 68°C for 1.5 minutes); extension at 68°C for 7 minutes.

2.2.2. Hemostatic vascular injury model

Hemostatic thrombus formation was observed in the cremaster muscle microcirculation of male mice aged 8-12 weeks essentially as previously described.[78] Alexa Fluor 568–labeled anti-CD41 F(ab')$_2$ fragments, Alexa Fluor 488–labeled anti–P-selectin, and Alexa Fluor 647-labeled anti-fibrin were administered via a catheter in the jugular vein. Arterioles 30-50 µm in diameter were studied. Penetrating vascular injuries were produced with a pulsed nitrogen dye laser fired through the microscope objective. Thrombus formation was observed for 3 min at 1.9 frames per second and analyzed using SlideBook 6 software (Intelligent Imaging Innovations, Denver, CO). For embolization studies, anti-CD41 labeled platelets accumulating at the injury site were acquired with 4x4 binning and 4 millisecond exposure time; only the red channel was used in order to increase image acquisition to 35.5 frames/sec, with a total of 6300 frames collected in 3 minutes. Data were collected in a region of interest drawn downstream of the thrombus.

2.2.3 Clot retraction

Visual assay: Whole mouse blood was drawn in 0.38% sodium citrate and centrifuged at 200 × g to obtain platelet rich plasma. Samples were adjusted with platelet-poor plasma to 6×10^8 platelets/mL, recalcified with 2 mM $CaCl_2$ and stimulated with 10 U/ml thrombin. Clot retraction was recorded at 15-minute intervals at 37° C with a digital camera and analyzed using ImageJ software.

Automated light scattering assay: Blood was collected from the inferior vena cava of anesthetized mice into 3.8% sodium citrate. Clot size dynamics were tracked by measuring light scattering over time followed by computational processing of the serial images using a Thrombodynamics Analyzer System (HemaCore, Moscow, Russia). Plastic cuvettes (12 x 7 x 1 mm) were prelubricated with a residual layer of 4% (v/v) Triton X-100 in phosphate-buffered saline to prevent fibrin sticking to the chamber. Samples were incubated with 2 mM $CaCl_2$ at 37°C for 3 minutes followed by addition of 5 U/mL thrombin to initiate clotting. Samples (80 µL) were quickly transferred to the cuvette, which was placed into the thermostatic chamber (37°C) between a red light-emitting diode and a CCD camera. Clot size was tracked from digitized images every 15 seconds for 20 minutes and analyzed using ImageJ software.[79]

2.2.4 Flow cytometry

Platelet activation via flow cytometry was detected as previously described.[80] Briefly, heparinized whole mouse blood was diluted 1:40 in modified Tyrode's buffer (137 mM NaCl, 20 mM HEPES, 5.6 mM glucose, 1 g/liter BSA, 1 mM $MgCl_2$, 2.7 mM KCl, 3.3 mM, NaH_2PO_4, pH 7.4). and incubated with 1 mM aspirin and 1 U/ml apyrase for 30 mins at 37°C to eliminate secondary signaling via released TxA_2 and ADP. The blood was incubated with agonists in presence of saturating amounts of fluorophore-conjugated mAbs directed towards activated $\alpha_{IIb}\beta_3$ integrin (Jon/A-PE; Emfret Analytics, Wuerzburg, Germany) and P-selectin (FITC-labeled; BD Biosciences, San Jose, CA) for 15 min at room temperature and analyzed on a FACSCanto II (BD Biosciences, San Jose, CA). The platelet population was gated based on FSC/SSC and CD41 positivity (Alexa

Fluor 647–labeled F(ab')$_2$; BD Biosciences, San Jose, CA). For activation studies with ADP, platelets were incubated with 1 mM aspirin alone.

2.2.5 Intracellular calcium mobilization

Intracellular calcium was measured as previously described.[81] Briefly, isolated platelets were suspended in Tyrode's buffer without Ca^{++} and loaded with fura-2/AM (5 μM) in the presence of Pluronic F-127 (0.2 μg/mL) for 20 minutes at 37°C. The platelets were then washed and resuspended in Tyrode's buffer with no extracellular Ca^{++}. Changes in fura-2 fluorescence were detected with an SLM/Aminco AB2 spectrophotometer, exciting at 340 and 380 nm, and measuring emission at 510 nm.

2.2.6 Akt phosphorylation

Blood was collected from the inferior vena cava of anesthetized mice into 200 U/mL heparin diluted 9:1 by volume and centrifuged at 280 x g for 5 min. Platelet rich plasma (PRP) was carefully removed from the supernatant and supplemented with 1 μM PGE1 (Sigma-Aldrich, St. Louis, MO). PRP was loaded onto a 2 mL column of Sepharose 2B and eluted with Tyrode's buffer containing 1 mg/ml bovine serum albumin. The most turbid fractions collected were counted and adjusted with Tyrode's buffer to 2 x 10^8 platelets/mL. Platelets were incubated with vehicle, agonists or antagonists at the concentrations outlined in the figures. Lysates were boiled in sample buffer prior to SDS-PAGE analysis. Immunoblots were performed with an anti-pAkt (Ser473) antibody before re-probing with anti-Akt antibody (Cell Signaling Technology, Danvers, MA).

2.2.7 Washed human platelets

Blood was obtained from healthy donors using protocols approved by the University of Pennsylvania IRB. Written informed consent of all donors was obtained prior to blood collection. Blood was anticoagulated 1:5 with ACD (65 mM Na_3 citrate, 70 mM citric acid, 100 mM dextrose, pH 4.4) and centrifuged at 129 x g for 20 min to obtain platelet rich plasma (PRP). PRP was then diluted 1:4 with HEN buffer (150 mM NaCl, 1 mM Na_2EDTA, 10 mM HEPES, pH 6.5) containing 1

μM PGI_2 prior to sedimentation at 341 x g for 10 min. Washed platelets were then resuspended in Tyrode's buffer to the desired concentration.

2.2.8 Phosphorylation of RGS10

Washed human platelets (prepared as outlined in 2.2.7) were adjusted to 1 x 10^9 /mL and supplemented with 1 mM $CaCl_2$. Following preincubation with inhibitors, platelet suspensions were treated with agonists, as indicated, and then lysed with HaloTag buffer [150 mM KCl, 50 mM HEPES, 0.1% (w/v) CHAPS, 4% NP40, pH 7.4, 1X cOmplete EDTA-free protease inhibitor cocktail, 1X PhosSTOP phosphatase inhibitor cocktail (Roche Diagnostics, Mannheim, Germany)]. Samples were then boiled in 1X Laemmli Sample Buffer (Biorad, Hercules, CA) and separated using a 12.5% SuperSep Phos-tag gel (198-17981; Wako Pure Chemical Industries, Osaka, Japan) according to manufacturer instructions. Following transfer to polyvinylidene difluoride membrane, immunoblotting was performed using goat α-RGS10 (sc-6206; Santa Cruz Biotechnology, Santa Cruz, CA).

2.2.9 Pull-down of platelet RGS10

Halo-tagged human $G_{i2}\alpha$ (Halo-GNAI2) was overexpressed in CHO cells transfected with pFC27A-$G_{i2}\alpha$ vector (Promega, Madison, WI). Following sonication to lyse cells and centrifugation at 10,000 x g to pellet membranes, protein from supernatant was conjugated to Magne HaloTag beads (Promega, Madison, WI) according to manufacturer recommendations. Resting or 10 U/mL thrombin-stimulated washed human platelets (prepared as in 2.2.7) were immediately centrifuged at 775 x g for 3 minutes at RT, resuspended in HaloTag Buffer (as prepared in 2.2.9), and lysed by sonication. Following centrifugation at 10,000 x g to pellet membranes, supernatant containing soluble protein was supplemented with either GDP buffer (10 mM HEPES, 150 mM NaCl, 50 μM EDTA, 0.0005% Triton X-100, 100 μM GDP, pH 7.5) or AMF buffer (GDP buffer, 10 mM $MgCl_2$, 10 mM NaF, 30 μM $AlCl_3$, pH 7.5). Washed Halo-GNAI2-Magne beads were added to samples and incubated for 2 hours while rotating at 4°C. Following three additional washes, $G_{i2}\alpha$ and bound

proteins were eluted from the magnetic beads with 1 µL of ProTEV tobacco etch virus protease (Promega, Madison, WI) for 90 minutes while rotating at room temperature. His-tagged ProTEV was removed from the solution by further incubation with HisLink resin (Promega, Madison, WI) for an additional 20 minutes. After allowing HisLink beads to settle in a magnetic rack, Input, Wash (first after coincubation), and Eluate samples were carefully removed and analyzed by SDS-PAGE with Phos-tag gels and immunoblotting (as outlined in 2.2.9).

2.3 Results

2.3.1 RGS10 deletion modifies the structure of hemostatic plugs

To assess hemostatic platelet function *in vivo*, mice were injected with fluorescent antibodies and imaged using confocal intravital microscopy following a penetrating laser injury. Our lab has previously demonstrated this to be a model of hemostasis rather than thrombosis because the endothelium is completely penetrated, blood leaks out initially, and the hole is rapidly sealed in a platelet-dependent manner.[78] The platelet plug that follows consists of a highly activated, densely packed, P-selectin(+) core overlaid by a less activated, more loosely packed, P-selectin(-) shell. And while growth of the shell relies primarily upon the release of secondary signaling agonists such as TxA_2 and ADP,[82] the initial core of platelets (as well as fibrin deposition) depends upon thrombin, which remains localized to the site of the injury.[83]

When comparing $RGS10^{-/-}$ mice to their respective WT controls, the initial rate of accumulation as well as peak total platelet accumulation does not differ appreciably (Figure 2-1A, B). Furthermore, we observed no significant difference between the two genotypes with respect to growth of the P-selectin$^{(+)}$ core (Figure 2-1A,C) or fibrin deposition (Figure 2-1D). However, while the WT platelet area tends to decrease after reaching peak growth, $RGS10^{-/-}$ platelet area remains stable until the endpoint, which we can attribute to the P-selectin$^{(-)}$ shell (Figure 2-1A).

At least two known phenomena contribute to the decrease in plug size following peak platelet accumulation in a normal mouse: embolization and retraction. Embolization, under these

conditions, occurs when less-activated platelets in the shell detach and are carried away, which suggests that a greater activation state is required for firm adhesion at the site of injury.[78] To test for differences in embolization, the passage of platelet aggregates downstream of a growing hemostatic plug were measured. While the number of emboli did not differ significantly during the initial growth phase of the plug up to peak accumulation, fewer emboli were observed for the RGS10$^{-/-}$ hemostatic plugs after peak accumulation (Figure 2-1E).

Retraction of hemostatic plugs depends, in large part, on outside-in signaling via $\alpha_{IIb}\beta_3$ integrin.[84,85] Interestingly, using two distinct assays, we observed a small but significant *delay* in retraction for the RGS10$^{-/-}$ blood when compared to WT controls following thrombin stimulation (Figure 2-1F,G). However, there was no difference in the degree of clot retraction at the endpoint in either assay. It is important to note, though, that the time scales for these various assays differ considerably. While cremaster laser injuries are captured over the course of 3 minutes, the visual and light scattering clot retraction assays occur over the course of 1 hour and 20 minutes, respectively. Thus, it is possible that RGS10$^{-/-}$ hemostatic plugs could consolidate to a similar degree as WT controls over a longer time course.

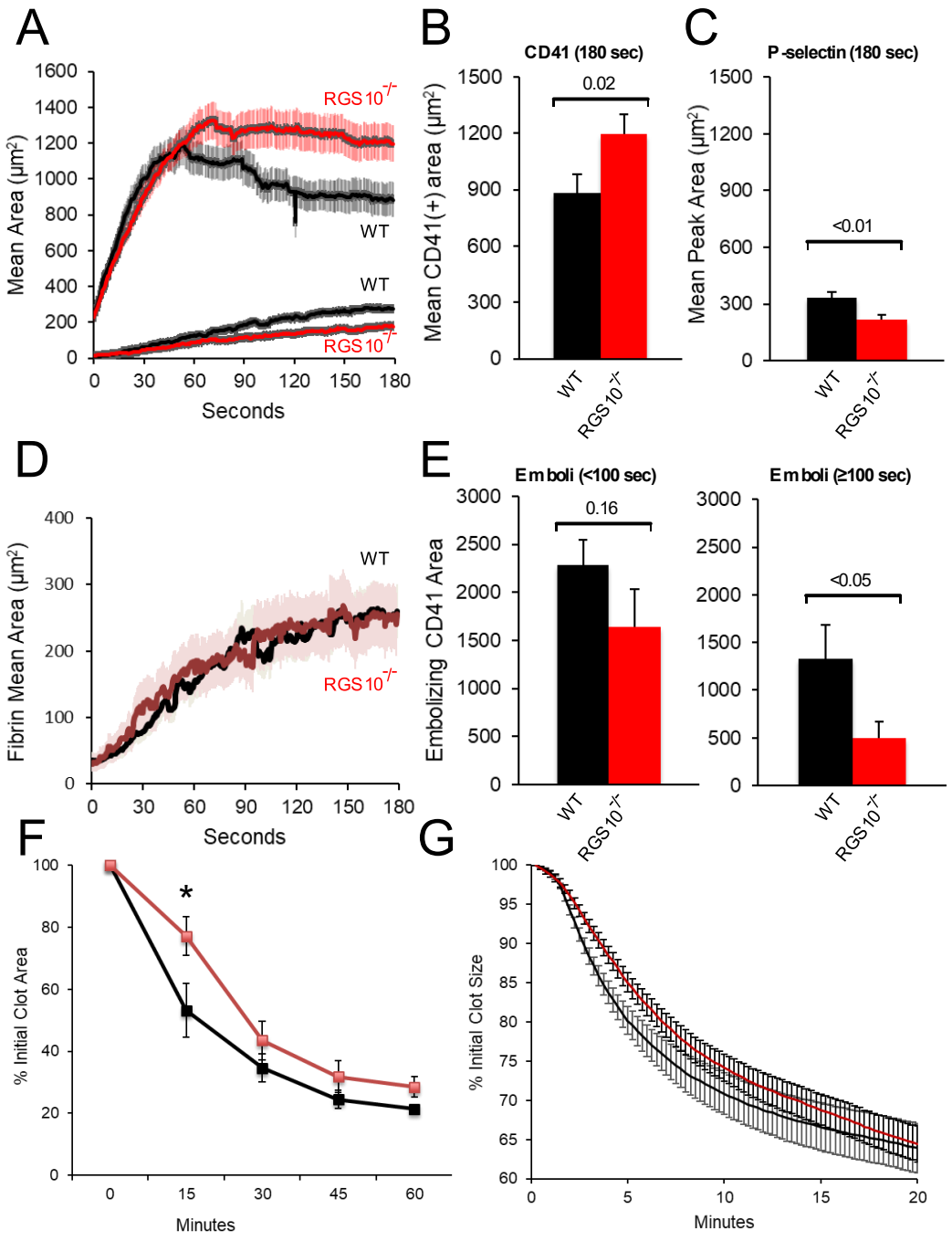

Figure 2-1. RGS10 deletion enhances the initial hemostatic response but delays clot retraction. Confocal intravital fluorescence microscopy was used to measure (A, B) platelet accumulation, (A, C) P-selectin expression, and (D) fibrin deposition. N = 78 injuries in 11 mice. (E) Embolization of platelets was measured by placing a virtual analysis window downstream of the site of injury and pooled into early and late time points for analysis. N = 19 injuries for WT and 18 injuries for RGS10$^{-/-}$ in 3 mice. Clot retraction was measured in (F) platelet rich plasma treated with 10 U/mL thrombin via a visual assay and (G) in whole blood samples incubated with 5 U/mL thrombin via a light scattering assay. N = 6 for WT and 7 for RGS10$^{-/-}$. * = P < 0.05.

2.3.2 RGS10 differentially affects specific GPCR signaling pathways

To assess the activation-dependent hemostatic function of platelets *in vitro*, we used flow cytometry to measure α-granule exocytosis and activated $\alpha_{IIb}\beta_3$ integrin with anti-P-selectin-FITC antibodies and Jon/A-PE, respectively. Platelets in these studies were pretreated with apyrase and aspirin to limit secondary signaling effects via ADP and TxA_2, respectively (except when using ADP as the agonist, pretreatment was with aspirin only). For PAR4 activating peptide (AYPGKF)-mediated P-selectin exposure, $RGS10^{-/-}$ platelets exhibited a left-shift in the dose-response but were no different at minimally or maximally activating concentrations (Figure 2-2A). In contrast, $RGS10^{-/-}$ platelets had a 6.7-fold increase in maximum P-selectin exposure in response to U46619, a TxA_2 mimetic (Figure 2-2C) and a similar pattern for ADP, with a 10.3-fold increase in maximum P-selectin exposure (Figure 2-2E). Additionally, nearly identical $\alpha_{IIb}\beta_3$ integrin activation response patterns were observed for all agonists, with a left-shift in dose-response for AYPGKF (Figure 2-2B), a 4.1-fold increase in maximal signal for U46619 (Figure 2-2D), and a 5.5-fold increase in maximal signal for ADP (Figure 2-2F). These results support the notion that both α-granule exocytosis and $\alpha_{IIb}\beta_3$ integrin activation as a measure of GPCR-dependent platelet activation are normally attenuated by RGS10.

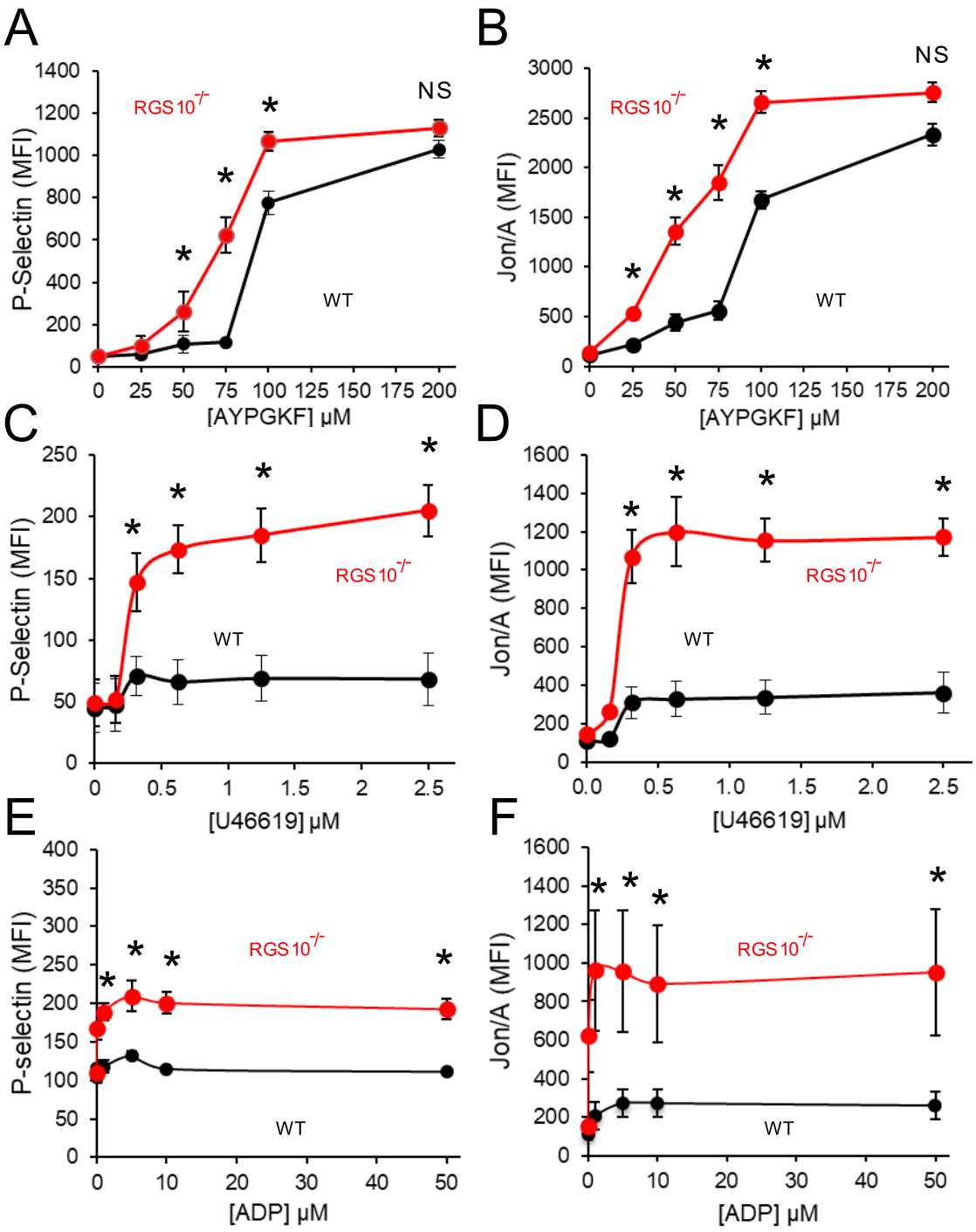

Figure 2-2. RGS10 deletion increases integrin activation and α-granule exocytosis. Platelets were stained with fluorophore-conjugated antibodies against (A, C, E) P-selectin or (B, D, F) $\alpha_{IIb}\beta_3$ integrin (Jon/A) after incubation with (A, B) PAR4 agonist peptide (AYPGKF), (C, D) a TxA2 mimetic (U46619), or (E, F) ADP at the concentrations indicated. N = 7 per genotype. Results are mean ± SEM. * = $P < 0.05$; NS = not significant.

2.3.3 RGS10 regulates G_q- and G_i-mediated signaling in platelets

As mentioned in 1.2, G_q-mediated responses result in, amongst other things, production of IP_3 that stimulates Ca^{2+} release from the platelet dense tubular system. As a potent secondary signaling molecule, Ca^{2+} is involved in various activation events, including cytoskeletal rearrangements mediated, in part, by myosin light chain phosphorylation.[86] To probe the magnitude and kinetics of Ca^{2+} mobilization, platelets were preloaded with the ratiometric Ca^{2+} sensor, fura-2, prior to agonist stimulation. For lower doses of PAR4 activating peptide (100 μM), the initial rate and the maximum amplitude of Ca^{2+} release is increased significantly in RGS10$^{-/-}$ platelets (Figure 2-3A, B). However, those differences are no longer observed at higher concentrations of agonist (500 μM). Interestingly, in response to both U46619 and ADP, there appears to be a significant increase in the maximum amplitude of Ca^{2+} release but no difference in initial rates (Figure 2-3A, B). These results would appear to be largely consistent with what we had observed using flow cytometry. Furthermore, RGS10$^{-/-}$ platelets exhibit a significant increase in myosin light chain phosphorylation following stimulation with PAR4 activating peptide, a secondary readout for G_q-mediated signaling (Figure 2-3C).

$G\beta\gamma$ subunits, derived from $G_i\alpha$ subunit dissociation, activate PI3Kβ which is involved in the phosphorylation and subsequent activation of the serine/threonine kinase, Akt.[87-89] Thus, to specifically probe effects of RGS10 deletion on G_i-mediated signaling, we measured Akt serine 473 phosphorylation (pAkt) in stimulated platelets via phosphospecific antibodies and immunoblotting. In response to ADP, pAkt was significantly increased in RGS10$^{-/-}$ platelets. This pattern was unaffected by the $P2Y_1$ inhibitor, MRS2500, but the response was ablated by the $P2Y_{12}$ inhibitor, cangrelor, consistent with the notion that Akt phosphorylation is mediated by $P2Y_{12}$ but not $P2Y_1$ (Figure 2-3D).[88] Furthermore, we observed no differences between RGS10$^{-/-}$ and WT platelets in response to high dose PAR4 activating peptide (350 μM), which directly stimulates G_q-mediated signaling. However, like with ADP, we did see decreases in pAkt responses of both genotypes in

the presence of cangrelor but not MRS2500, suggesting that the PAR4 response is mediated, at least in part, by secondary signaling via released ADP acting upon $P2Y_{12}$ (Figure 2-3D).

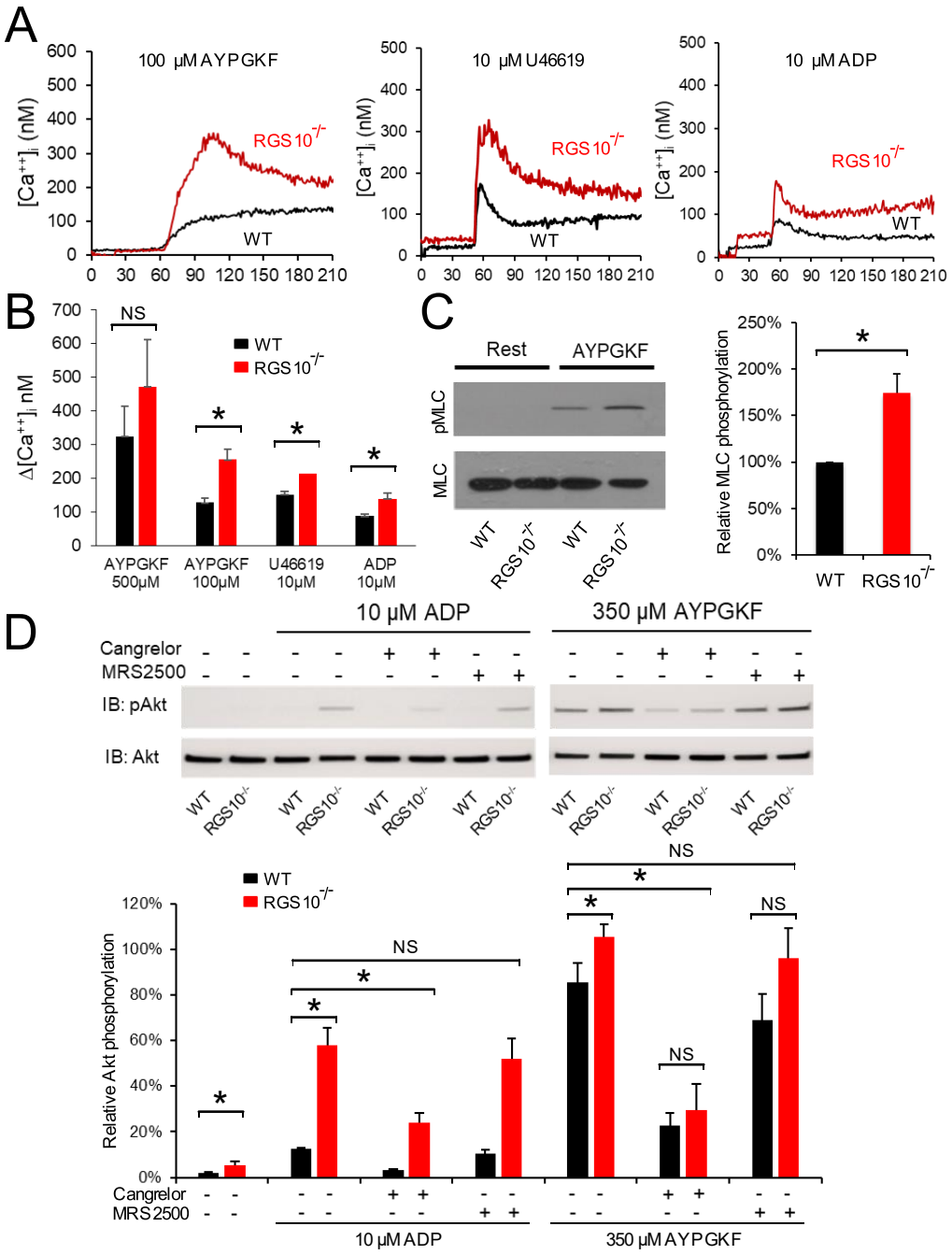

Figure 2-3. RGS10 regulates G_q- and G_{i2}-mediated signaling in platelets. (A) Fura-2-loaded platelets were stimulated with agonists as indicated to measure Ca^{2+} mobilization. (B) Quantification of Ca^{2+} experiments. N = 4. (C) Washed platelets incubated for 3 minutes with 350 μM AYPGKF were lysed and analyzed by immunoblotting for myosin light chain Thr18 and Ser19 phosphorylation. N = 4 (D) Gel-filtered platelets were stimulated with agonist ± inhibitors as indicated, lysed and analyzed by immunoblotting for Akt Ser473 phosphorylation. N = 5. All results represented as mean ± SEM; * = $P < 0.05$.

2.3.4 Interactions between RGS10 and putative regulators in platelets

Previous work from our lab has shown that both RGS10 and RGS18 are capable of binding to spinophilin (SPL) at rest but dissociate following G_q- or G_s-mediated stimulation (see 1.4.3). Additional studies with $SPL^{-/-}$ mice and RGS binding-deficient variants have led to hypothesis that binding to SPL inhibits RGS function in platelets and that RGS release constitutes a mode of negative feedback regulation, although this has yet to be tested directly.[74,75] Additionally, others have shown that binding of RGS18 to 14-3-3γ is enhanced by G_q-mediated signaling, but inhibited by G_s-mediated signaling, suggesting another mode of negative feedback regulation.[70,71] Therefore, we sought to explore how these adapter proteins might be interacting with RGS10 using immunoprecipitation. It is important to note, however, that due to limitations with available antibodies, these analyses were carried out with human platelets rather than mouse platelets.

In response to more potent G_q-stimulating agonists, such as PAR1 activating peptide (SFLRRN) or U46619, RGS10 appears to dissociate from SPL within 3 minutes (Figure 2-4A). However, in response to weaker G_q- and G_i-specific agonist, ADP, dissociation is primarily dependent upon secondary signaling, likely through TxA_2, as the amount of dissociation is considerably diminished in the presence of aspirin (Figure 2-4B). As for the non-GPCR agonist, collagen, dissociation is entirely dependent upon secondary signaling, as aspirin and apyrase pretreatment blocks any appreciable dissociation (Figure 2-4A). Furthermore, forskolin, which directly activates adenylyl cyclase (AC), or PGI_2 which activates G_s-coupled receptors upstream of AC, also results in dissociation of this complex, which is more robust in the presence of the phosphatase inhibitor, okadaic acid (Figure 2-4C). These results are consistent with what has previously been demonstrated for RGS18, suggesting that agonist-dependent phosphorylation of SPL impacts RGS interactions. Additionally, within 1 minute of thrombin stimulation, RGS10 completely dissociates from 14-3-3γ (Figure 2-4D), which is in direct contrast to what had previously been observed for RGS18.

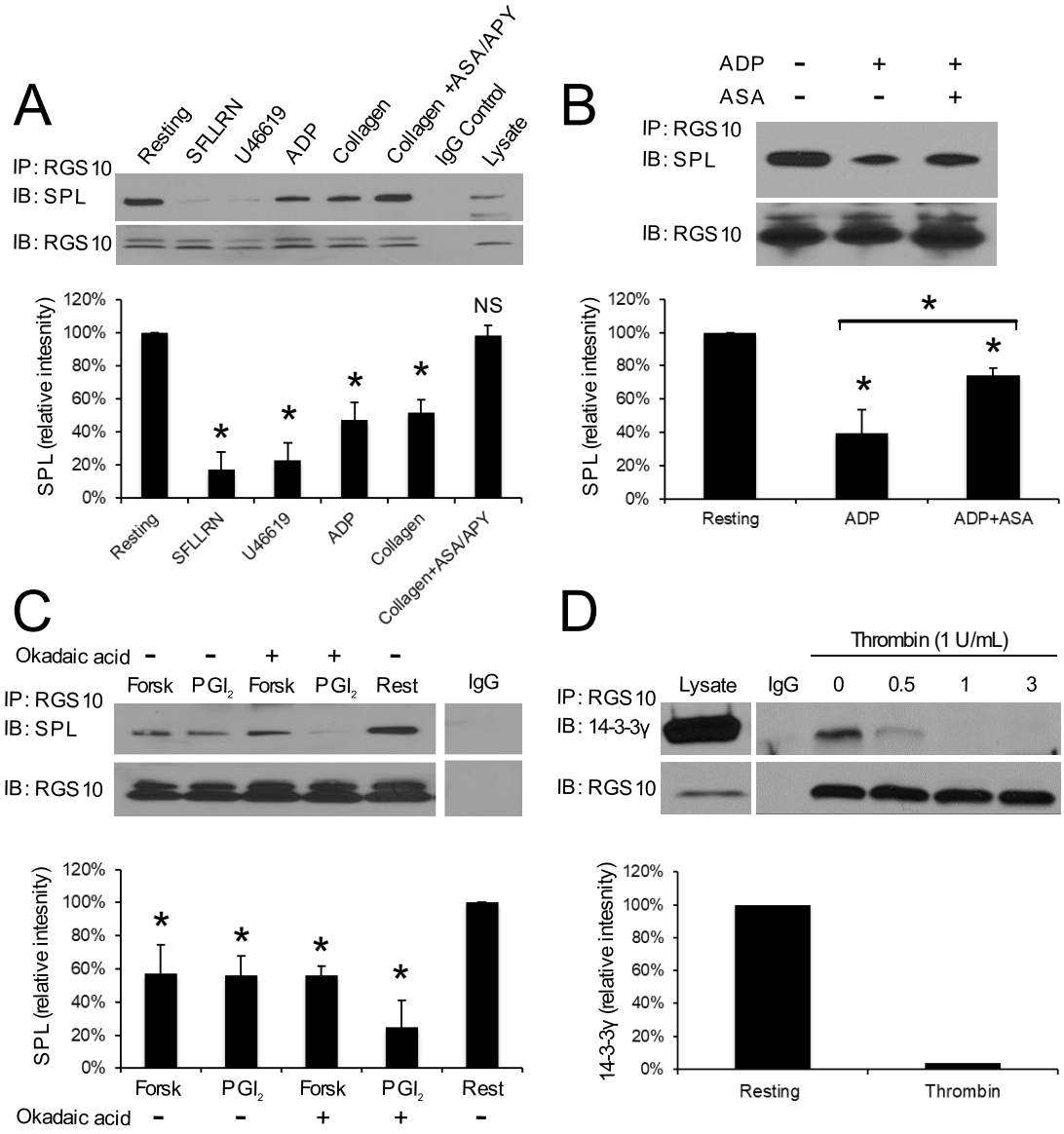

Figure 2-4. RGS10 interacts with spinophilin and 14-3-3γ. (A) Human platelets were incubated for 3 minutes with 50 μM PAR1 agonist peptide (SFLLRN), 10 μM TxA_2 mimetic (U46619), 10 μM ADP, or 10 μg/mL collagen in the presence of absence of 100 μM aspirin (ASA) and 1 U/mL apyrase (APY), as indicated. Lysates were precipitated with anti-RGS10 and probed for spinophilin (SPL) before reprobing for RGS10. N = 3. (B) Human platelets were incubated for 3 minutes with 10 μM ADP in the presence or absence of 100 μM aspirin (ASA), as indicated. Proteins were precipitated and immunoblotted as in A. N = 4. (C) Human platelets were incubated with 20 μM forskolin (Forsk) or 15 μM PGI_2 in the presence or absence of okadaic acid, a phosphatase inhibitor, as indicated. Proteins were precipitated and immunoblotted as in A. N = 4. (D) Human platelets were incubated with 1 U/mL thrombin for the times indicated and then lysed. 14-3-3γ was precipitated with anti-RGS10 prior to immunoblotting. N = 2. All quantifications, except those shown in D, are represented as mean ± SEM; * = $P < 0.05$.

2.3.5 Platelet activation-dependent RGS10 phosphorylation may impact Gα interactions

Prior work in cultured nucleated cells has shown that RGS10 is phosphorylated on S168 in a PKA-dependent manner. This results in translocation of RGS10 to the nucleus, where it can no longer interact with Gα subunits in the plasma membrane but has no apparent direct impact on GTPase activity.[56] Additional work with phospho-resistant variants of RGS10 (S168A) suggests that PKA-dependent phosphorylation may be important in mediating its role in protection against neurotoxicity, although the precise mechanisms of this role have not yet been clearly defined.[90] Thus, we sought to explore whether or not RGS10 undergoes phosphorylation in platelets and what signaling pathways may be involved.

Human platelets were stimulated with several agonists, lysed and separated on Phos-tag gels, which provide improved resolution of phosphorylated species that bind specifically to the embedded Phos-tag molecule. Unexpectedly, PGE_1 incubation, which stimulates $G_s\alpha$ and subsequent PKA activation in platelets, did not result in any band shifts indicative of a phosphorylation event, as was hypothesized based on observations in the literature (Figure 2-5A). However, PAR1 activating peptide (SFLLRN) results in at least one (and possibly two) distinct band shift(s) to a higher apparent molecular weight (p2 and p1) indicative of a phosphorylated species. The same is true for ADP, although to a lesser extent (Figure 2-5A). Incubation with phosphatase led to a partial reduction in the intensity of p2 bands and an increase in the basal (b) bands, suggesting that these shifts are indeed due to phosphorylation. Additionally, we observed a dose-dependent increase in phosphorylation of RGS10 in response to thrombin (PAR1 and PAR4 activator), although the p1 band only becomes visible after partial dephosphorylation with calf intestinal phosphatase (Figure 2-5B). We also demonstrate that stimulation with high doses of either SFLLRN, AYPGKF or both results in RGS10 phosphorylation, indicating contributions from both PAR1 and PAR4 receptors (Figure 2-5C). Since these receptors couple to $G_q\alpha$, which results in calcium flux, we stimulated with the calcium ionophore, A23187, to see if phosphorylation was calcium dependent. A23187 can directly induce RGS10 phosphorylation, which is almost

completely reversed by treatment with phosphatase, indicating the involvement of calcium in RGS10 phosphorylation (Figure 2-5C). Incomplete loss of these p1 or p2 bands after phosphatase incubation indicates incomplete dephosphorylation, which is likely due to non-ideal conditions for phosphatase activity. It is also worth noting that Phos-tag gels are extremely sensitive to minor differences in buffer composition, which is why we often observe warping of the protein molecular weight ladder lanes and inconsistent resolution of bands from experiment to experiment.

A similar result was observed for PAR4 activating peptide (AYPGKF) stimulation of mouse platelets, with only a single distinct low molecular weight band at rest (b) and two distinct higher molecular weight species appearing after stimulation (p1 and p2) (Figure 2-5D). Since the magnitude of band shifts in Phos-tag gels is proportional to the degree of phosphorylation, we hypothesize that these bands indicate a singly (p1) and doubly (p2) phosphorylated species. Further, the pattern is similar but significantly weaker in intensity for $RGS10^{+/-}$ mouse platelets, providing further evidence that this signal is specific to RGS10. These results, combined with those observed above, indicate that activation-dependent RGS10 phosphorylation is common to both human and mouse platelets.

To further elucidate the signaling mechanisms involved in RGS10 phosphorylation, we preincubated human platelets with inhibitors and stimulated with a variety of agonists (Figure 2-5E). Thrombin stimulation results in a band shift that is consistent with previous observations, and this is not inhibited by preincubation with aspirin (to block secondary signaling via TxA_2), apyrase (to block secondary signaling via ADP), KT 5720 (a PKA inhibitor), Saracatinib (a Src Family Kinase inhibitor), or CAY10505 (a PI3K inhibitor).[91-93] This indicates that secondary signaling is not required for RGS10 phosphorylation via thrombin and that these various kinases are not involved. U46619 (a TxA_2 mimetic) results a similar pattern although the p1 band appears to predominate over the p2 band and is unaffected by treatment with aspirin and apyrase. ADP stimulation only results in a very weak band shift and only of the p1 species, which is almost completely blocked by treatment with aspirin (Figure 2-5E). This suggests that ADP-mediated phosphorylation of RGS10

is primarily mediated by secondary signaling via TxA_2, and thus not likely dependent on primary $P2Y_1$ or $P2Y_{12}$ signaling. Interestingly, GPVI stimulation via convulxin also results in the appearance of both p1 and p2 species which is unaffected by secondary signaling inhibitors (Figure 2-5E). This suggests that RGS10 phosphorylation may be mediated by signaling mechanisms that are common to GPVI and GPCR signaling pathways.

Since our previous evidence suggested that calcium ionophore could induce RGS10 phosphorylation, we hypothesized that calcium mobilization would be upstream of the responsible kinase(s). This is consistent with our results for both G_q-coupled GPCR agonists as well as GPVI agonists, because these two signaling pathways converge at PLC activation, which generates IP_3 to stimulate calcium flux and DAG to stimulate PKC activation. To further test this, platelets were preloaded with BAPTA-AM, an intracellular calcium chelator, and then stimulated with thrombin in the presence or absence of extracellular calcium. BAPTA-AM dose dependently inhibited RGS10 phosphorylation (at least of the p2 species), which was further reduced if no extracellular calcium was present (Figure 2-5F), indicating that calcium plays at least a partial role in mediating RGS10 phosphorylation. Because PKC isoforms are activated downstream of these signaling pathways, we next asked whether inhibition would reduce RGS10 phosphorylation. Treatment with a pan-PKC inhibitor, GF109203X, resulted in a similar dose dependent decrease in phosphorylation of RGS10.[94] And at the highest concentrations tolerated by platelets, RGS10 phosphorylation was almost completely ablated (Figure 2-5F), suggesting that PKC isoforms are likely responsible for RGS10 phosphorylation. This was further confirmed by direct stimulation with phorbol 12-myristate 13-acetate (PMA), which directly activates PKC.[95] The response to PMA was virtually identical to that of thrombin and was inhibited to a similar extent by GF109203X (Figure 2-5G). Lastly, we lysed resting or thrombin-stimulated human platelets and attempted to pull-down RGS10 with Halo-$G_{i2}\alpha$ in the presence of GDP alone (to mimic the inactive state) or GDP + AlF^{4-} (to mimic the transition state). RGS10 was partially phosphorylated in the resting condition, but the predominant species was unphosphorylated. Interestingly, $G_{i2}\alpha$ was unable to pull down the largely

dephosphorylated species of RGS10. However, after thrombin stimulation, almost all the RGS10 was phosphorylated, and a at least a portion appeared to bind to $G_{i2}\alpha$ (Figure 2-5H). This suggests that phosphorylation of RGS10 may mediate interactions with $G\alpha$ subunits directly or indirectly via adapters.

Figure 2-5. Platelet RGS10 undergoes activation-dependent phosphorylation (on following page). (A) Washed human platelets were incubated with 50 μM SFLLRN, 20 μM ADP, or 10 μM PGE_1, lysed, and incubated in the presence or absence of 400 U of lambda phosphatase as indicated prior to Phos-tag immunoblotting. (B) Washed human platelets were incubated with increasing concentrations of thrombin as indicated, lysed and then incubated in the presence or absence of 20 U calf intestinal phosphatase (CIP) prior to Phos-tag immunoblotting.(C) Washed human platelets were treated with SFLLRN (PAR1 agonist peptide), AYPGKF (PAR4 agonist peptide), a combination of the two, or A23187 (calcium ionophore), lysed, and incubated in the presence or absence of 20 U CIP prior to Phos-tag immunoblotting. (D) Washed platelets from wild type or $RGS10^{+/-}$ mice were incubated with 350 μM AYPGKF, lysed and analyzed by Phos-tag immunoblotting. (E) Washed human platelets were stimulated with 10 U/mL thrombin, 50 μM TxA_2 mimetic (U46619), 20 μM ADP, or 1 μg/mL convulxin (CVX) in the presence or absence of 1 mM aspirin (ASA), 1 U/mL apyrase (APY), 0.1 μM PKA inhibitor (KT 5720; PKAi), 0.1 μM Src Family Kinase inhibitor (Saracatinib; SFKi), 20 μM PI3K inhibitor (CAY10505; PI3Ki), and 5 mM EGTA. Lysed samples were then analyzed by Phos-tag immunoblotting. (F) Washed human platelets were treated with 1 U/mL thrombin in the presence or absence of increasing concentrations of intracellular calcium chelator (BAPTA-AM) or PKC inhibitor (GF109203X), and/or 1 mM $CaCl_2$ (Ca^{2+}), lysed and analyzed by Phos-tag immunoblotting. (G) Washed human platelets were treated with 1 U/mL thrombin or 1 μM phorbol 12-myristate 13-acetate (PMA) in the presence or absence of PKC inhibitor (GF109203X), lysed and analyzed by Phos-tag immunoblotting. (H) Washed human platelets were incubated in the presence or absence of 1 U/mL thrombin, lysed and subject to pull-down via magnetic bead-bound Halo-$G_{i2}\alpha$ in the presence of GDP or GDP + AlF^{4-}. Total lysate (Input), washes after the final incubation with Halo-$G_{i2}\alpha$ (Wash) and eluate (E1) after tobacco etch virus cleavage of $G_{i2}\alpha$ from the magnetic beads were analyzed by Phos-tag immunoblotting. Arrows indicate: b, basally phosphorylated or unphosphorylated species; p1, first phosphorylated species; and p2, second phosphorylated species.

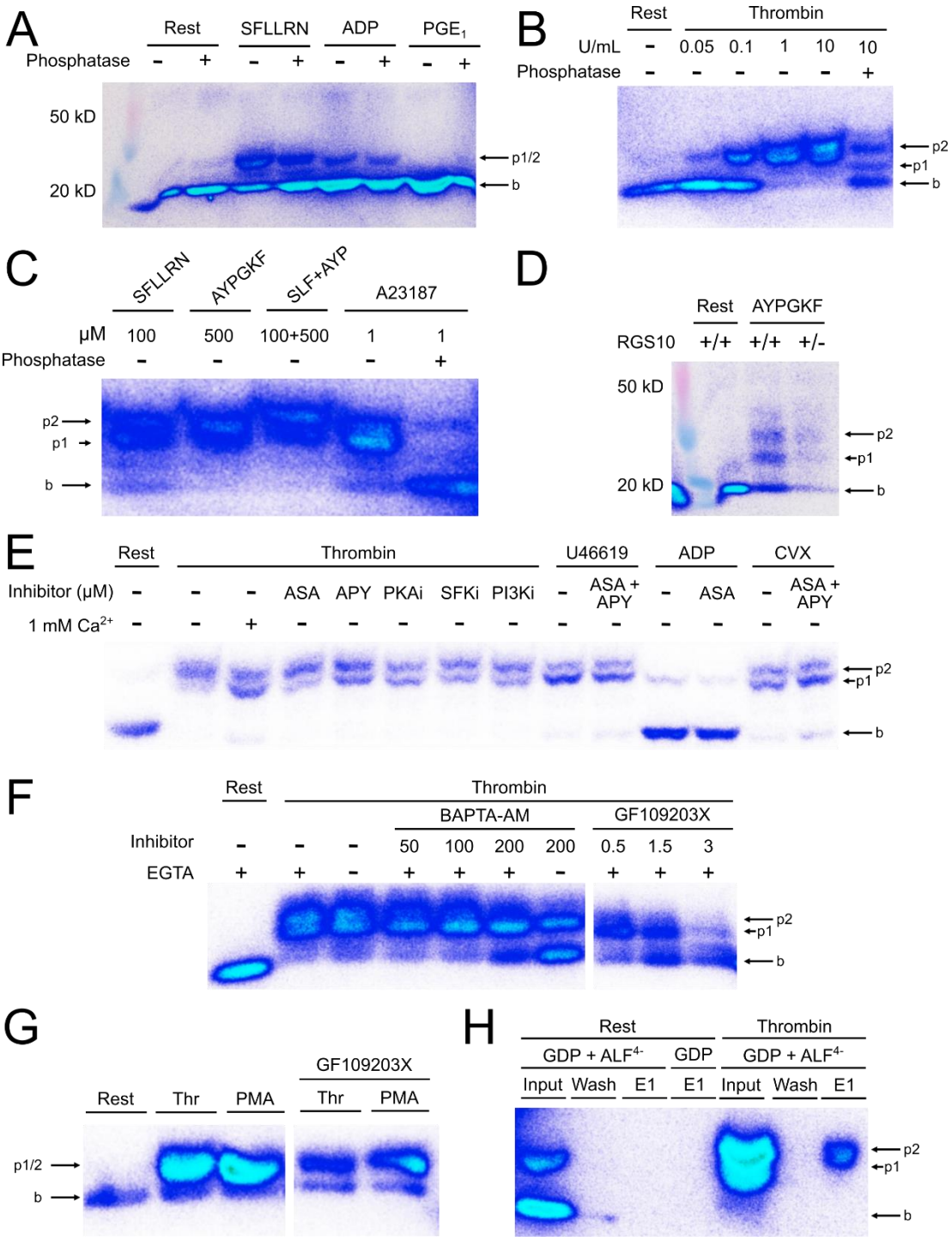
A
Rest
SFLLRN
ADP
PGE1
Phosphatase
50 kD
20 kD
p1/2
b
B
Rest
Thrombin
U/mL
0.05
0.1
1
10
10
Phosphatase
p2
p1
b
C
SFLLRN
AYPGKF
SLF+AYP
A23187
μM
100
500
100+500
1
1
Phosphatase
p2
p1
b
D
Rest
AYPGKF
RGS10
+/+
+/+
+/-
50 kD
20 kD
p2
p1
b
E
Rest
Thrombin
U46619
ADP
CVX
Inhibitor (μM)
ASA
APY
PKAi
SFKi
PI3Ki
ASA + APY
ASA
ASA + APY
1 mM Ca2+
p2
p1
b
F
Rest
Thrombin
BAPTA-AM
GF109203X
Inhibitor
50
100
200
200
0.5
1.5
3
EGTA
p2
p1
b
G
GF109203X
Rest
Thr
PMA
Thr
PMA
p1/2
b
H
Rest
Thrombin
GDP + ALF4-
GDP
GDP + ALF4-
Input
Wash
E1
E1
Input
Wash
E1
p2
p1
b

2.4 Discussion

Using the cremaster laser injury model to study hemostasis *in vivo*, we've gained valuable insights into the biochemical and biophysical determinants of hemostatic plug formation that are modulated by RGS10 deletion. And in combination with our *in vitro* studies, we have expanded our working model for hemostasis that highlights the importance of RGS10 and its regulation.

Deletion of RGS10 results in stabilization, but no difference in peak accumulation, of the P-selectin$^{(-)}$ shell *in vivo*, which is driven primarily by released ADP and TxA_2. A similar pattern was also previously observed for $G_{i2}\alpha^{G184S/+}$ mice, hemizygous for a substitution that makes $G_{i2}\alpha$ insensitive to RGS regulation, with an expansion of the shell.[78] However, in this model, the peak accumulation of P-selectin$^{(-)}$ platelets was significantly greater, in addition to being more stable over time. This would indicate that the net effect of RGS-insensitive $G_{i2}\alpha^{G184S/+}$ is greater than that of RGS10 deletion alone and suggests contributions to G_{i2}-mediated signaling from additional RGS in platelets, such as RGS18. Furthermore, while the effects of RGS-insensitive $G_{i2}\alpha^{G184S/+}$ are limited to G_{i2}-mediated signaling, RGS10 deletion appears to impact both G_q and G_i signaling pathways, as demonstrated by our Ca^{2+} and Akt phosphorylation assays, respectively. This would indicate that RGS10 regulates both $G_q\alpha$ and $G_{i2}\alpha$ in platelets, although the extent to which it does so is not entirely clear. This is consistent with concurrent studies by Hensch *et al*, which showed that pretreatment of RGS10-deficient platelets with apyrase led to transient aggregation following stimulation with low-dose PAR4 agonist peptide (40 μM) that was not observed in the absence of apyrase.[63] Since apyrase indiscriminately hydrolyzes ADP, which stimulates both G_q-coupled $P2Y_1$ receptors and G_{i2}-coupled $P2Y_{12}$ receptors, it is likely that RGS10 limits signaling downstream of both of these secondary signaling pathways to prevent aggregation in response to submaximal PAR stimulation.

In contrast to our U46619 and ADP flow cytometry results, we see only a slight but significant left-shift in the dose response curve for PAR4 agonist peptide stimulation with no increase in the maximal signal. However, we also do not see any differences in the P-selectin$^{(+)}$

core, driven by local concentrations of thrombin, which cleaves and activates PARs. One possible explanation for this apparent discrepancy is that platelets in the core of a hemostatic plug, where thrombin concentrations are high and limited in diffusion by high packing density,[85] are uniformly reaching maximal activation and fully degranulating. Since the differences that we observed for PAR activation *in vitro* disappear at maximal dose, the inability for thrombin to diffuse outward to less activated platelets could explain why the core size does not differ significantly. Another possibility is that RGS10, in isolation, does not significantly contribute to limiting platelet activation (and more specifically degranulation) once a certain threshold of activation has been reached. While we may not actually be able to reach this threshold *in vitro* with individual agonists, the complex microenvironment of a growing hemostatic core *in vivo* contains a milieu of additional stimuli that may overwhelm or downregulate RGS10-mediated regulation.

Additionally, we have shown that RGS10, much like RGS18, can bind to spinophilin and 14-3-3γ in an agonist dependent manner. Interestingly, stimulation with activators like PAR1 activating peptide or U46619 (G_q- and G_{13}-coupled agonists) but not ADP (G_q- and G_{i2}-coupled agonist) or collagen (non-GPCR agonist) results in dissociation of the RGS10:SPL complex. Furthermore, platelet inhibitors, like PGI_2 (G_s-coupled agonist) also cause dissociation of the complex. Why, then, might signaling pathways that are classically thought to have opposing outcomes, generate similar results? And why do only a subset of platelet activating agonists cause dissociation of the RGS10:SPL complex? While there is little available evidence to support concrete conclusions, we propose a model in which RGS10 serves dual purposes: negative feedback regulation and constitutive attenuation.

When the platelet is in circulation, multiple mechanisms, including PGI_2 released from the endothelium, maintain platelets in a quiescent state. It would thus stand to reason that, under these conditions, RGS10 dissociates from spinophilin to act as a constitutive break to limit aberrant G_q or G_{i2} signaling *in vivo*. Conversely, when platelet activation is required to stem bleeding, the process needs to occur rapidly. Thus, having RGS10 bound to SPL to inhibit its function in the earliest

stages of platelet activation may be beneficial for the most rapid and robust response. However, an excessive response would prove to be just as deleterious as an insufficient one, so RGS10 is released from SPL after signaling is initiated to limit excessive platelet deposition and clot growth via G_q and G_{i2} signaling. What remains unclear, however, are the *in vivo* conditions under which RGS10 becomes bound to SPL initially. It is possible that there is a rapid transition during initial platelet deposition where ADP-mediated G_{i2}-coupled $P2Y_{12}$ activation counteracts PGI_2-mediated inhibition prior to thrombin and TxA_2 generation. Under these conditions, RGS10 would thus bind to spinophilin, allow rapid platelet activation via G_q- and G_{i2}-dependent signaling, and then dissociate from spinophilin to attenuate signaling before it leads to uncontrolled clot growth.

Lastly, we present evidence that RGS10 is phosphorylated in platelets in an agonist-specific manner that may impact its interactions with $G\alpha$ subunits. Notably, TP and PAR stimulation, which result in dramatic dissociation from SPL, also result in robust RGS10 phosphorylation. It is thus possible that phosphorylation of RGS10 plays a role in mediating its interactions with SPL (and 14-3-3γ). However, G_s stimulation does not appear to impact RGS10 phosphorylation while it does result in SPL dissociation. This could indicate that G_s-mediated RGS10:SPL dissociation occurs via mechanisms that are distinct from G_q-mediated RGS10:SPL dissociation, as was reported for RGS18.[75] Why G_s/PKA is involved in RGS10 phosphorylation in nucleated cells but not platelets remains unclear. It is possible that these cells possess an intermediate kinase that platelets lack. Further, it is yet unclear what functional impact phosphorylation has on RGS10 in platelets. While it appears that it may impact interactions with $G\alpha$ subunits, it remains to be seen whether this is effect is direct or indirect via interactions with an intermediate, such as SPL or 14-3-3γ. Additionally, we observe at least two distinct phosphorylated species in response to platelet activation, particularly under circumstances where we achieve optimal resolution. For more robust stimuli like thrombin (or PAR1/4 agonist peptides), the p2 species appears to predominate. Since the degree of shift in a Phos-tag gel is proportional to the degree of phosphorylation, it is conceivable that this species is multiply phosphorylated. With less robust stimuli, such as U46619

and ADP, the p1 species appears to predominate. This suggests that weaker stimuli do not result in the same degree of phosphorylation. Further, this correlation suggests that the p1 species may be a required intermediate to sequentially generate the p2 species. While we have yet to identify the exact kinases involved, our data suggest that this process is Ca^{2+} and PKC-dependent, consistent with the ability of both G_q GPCR and GPVI ITAM signaling to generate similarly phosphorylated species. Interestingly, we see that BAPTA-AM, an intracellular calcium chelator, in the absence of intracellular calcium is still unable to reduce phosphorylation to the same degree as GF109203X, a pan-PKC inhibitor. While it is certainly possible that our highest concentration of BAPTA-AM is insufficient to completely chelate all calcium, it may also suggest that at least some degree of phosphorylation is calcium independent. Indeed, in the presence of BAPTA-AM the p2 species appears to completely disappear while the p1 species remains robust. Based on these results and those for PKC inhibition, we hypothesize that the p1 species is dependent upon novel PKC isoforms (which require DAG but do not require Ca^{2+} for activation) while the p2 species is dependent upon conventional PKC isoforms (which require both DAG and Ca^{2+} for activation).[96] Finally, when attempting to pull-down RGS10 from human platelets with Halo-$G_{i2}\alpha$, we observed some degree of RGS10 phosphorylation in the resting condition not observed previously. The reasons for this are not entirely clear, but it could potentially be due to some degree of preactivation during the preparation of the platelets or phosphorylation of RGS10 following lysis of platelets and incubation. However, interestingly, the phosphorylated species in the resting platelets appears to be the p1 species, which is not precipitated by Halo-$G_{i2}\alpha$ in the presence of GDP + AlF^{4-} (to mimic the transition state). Conversely, thrombin stimulated platelet lysate leads to the presence of both p1 and p2 species but only the p2 species appears to be precipitated by Halo-$G_{i2}\alpha$. This could imply that the p1 species cannot interact with $G_{i2}\alpha$ while the p2 species can. Whether p1 phosphorylation directly interrupts interactions or enhances interactions with inhibitory molecules, like SPL and 14-3-3γ, while p2 phosphorylation directly enhances interactions or disrupts those with inhibitory molecules will require further investigation.

CHAPTER 3: RGS10 and RGS18 Differentially Regulate Platelet Biology

3.1 Introduction

While deletion of single RGS proteins has provided evidence for their individual roles, questions remain as to the net contributions of RGS proteins as a family to the regulation of platelet activation during hemostasis and the homeostatic maintenance of platelet counts in circulation. Deleting more than 20 canonical RGS proteins in mice simply isn't feasible and would likely not yield viable offspring. And while $G_{i2}\alpha$ RGS-insensitive variants exist and produce mice that are least somewhat viable, identifying functional $G_q\alpha$ RGS-insensitive variants in mice has proven more difficult (see Chapter 4). Thus, our approach was to focus on the two predominantly expressed and common RGS proteins in both human and mouse platelets: RGS10 and RGS18.[41-43] We also sought to compare single deletions of each protein to the dually deleted mice to better assess the individual contributions of each protein.

Deleting RGS10 or RGS18 alone has measurable effects, largely consistent with previous reports, but the full impact of these proteins can only be appreciated when both are absent. Deleting RGS10 has no impact on platelet counts, while deleting RGS18 results in a reduction of ~15%. Dual deletion of both RGS10 and RGS18 results in a further decrease in platelet counts of ~40%. Platelets from $RGS10^{-/-}RGS18^{-/-}$ (but not $RGS10^{-/-}$ or $RGS18^{-/-}$ mice) exhibit an increased rate of clearance from circulation, increased basal surface expression of TLT-1 and increased thiazole orange staining. Further, treating $RGS10^{-/-}RGS18^{-/-}$ mice with dual anti-platelet therapy (DAPT) consisting of aspirin and $P2Y_{12}$ ADP receptor antagonist, prasugrel, normalizes their platelet counts to levels comparable to $RGS18^{-/-}$ mice, suggesting that their decrease in platelet counts can be explained, in part, by premature clearance of hyperactive platelets in circulation. In addition, $RGS10^{-/-}RGS18^{-/-}$ and $RGS18^{-/-}$ mice (but not $RGS10^{-/-}$) exhibit delayed recovery of platelet counts after depletion and a trend towards a decreased capacity to produce proplatelets, indicating that the remainder of the decrease in platelet count is likely due to defects in platelet production from megakaryocytes. Taken together, this data suggests that RGS18 plays a minor role in signaling

that promotes platelet production from megakaryocytes, while both proteins combine to attenuate aberrant signaling under basal conditions that would otherwise result in platelet activation and subsequent clearance.

In addition to their roles in regulating platelet lifespan, RGS10 and RGS18 also have a significant impact on hemostasis. Responses to platelet activating GPCR agonists *ex vivo*, including PAR4 activating peptide, TP-activating TxA2 mimetic (U46619) and $P2Y_1$- and $P2Y_{12}$-activating ADP, are increased for the $RGS10^{-/-}RGS18^{-/-}$ platelets relative to controls. And while previous reports by ourselves (see Chapter 2) and others suggest a modest role in regulating hemostatic plug formation and preventing blood loss for RGS10 and RGS18 deletion in isolation,[62,63] penetrating hemostatic injuries in $RGS10^{-/-}RGS18^{-/-}$ mice evoke a response that is significantly exaggerated to the point of vessel occlusion, a rare occurrence in this model. These results, taken together with those above, suggest that RGS10 and RGS18 cooperate to attenuate signaling under basal and hemostatic conditions to prevent unnecessary clearance and vascular occlusion, respectively.

3.2 Materials and Methods

3.2.1 $RGS10^{-/-}$ $RGS18^{-/-}$ mouse model

Generation of *Rgs10/18* double knockout mice using CRISPR-Cas9 genome-editing system was performed essentially as described by Henao-Mejia et al[97] and all mouse protocols and procedures were approved by the Institutional Animal Care and Use Committee of the University of Pennsylvania. Briefly, Cas9 mRNA was generated from pMJ920-Cas9 plasmid using mMESSAGE mMACHINE T7 Ultra Transcription Kit according to the manufacturer's instructions (Life Technologies, AM1345). The quality of the Cas9 mRNA was determined by analyzing Cas9 mRNA pre- and post-polyadenylation with a 2100 Bioanalyzer. gRNAs were designed for *Rgs10* and *Rgs18* genes by following the protocol described in Ran et al.[98] T7 promoter was added to the gRNA templates by PCR amplification. The PCR product was purified and then used as a template

for in vitro transcription according to the manufacturer's specifications (MEGAshortscript T7 kit, Life Technologies). The gRNAs were then purified using the MEGAclear kit (Life Technologies). gRNA quality was verified on agarose gel. Zygotes from C57BL/6 mice were injected with Cas9 mRNA (100 ng/µl) and gRNAs (50 ng/µl). Embryos were then transferred to pseudo-pregnant C57BL/6 females. After birth, 10-day-old mice were tail-snipped and genomic DNA was extracted for genotyping and sequencing. The lone founder mouse (*Rgs10*$^{-/-}$*Rgs18*$^{+/-}$) was backcrossed to genetically identical parental WT C57BL/6 mice. Successive breeding with mice from the same colony was performed as necessary to generate *Rgs10*$^{+/+}$*Rgs18*$^{+/+}$, *Rgs10*$^{-/-}$*Rgs18*$^{+/+}$, *Rgs10*$^{+/+}$*Rgs18*$^{-/-}$, and *Rgs10*$^{-/-}$*Rgs18*$^{-/-}$ mice. Age- and sex-matched WT, single and double knockouts for experimental use were generated from homozygous parents for each genotype.

3.2.2 RGS10$^{-/-}$ RGS18$^{-/-}$ genotyping

Mice were genotyped for Rgs10 using a three primer PCR-based strategy. Forward Primer: 5'-GTGGATAACAGTCCAGCTTCTC-3', Reverse Primer 1: 5'-CCAGAGCCCATCTCACATTTA-3', Reverse Primer 2: 5'- GTTCCTCAGCCTTCGTCAAT-3'. PCR was performed with the following conditions: Denaturation at 95°C for 5 minutes; 35 cycles of (95°C for 30 seconds, 58°C for 30 seconds, and 72°C for 1 minute); extension at 72°C for 7 minutes. Mice were genotyped for Rgs18 by PCR and endonuclease digestion strategy. Forward Primer: 5'-TGTGTAAATGTGTGGATCCTTGT-3', Reverse Primer: 5'-ACTTTCAATCCATAATCATACGCTGTATTCTG-3'. PCR was performed with the following conditions: Denaturation at 95°C for 2 minutes; 35 cycles of (95°C for 30 seconds, 59°C for 45 seconds, and 72°C for 45 seconds); extension at 72°C for 5 minutes. Samples were then incubated with ApoI-HF according to manufacturer protocol. Additionally, to routinely verify PCR genotyping results, samples were processed with ExoSAP-IT PCR Product Cleanup Reagent (Affymetrix, Santa Clara, CA) according to manufacturer protocol prior to addition of Forward Primer for Sanger sequencing through the Genomics Analysis Core at the University of Pennsylvania.

3.2.3 Preparation of diluted whole blood for flow cytometry

Whole blood was isolated via the retro-orbital plexus from isoflurane-anesthetized mice using heparinized micro-hematocrit capillary tubes. Blood was diluted 1:20 with modified Tyrode's bufffer (137 mM NaCl, 20 mM HEPES, 5.6 mM glucose, 1 g/liter BSA, 1 mM MgCl2, 2.7 mM KCl, 3.3 mM, NaH2PO4, pH 7.4) and stored at 37°C prior to analysis.

3.2.4 Flow cytometric analysis of platelet activation

Diluted whole blood was prepared as outlined in 3.2.3 and incubated with 1 mM aspirin and 1 U/mL apyrase for 30 minutes at 37°C to eliminate secondary signaling (except for ADP measurements, incubated only with 1 mM aspirin). Following inhibitor treatment, diluted blood was treated with agonist for 15 minutes at 37° C in the presence of saturating concentrations of fluorescently-labeled mAb against P-selectin, activated $\alpha_{IIb}\beta_3$ integrin (Jon/A) and $F(ab')_2$ fragments against CD41 (α_{IIb}) and analyzed on a FACSCanto II cell analyzer (BD Biosciences, San Jose, CA). The platelet population was gated based on FSC/SSC and CD41 positivity. For thiazole orange (TO) studies, platelets were incubated with 1 μg/mL of TO for 20 minutes at 37° C prior to staining with CD41 (α_{IIb}). For TLT-1 studies, platelets were co-incubated with Alexa Fluor 488-labeled mAb against TLT-1 in place of P-selectin.

3.2.5 Platelet and fibrin accumulation following penetrating vascular injury

Hemostatic thrombus formation was observed in the cremaster muscle microcirculation of male mice aged 8-12 weeks, as previously described.[78] Briefly, Alexa Fluor 568–labeled anti-CD41 F(ab')2 fragments, Alexa Fluor 488–labeled anti–P-selectin, and Alexa Fluor 647-labeled anti-fibrin were administered via a catheter in the jugular vein. Arterioles 30-50 μm in diameter were studied. Penetrating vascular injuries were produced with a pulsed nitrogen dye laser fired through the microscope objective. Thrombus formation was observed for 3 min at 1.9 frames per second and analyzed using SlideBook 6 software (Intelligent Imaging Innovations, Denver, CO). Transient occlusions were defined as hemostatic thrombi that filled the diameter of the blood vessel, but

either did not fully block blood flow or blocked it temporarily. Stable occlusions were defined as fully occluded vessels that did not recover flow by the end of the observation period.

3.2.6 Bone marrow megakaryocyte immunohistochemistry

Femurs were harvested from mice and fixed for at least 48 hours in 10% neutral buffer formalin. Decalcification, paraffin embedding, sectioning and slide mounting was performed by the Comparative Pathology Core at the University of Pennsylvania School of Veterinary Medicine. Immunohistochemistry to stain for α_{IIb} was performed as previously described.[99] Briefly, slides were incubated with goat anti-human integrin α_{IIb} followed by peroxidase-conjugated anti-goat secondary, stained with DAB Peroxidase Substrate Kit, and counterstained with hematoxylin. Imaging was performed using a 20X objective on a Nikon Eclipse E600 microscope and quantification of megakaryocytes performed blinded by counting large, positively stained brown cells with multi-lobed nuclei.

3.2.7 Platelet depletion and recovery

Twenty-four hours prior to depletion, mouse whole blood was acquired from the retro-orbital plexus and counted with a Procyte Hematological Analyzer (Idexx Laboratories, Westbrook, ME) to establish base-line counts. To assess the rate of platelet production, mice were injected via the retro-orbital plexus with 0.2 μg/g bodyweight of platelet-depleting rat anti-GPIbα antibody (Emfret Analytics, Eibelstadt, Germany) multiplied by the percent of platelets relative to Wild type (WT) baseline (to account for differences in base-line platelet counts between genotypes). Twenty minutes post-injection, platelets counts were <5% of baseline for each genotype. Every 24 hours for five days, whole blood was obtained from the retro-orbital plexus and analyzed for platelet counts as they recovered.

3.2.8 Platelet clearance from circulation

To assess the rate of platelet clearance, mice were injected via the retro-orbital plexus with non-saturating concentrations (1 μg/g body weight) of rat anti-GPIbβ-Dylight488 (Emfret Analytics,

Eibelstadt, Germany) to label the existing platelet pool while avoiding excess free antibody in circulation. Twenty minutes post-injection, ~90% of CD41(+) platelets were GPIbβ(+) for each genotype as assessed by flow cytometry. The percent of GPIbβ(+) CD41(+) platelets was then tracked every 24 hours for four days to assess the rate of platelet clearance.

3.2.9 Treatment with dual anti-platelet therapy

Mice were administered 50 mg/kg of aspirin and 1.875 mg/kg of prasugrel in 0.5% methylcellulose via oral gavage daily for 10 days total. Prior to the first dose and every 5 days after, blood was obtained via the retro-orbital plexus and platelet counts were determined with a Procyte Hematological Analyzer (Idexx Laboratories, Westbrook, ME). 5 days after treatment ceased, platelet counts were determined once more as described.

3.2.10 Megakaryocyte progenitor analysis

Bone marrow was isolated from femurs and tibias by flushing with PBS + 1X Penicillin-Streptomycin (Gibco, Waltham, MA) and counted using an automated trypan blue cell counter. To quantitate numbers of healthy, immunophenotypic bone marrow megakaryocyte progenitors (MegPs), cells were stained with the following fluorescently labeled antibodies: Pacific blue-anti-mouse lineage cocktail (Lin), PerCP/Cy5.5 anti-Sca-1, APC/Cy7 anti-c-Kit, PE anti-CD16/CD32, PE/Dazzle 594 anti-CD150, FITC anti-CD41, and fluorescent BUV395 Annexin V (to exclude apoptotic cells) and analyzed by flow cytometry. Healthy MegPs were defined as Annexin $V^{(-)}Lin^{(-)}Sca\text{-}1^{(-)}c\text{-}Kit^{(+)}CD16/32^{(-)}CD150^{(+)}CD41^{(+)}$ cells.

3.2.11 Cultured megakaryocyte analysis

Unfractionated bone marrow cells isolated as outlined above were seeded at 5×10^6 cells per well in a 6-well plate in Iscove's Modified Dulbecco's Medium (IMDM) containing 10% FBS (HyClone, Chicago, IL), 100 U/mL Pen/Strep (Gibco, Waltham, MA), 2 mM Glutamine (Gibco, Waltham, MA), and 50 ng/mL mouse thrombopoietin (TPO; R&D Systems, Minneapolis, MN). Cells were cultured for 5 days and media was replenished on Day 3 of culture. On Day 5, terminal

megakaryocytes (Megs) and Meg ploidy were quantitated by staining with APC anti-mouse CD42d, FITC anti-mouse CD41, and Vybrant DyeCycle followed by flow cytometric analysis. Megs were defined as $CD42d^{(+)}CD41^{(+)}$ cells and ploidy was determined by measuring distinct histogram peaks in DyeCycle within the $CD42d^{(+)}CD41^{(+)}$ subpopulation. Following enrichment via a 1.5%/3% BSA gradient, cells were seeded into 24-well plates coated with fibronectin (Thermo Fisher, Waltham, MA) and containing 10% FBS, 100 U/mL Pen/Strep, and 10 ng/mL TPO. After 48 hours, cells extending at least one proplatelet protrusion were counted and imaged using a phase contrast inverted microscope at 200X total magnification attached to an 18 mega pixel digital camera (OMAX, Kent, WA). Three wells were examined per condition and at least 100 cells quantitated per well.

3.2.12 Bone marrow chimeras

Four days prior to irradiation, mice began treatment *ad libitum per os* with Sulfamethoxazole and Trimethoprim (Aurobindo Pharma, Hyderabad, India) to prevent infections. Mice were then irradiated with two doses of 550 rad each spread 2 hours apart. Following irradiation, donors were retro-orbitally injected with 2×10^7 unfractionated bone marrow cells in sterile DMEM isolated from recipients as outlined above. After reconstitution of bone marrow was complete, platelet counts were determined as described, mice were euthanized and their spleens were harvested and weighed for analysis.

3.2.13 Mouse lung immunofluorescence

Mice were injected with DyLight488-labelled anti-mouse GPIbβ (Emfret Analytics, Eibelstadt, Germany) 24 hours prior to experiment. Three minutes prior to euthanasia, mice were either injected with either saline as a vehicle control or 18 µg/mL collagen and 150 µg/mL epinephrine to induce systemic thrombosis as a positive control. Following euthanasia, lung was harvested, fixed for 24 hours in 4% neutral buffered formalin, cryoprotected with sucrose, and then frozen in optimal cutting temperature (OCT) compound (Sakura Finetek, Torrance, CA). After 5 µm sections were cut, samples were mounted with VECTASHIELD Antifade Mounting Medium with

DAPI (Vector Labs, Burlingame, CA). Images were acquired from at least three fields per sample using a Nikon Eclipse TE2000-U at 20X magnification equipped with blue (DAPI) and green (FITC) filters and analyzed with Slidebook6 software.

3.3 Results

3.3.1 RGS18$^{-/-}$ and RGS10$^{-/-}$18$^{-/-}$ mice have fewer platelets but are otherwise normal

To generate RGS10$^{-/-}$18$^{-/-}$ mice *via* CRISPR-Cas9, two single guide RNAs were designed for each gene, each targeting Exon 4 and Intron 4 (Figure 3-1A). Exon 4 encodes part of the RGS domain for both proteins. Complete regional deletion within the *Rgs10* gene results in loss of RGS10 expression (Figure 3-1B left). The same founder possessed a 5 base pair deletion in Exon 4 of *Rgs18*, producing a premature stop codon and loss of RGS18 expression (Figure 3-1B right).

RGS10$^{-/-}$18$^{-/-}$ mice were viable, grossly normal in appearance and gained weight normally compared to age- and sex-matched wild type (WT) controls (Supplemental Figure 3-7A). RGS10$^{-/-}$ 18$^{-/-}$ blood parameters were also normal, except for their platelet counts, which were reduced by ~40% (Figure 3-1C; Supplemental Figure 3-7B). In agreement with previous reports, RGS10$^{-/-}$ and RGS18$^{-/-}$ mice were grossly normal in appearance and did not differ significantly in initial weight gains (Supplemental Figure 3-7A).[63,100,101] Also consistent with our previous work and reports by Delesque-Touchard et al., RGS10$^{-/-}$ mice had normal blood parameters, while RGS18$^{-/-}$ mice had a reduction in platelet counts of ~15% (Figure 3-1C).[63,101,102] Because of the low probability of generating useable genotypes from *Rgs10*$^{+/-}$*Rgs18*$^{+/-}$ parents, breeding was performed with homozygous parents of each individual genotype.

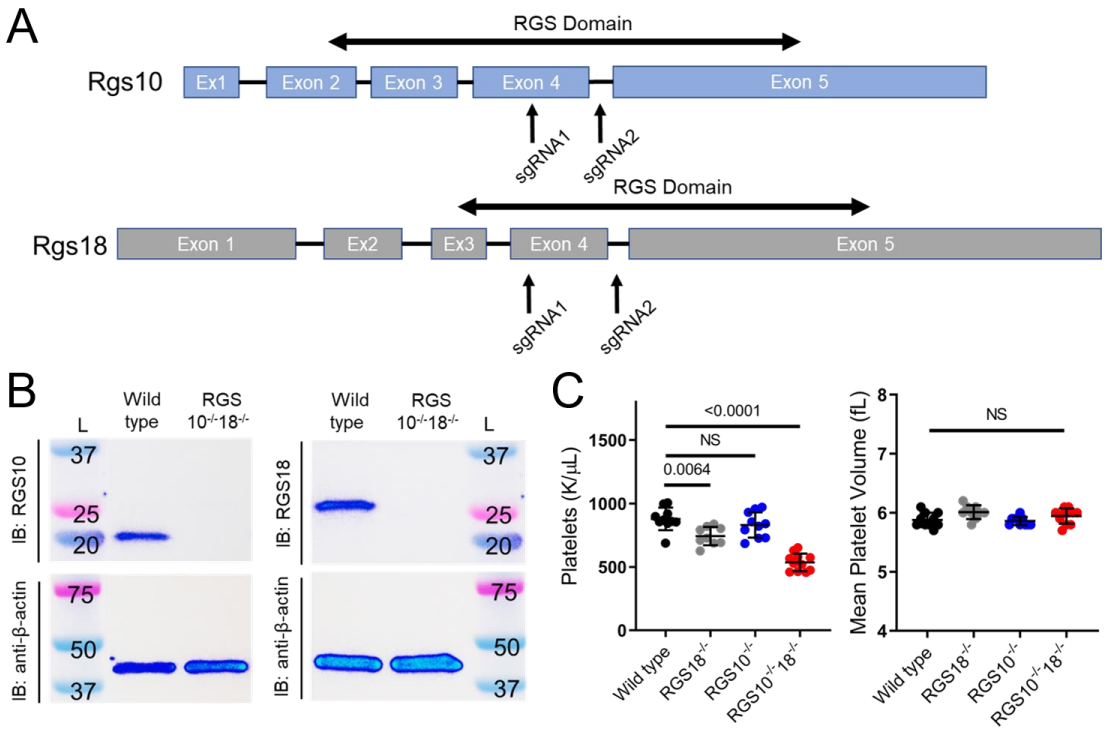

Figure 3-1. Generation and characterization of Rgs deletion mice. (A) Graphical depiction of Rgs10 and Rgs18 genes. Arrows indicate approximate locations targeted by single guide RNAs during CRISPR-Cas9. In both cases, regions within the sequence that encode the RGS domain were targeted. (B) Representative RGS10 and RGS18 immunoblots (top) of platelet lysates from RGS10$^{+/+}$18$^{+/+}$ (denoted Wild type) and RGS10$^{-/-}$18$^{-/-}$ mice with β-actin (bottom) as the loading control. (C) Platelet counts and mean platelet volume of 8-week-old WT, RGS18$^{-/-}$, RGS10$^{-/-}$ and RGS10$^{-/-}$18$^{-/-}$ mice. At least 9 measurements were collected per genotype. NS indicates $P > 0.05$, mean ± SEM.

3.3.2 RGS10$^{-/-}$ and RGS18$^{-/-}$ differentially impact GPCR-dependent agonist responses

Flow cytometry was used to assess agonist-mediated platelet activation via two independent markers: P-selectin, exposed on the platelet surface during α granule exocytosis,[103,104] and activated $\alpha_{IIb}\beta_3$ integrin.[105] While there was no difference between resting or maximal P-selectin exposure amongst genotypes in response to PAR4 agonist peptide (PAR4P, AYPGKF), there was a pronounced leftward shift in the dose/response curve for RGS10$^{-/-}$ and RGS10$^{-/-}$18$^{-/-}$ platelets (EC50 of 78.5 and 73.75 µM, respectively) relative to WT (EC50 of 126 µM), indicating an increase in sensitivity. A smaller but still significant shift was observed for RGS18$^{-/-}$ platelets (EC50 of 99.62 µM; Figure 3-2A; Supplemental Figure 3-8A), suggesting a more limited contribution of RGS18 to PAR4 signaling. A nearly identical pattern was observed using the Jon/A monoclonal antibody, which recognizes the activated conformation of the integrin $\alpha_{IIb}\beta_3$. We observed a similar left-shift for both RGS10$^{-/-}$ and RGS10$^{-/-}$18$^{-/-}$ platelets (EC50 of 89.2 and 83.19 µM, respectively) with a more moderate shift for RGS18$^{-/-}$ platelets (EC50 of 103.6) (Figure 3-2B; Supplemental Figure 3-8B; Supplemental Table 3-1). Compared to the EC50 of wild type controls (129.5 µM), this supports the notion that RGS10 plays a more substantial role regulating PAR4 signaling than RGS18.

In contrast to our results with PAR4 agonist peptide, RGS10$^{-/-}$ and RGS10$^{-/-}$18$^{-/-}$ platelets showed a marked increase in their maximal P-selectin and integrin activation responses to ADP and the TxA_2 mimetic, U46619, that was not seen with RGS18$^{-/-}$ platelets (Figure 3-2C-F; Supplemental Figure 3-8C-F). This further suggests that RGS18 is contributing minimally (if at all) to regulating ADP and TxA_2 receptor signaling with respect to their roles in integrin activation and degranulation.

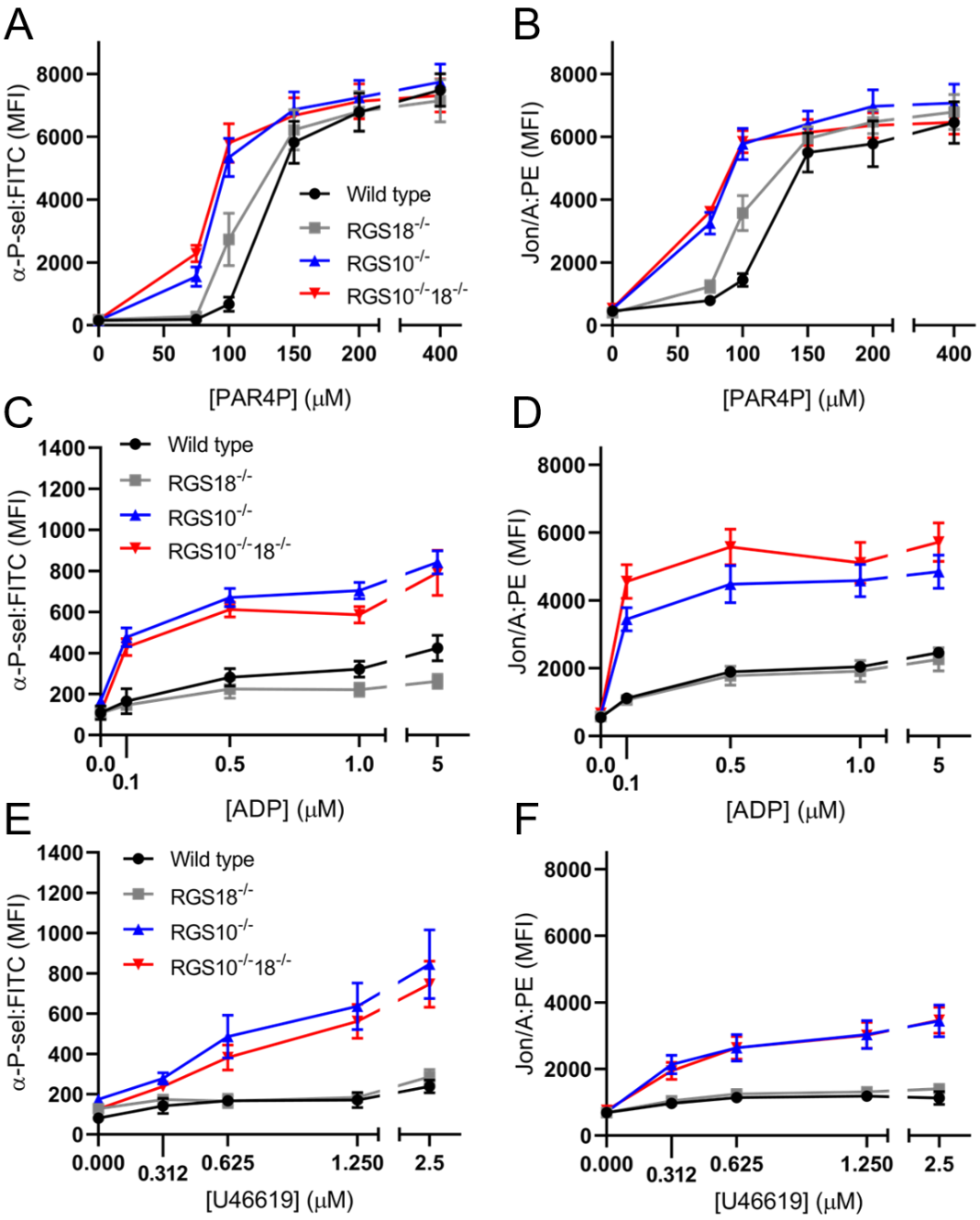

Figure 3-2. RGS10 and RGS18 differentially impact *in vitro* platelet dose-responses. Flow cytometric analysis of (A, C, E) P-selectin expression and (B, D, F) integrin $\alpha_{IIb}\beta_3$ activation of platelets from matched WT, RGS18$^{-/-}$, RGS10$^{-/-}$, and RGS10$^{-/-}$ 18$^{-/-}$ mice. Platelets were stimulated with increasing doses of: (A, B) PAR4 activating peptide (PAR4P, AYPGKF), (C, D) ADP and (E, F) TxA_2 analogue (U46619) and gated by FSC/SSC and CD41 positivity. At least 4 measurements were collected per genotype per condition, mean ± SEM. See Supplemental Figure 2 for statistical comparisons between genotypes.

3.3.3 RGS10$^{-/-}$18$^{-/-}$ results in excessive hemostatic platelet activation and thrombosis

Platelet function *in vivo* was assessed with real time intravital confocal fluorescence microscopy following a laser-inflicted penetrating injury in cremaster muscle arterioles.[78] Because the vessel wall is penetrated and blood escapes, we view this as a model of hemostasis, rather than thrombosis, and have previously shown that results obtained using a laser are identical to those produced with a mechanical puncture. The hemostatic plugs that form in this setting have a characteristic architecture in which a densely-packed core of fully-activated, P-selectin$^{(+)}$ platelets is overlaid by a shell of loosely-packed, P-selectin$^{(-)}$ platelets.[78] We've shown that the core is driven primarily by high local concentrations of thrombin, which leads to fibrin deposition as well as platelet activation, while the shell is less activated and driven mainly by released ADP and TxA_2.[78,106]

Representative endpoint images of hemostatic plugs formed in WT and RGS10$^{-/-}$18$^{-/-}$ mice 3 minutes after injury are shown in Figure 3-3A. Mean platelet accumulation was greater in the RGS10$^{-/-}$18$^{-/-}$ mice than in controls, an increase of 77% (Figure 3-3B, E left; Supplemental Video 1). Similarly, we see a 111% increase in the area of P-selectin$^{(+)}$ platelets (Figure 3-3C, E middle). Further, by subtracting the P-selectin$^{(+)}$ core area from the total platelet area, we can extract the area of the P-selectin$^{(-)}$ shell, which was 69% larger in the RGS10$^{-/-}$18$^{-/-}$ mice (not shown). However, there was no significant difference in the percentage of P-selectin$^{(+)}$ core area between genotypes (18% for WT and 22% for RGS10$^{-/-}$18$^{-/-}$; not shown). Additionally, the kinetics and extent of fibrin accumulation in the RGS10$^{-/-}$18$^{-/-}$ mice was indistinguishable from the controls, suggesting that deleting both RGS proteins does not affect the generation of thrombin (Figure 3-3D, E right). Finally, the dramatic increase in platelet accumulation was accompanied by an increase in both transient and stable occlusion of the arterioles (Figure 3-3F; Supplemental Video 2), an event rarely observed in WT mice in this model. This suggests not only a prominent role for RGS proteins regulating the hemostatic response to injury but also a potential role in limiting thrombosis under pathological settings, such as vessel wall disease.

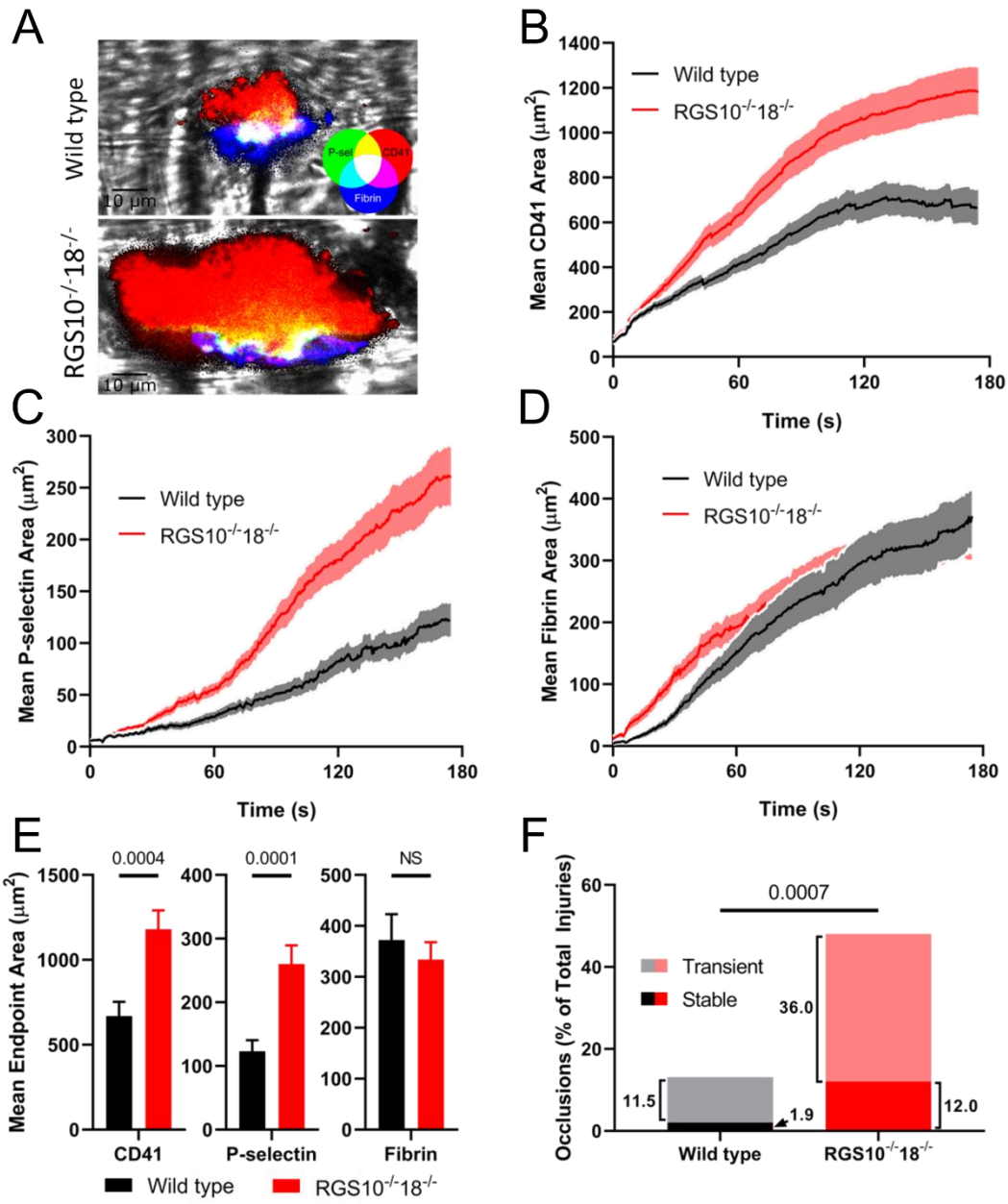

Figure 3-3. RGS10$^{-/-}$18$^{-/-}$ enhances the *in vivo* hemostatic response. Real time confocal intravital microscopy following penetrating laser injuries in cremaster muscle arterioles in WT and RGS10$^{-/-}$18$^{-/-}$ mice. (A) Representative endpoint images of hemostatic plugs. Platelets (CD41) are labeled red, P-selectin (P-sel) is green, and fibrin is blue. Overlay of CD41 and fibrin appears magenta, CD41 and P-selectin appears yellow, fibrin and P-selectin appears cyan, and overlay of all three channels appears white. Mean area of accumulation for each fluorophore was measured over time: (B) CD41 (α_{IIb} integrin), (C) P-selectin, and (D) Fibrin. (E) Mean endpoint area calculations for each individual fluorophore. (F) The fraction of injuries that produced stable or transient occlusions as defined in methods. N = 52 for WT injuries and N = 50 for RGS10$^{-/-}$18$^{-/-}$ injuries. Represented as mean ± SEM.

3.3.4 RGS18$^{-/-}$ reduces platelet counts due to decreased production

Because RGS18$^{-/-}$ and RGS10$^{-/-}$18$^{-/-}$ mice have reduced platelet counts of 15% and 40% of WT controls, respectively, we hypothesized that there may be a defect in platelet production. To assess this, we first quantified megakaryocytes in femurs obtained from RGS10$^{-/-}$, RGS18$^{-/-}$, RGS10$^{-/-}$18$^{-/-}$ and control mice stained with anti-CD41 and examined by light microscopy. Despite the reduction in platelet count in the RGS18$^{-/-}$ and RGS10$^{-/-}$18$^{-/-}$ mice, megakaryocyte counts were normal for all genotypes (Figure 3-4A-B), suggesting that the decrease in platelet count is not primarily due decreased megakaryocyte differentiation.

Next, to assess platelet production, we used a specific GPIbα antibody to deplete platelets in mice from each genotype and tracked the generation of new platelets over 96 hours. During the first 48 hours of this recovery, we saw no significant difference between the knockouts and WT controls. However, by 72 hours onward, we observed a delay in recovery for RGS18$^{-/-}$ and RGS10$^{-/-}$18$^{-/-}$ mice (Figure 3-4C). While the interpretation of such results is complicated by other factors, including concomitant clearance, this could indicate a decreased capacity to produce platelets.

Finally, we performed an *in vitro* analysis of megakaryocytes (Megs) to determine their capacity to differentiate and/or produce proplatelets. These results suggest a trend towards an increase in megakaryocyte progenitors and a decrease in proplatelet potential for RGS18$^{-/-}$ and RGS10$^{-/-}$18$^{-/-}$ Megs, but no difference in the transition from Meg progenitor to Meg or Meg ploidy (Supplemental Figure 3-9). Taken together, this suggests that at least some portion of thrombocytopenia observed in RGS18$^{-/-}$ and RGS10$^{-/-}$18$^{-/-}$ mice may be due to decreased platelet production but not reduced Meg differentiation.

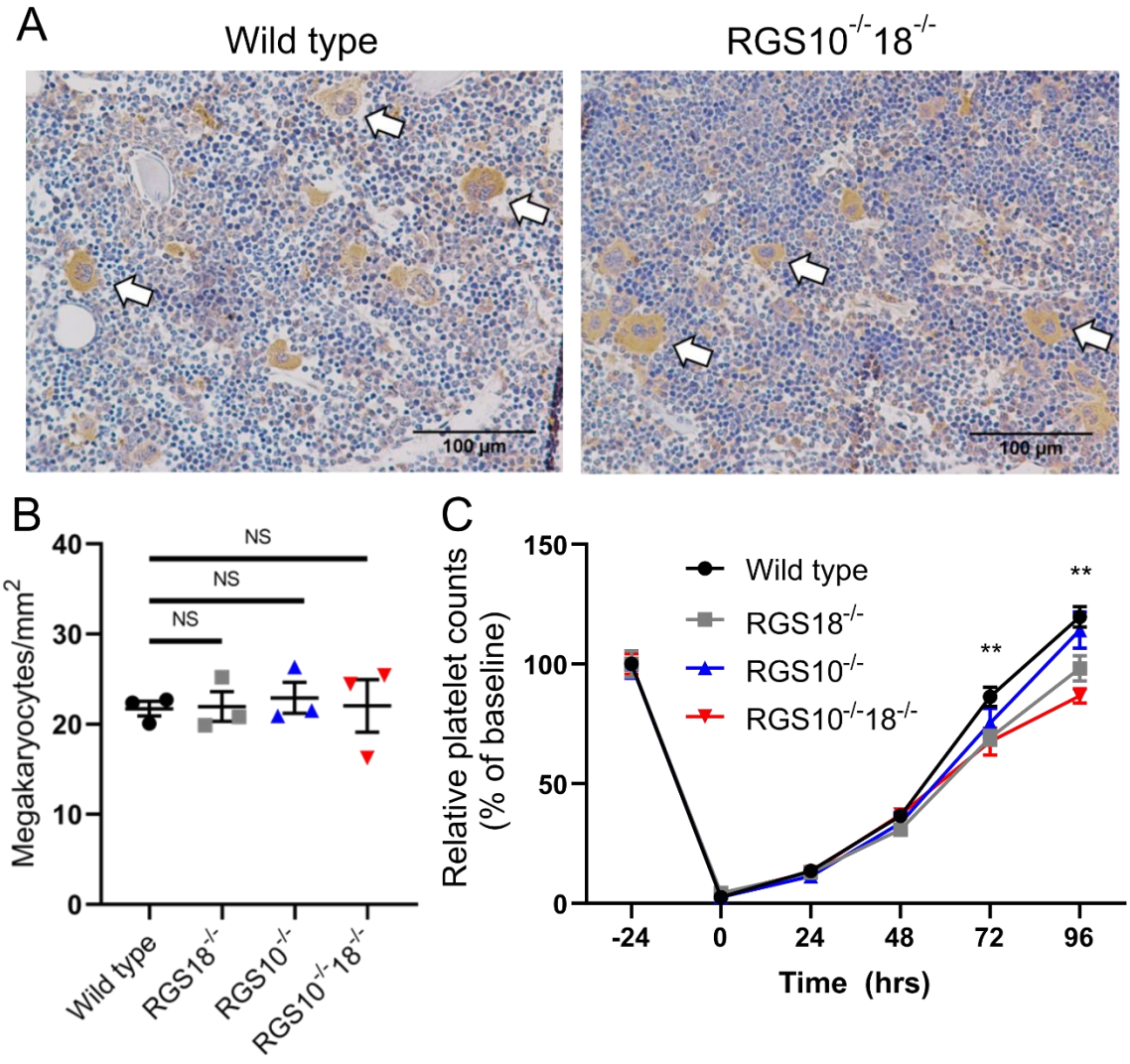

Figure 3-4. RGS18$^{-/-}$ and RGS10$^{-/-}$18$^{-/-}$ results in reduced platelet production. (A) Cross-sectioned femurs harvested from WT, RGS18$^{-/-}$, RGS10$^{-/-}$, and RGS10$^{-/-}$18$^{-/-}$ mice were stained for CD41 (α_{IIb} integrin) and counterstained with hematoxylin. Large, multinucleate CD41$^{(+)}$ cells were counted as megakaryocytes. White arrows point to representative examples. (B) Megakaryocyte counts from five randomly selected fields per mouse. N = 3, mean ± SEM. (C) Platelet depletion with an anti-GPIbα antibody followed by recovery over the course of 96 hours represented as a percentage of the baseline for each genotype. ****** indicates P ≤ 0.05 for WT vs RGS18$^{-/-}$ and RGS10$^{-/-}$18$^{-/-}$. N = 6, represented as mean ± SEM**.**

3.3.5 RGS10$^{-/-}$18$^{-/-}$ reduces platelet survival and increases preactivation in circulation

Although both RGS18$^{-/-}$ and RGS10$^{-/-}$18$^{-/-}$ mice appear to have a reduced platelet production potential, RGS10$^{-/-}$ mice do not. We thus hypothesized that the further decrease in RGS10$^{-/-}$18$^{-/-}$ platelet counts may be due to decreased survival in circulation. To assess platelet survival, mice of each genotype were injected with non-saturating concentrations of a GPIbβ antibody that has no effect on platelet activation.[107] At successive 24-hour intervals, blood was drawn and the percentage of remaining anti-GPIbβ$^{(+)}$ platelets was determined (Figure 3-5A). The results show that RGS10$^{-/-}$18$^{-/-}$ platelets have a significantly reduced survival ($t^{1/2}$ = 46 hours), clearing faster than either the single RGS protein knockouts or controls ($t^{1/2}$ = ~62 hours).

Next, we stained resting platelets from each genotype with thiazole orange (TO), which binds to RNA. Platelet RNA content declines as platelets age in the circulation, which means that TO positivity represents the population of younger platelets.[108] The results show that a significantly higher proportion of RGS10$^{-/-}$18$^{-/-}$ platelets were TO$^{(+)}$, when compared to other genotypes (Figure 3-5B), suggesting that a larger fraction of RGS10$^{-/-}$18$^{-/-}$ platelets are younger than single knockouts or controls.

Considering the evidence of increased clearance, we asked whether the hyperreactivity we observed in the absence of RGS10 and RGS18 translates into increased spontaneous platelet activation in the circulation that may reduce survival. To test this hypothesis, flow cytometry was used to detect the binding to freshly isolated platelets of three antibodies: Jon/A, anti-TLT-1, and anti-P-selectin. As noted earlier, Jon/A detects the activated conformation of $\alpha_{IIb}\beta_3$ and P-selectin expression is a marker for α-granule secretion. Triggering receptor expressed on myeloid cells (TREM)-like transcript-1 (TLT-1) is highly expressed in platelets, at least partially stored in α–granules and is reported to be an even more sensitive marker of platelet activation than P-selectin.[109,110] Our results show that the binding of Jon/A (Figure 3-5C) and anti-P-selectin (Supplemental Figure 3-10A) to resting platelets from the RGS protein knockouts was indistinguishable from controls. There was, however, an increase in TLT-1 expression on the

RGS10$^{-/-}$18$^{-/-}$ platelets that was not observed for single knockouts or WT controls (Figure 3-5D), suggesting that RGS10$^{-/-}$18$^{-/-}$ platelets are already partially activated in the circulation.

To test this conclusion further, we stimulated WT and knockout platelets with epinephrine and measured Jon/A binding and anti-P-selectin expression. Epinephrine activates platelet α_{2A}-adrenergic receptors coupled to the G_i family member, G_z.[111] It has been shown that epinephrine alone cannot cause platelet activation, but it potentiates activation when added with other platelet agonists, particularly those whose receptors couple to G_q.[111,112] The results show that epinephrine causes an increase in $\alpha_{IIb}\beta_3$ activation in RGS10$^{-/-}$ but not RGS18$^{-/-}$ platelets and an even greater increase on RGS10$^{-/-}$18$^{-/-}$ platelets (Figure 3-5E), supporting the conclusion that these platelets are already partially activated. There was also a trend towards an increase in P-selectin expression, but it did not reach statistical significance (Supplemental Figure 3-4B).

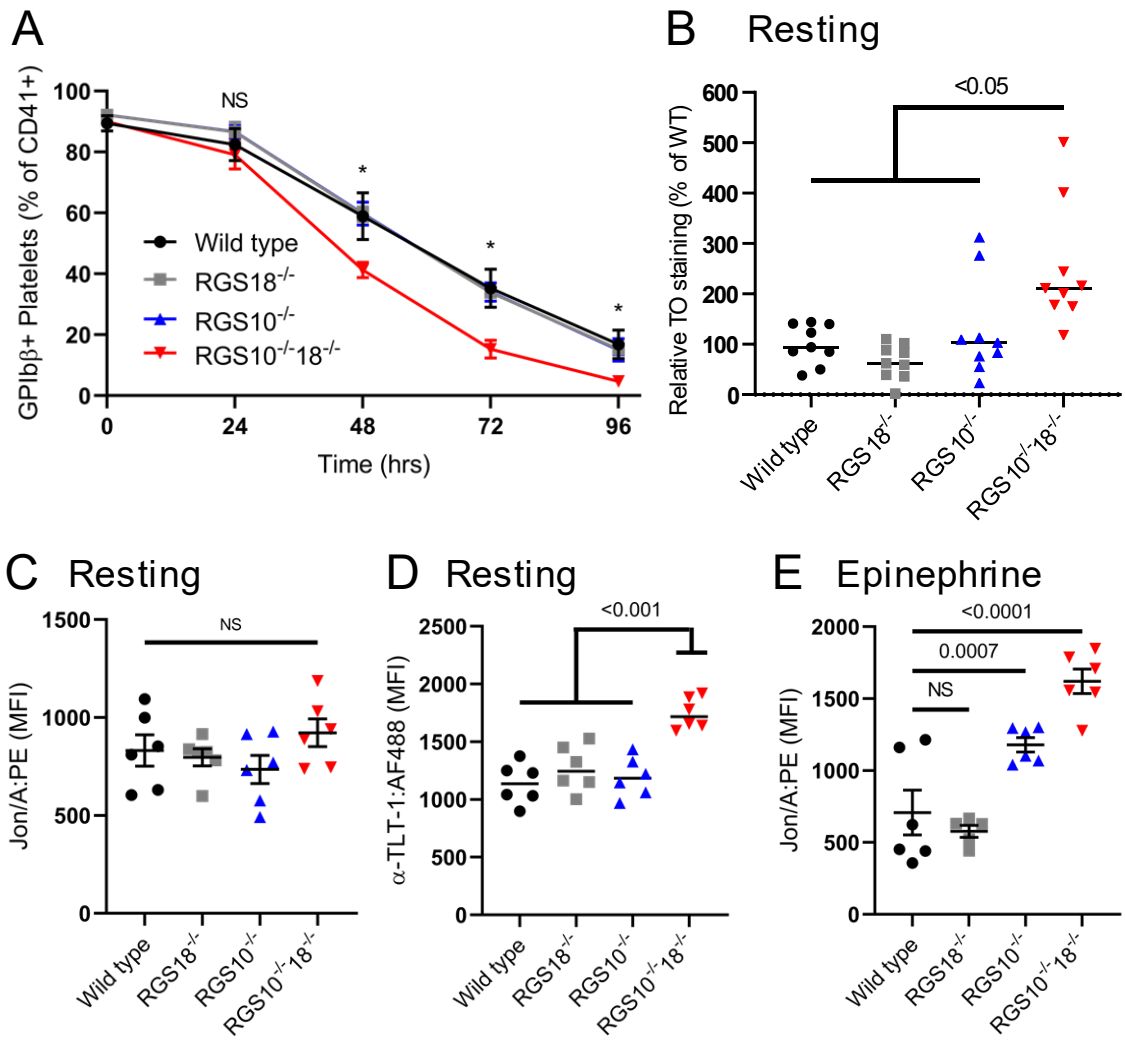

Figure 3-5. RGS10$^{-/-}$18$^{-/-}$ platelets are preactivated with shorter survival. Flow cytometry analysis for WT, RGS18$^{-/-}$, RGS10$^{-/-}$ and RGS10$^{-/-}$18$^{-/-}$ mice to measure: (A) clearance of anti-GPIbβ:DyLight488 *in vivo* labeled platelets over the course of 96 hours. At baseline and every 24 hours thereafter, platelets were identified using anti-CD41 (α_{IIb} integrin) and then analyzed for DyLight488$^{(+)}$ by flow cytometry. ***** indicates P ≤ 0.05 for WT vs RGS10$^{-/-}$18$^{-/-}$. N = 5, mean ± SEM; (B) Relative fraction of platelets that were positive for both anti-CD41 and thiazole orange (TO). N = 9, mean ± SEM; (C) Jon/A binding to resting platelets; (D) anti-TLT-1 binding to resting platelets; and (E) Jon/A binding to 10 μM epinephrine stimulated platelets. N = 6, mean ± SEM.

3.3.6 RGS10$^{-/-}$18$^{-/-}$ platelet preactivation can be reversed by dual antiplatelet therapy

Due to the observed increase in platelet clearance of RGS10$^{-/-}$18$^{-/-}$ platelets, we next explored potential mechanisms, the first being that loss of RGS10 and RGS18 causes premature desialylation of platelets, leading to enhanced clearance by Ashwell-Morell receptors in the liver.[113] However, we found no increase in RCA-I lectin binding to the platelet surface, which normally increases when sialylation decreases (Supplemental Figure 3-10C, D).[114] We next measured Annexin V binding to resting platelets to determine if enhanced phosphatidylserine exposure (indicative of apoptosis) is contributing to increased clearance.[115,116] No increase was observed (Supplemental Figure 3-10E). Third, we sought to determine if splenic sequestration of RGS10$^{-/-}$18$^{-/-}$ platelets might explain their decrease in systemic circulation.[117] However, we found no differences in the spleen to bodyweight ratio for WT -> WT or RGS10$^{-/-}$18$^{-/-}$ -> WT bone marrow chimeras, despite the RGS10$^{-/-}$18$^{-/-}$ chimeras having similarly reduced platelet counts (Supplemental Figure 3-10F, G). Finally, we asked if microvascular thrombosis was the cause of reduced platelet survival,[118] but we could not detect any GPIb$\beta^{(+)}$ platelet aggregates in the lungs of unstimulated RGS10$^{-/-}$18$^{-/-}$ mice via immunofluorescence (Supplemental Figure 3-11).

While the precise mechanism of clearance has remained elusive, we hypothesized that it was indeed dependent upon GPCR-mediated activation. Therefore, we asked whether administration of dual antiplatelet therapy to inhibit ADP responses and TxA_2 production would improve platelet survival and reduce the degree of thrombocytopenia found in RGS10$^{-/-}$18$^{-/-}$ mice. Platelet counts were measured before, during and after giving mice aspirin and the $P2Y_{12}$ antagonist, prasugrel, using a dosing regimen that was sufficient to blunt platelet responses to PAR4P and ADP (Supplemental Figure 3-12). While receiving treatment, the RGS10$^{-/-}$18$^{-/-}$ mice showed an increase in their platelet count to levels indistinguishable from RGS18$^{-/-}$ mice but still significantly less than RGS10$^{-/-}$ or WT controls. After withdrawing treatment, the platelet counts for RGS10$^{-/-}$18$^{-/-}$ mice fell to pre-treatment levels (Figure 3-6A). Furthermore, both basal TLT-1 expression on the platelet surface and staining of TO were normalized to levels comparable to WT controls during treatment (Figure 3-6B, C). Taken together, these data suggest that premature

platelet activation, but not desialylation, apoptosis or spontaneous thrombosis, is a mechanism underlying increased clearance of RGS10$^{-/-}$18$^{-/-}$ platelets *in vivo*.

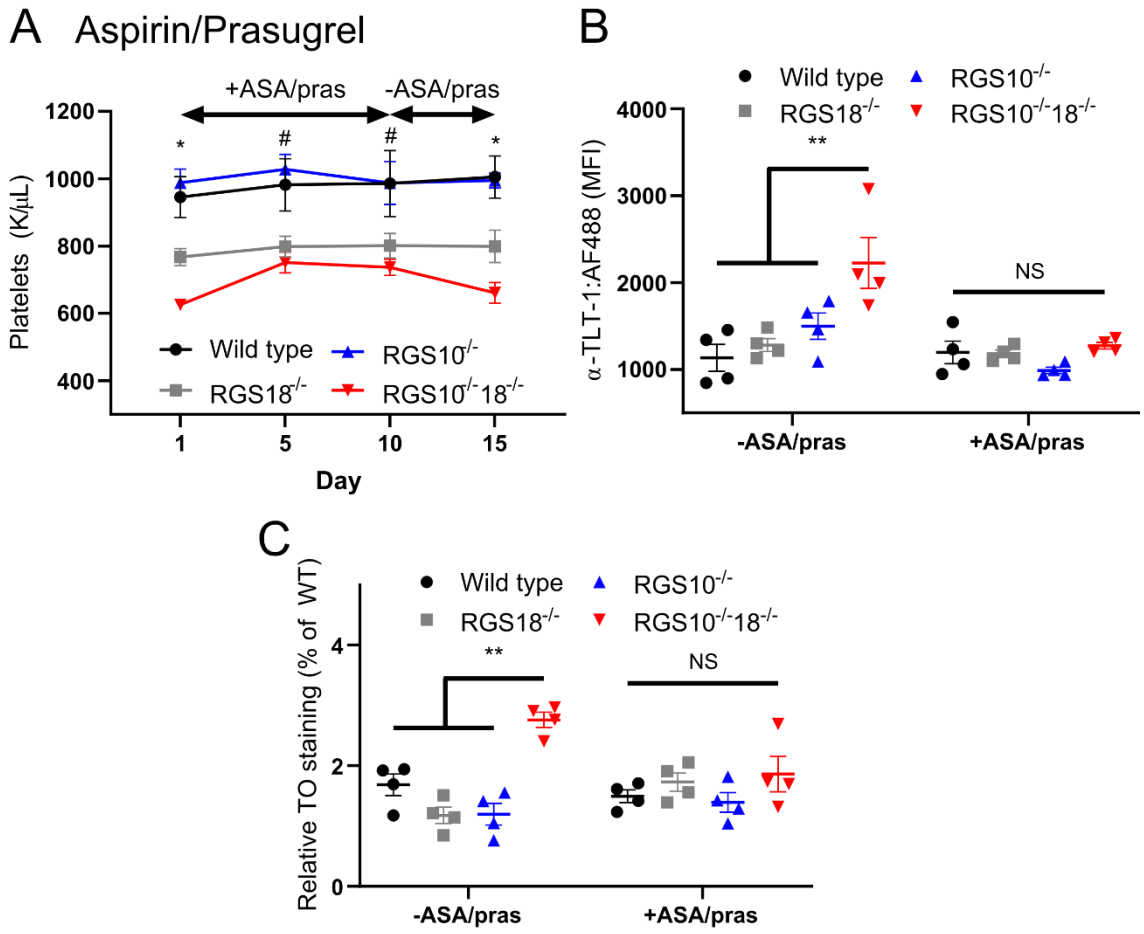

Figure 3-6. Aspirin/prasugrel reverses RGS10$^{-/-}$18$^{-/-}$ platelet preactivation. (A) Platelet counts in WT, RGS18$^{-/-}$, RGS10$^{-/-}$, and RGS10$^{-/-}$18$^{-/-}$ mice treated daily for 10 days with 50 mg/kg aspirin (ASA; cyclooxygenase inhibitor) and 1.875 mg/kg prasugrel (pras; P2Y$_{12}$ inhibitor) by oral gavage, followed by 5 days without treatment. N = 4, mean ± SEM. * indicates P ≤ 0.05 for WT and RGS10$^{-/-}$ vs RGS18$^{-/-}$ vs RGS10$^{-/-}$RGS18$^{-/-}$. # indicates P ≤ 0.05 for WT and RGS10$^{-/-}$ vs RGS18$^{-/-}$ **and** RGS10$^{-/-}$RGS18$^{-/-}$. Data showing the impact of these drugs on platelet activation is included in Supplemental Figure 4. (B, C) Flow cytometric analysis of (B) anti-TLT-1 binding and (C) thiazole orange (TO) staining prior to and 5 days after drug treatment. N = 4, mean ± SEM; NS = not significant.

3.4 Discussion

Platelets possess multiple receptors and signaling pathways through which they can respond to trauma and control bleeding, nearly all of which involve members of the GPCR superfamily. While these activating pathways have been mapped in detail, less is known about the intrinsic regulatory mechanisms that modulate the platelet signaling network to prevent unnecessary or premature platelet activation, which could be especially important in the setting of vessel wall disease. Here we sought to understand the collective impact of RGS proteins on platelet function, focusing for the first time on the consequences of deleting the two most prominently expressed in platelets. Additionally, we sought to extend observations by ourselves[102] and others[63,100,101] on individual knockouts of RGS10 and RGS18 by performing direct comparisons on the same background.

3.4.1 RGS10 and RGS18 differentially impact platelet GPCR signaling networks

Our results with single agonist measurements of platelet activation *in vitro* suggest that RGS10 has more pronounced role in regulating thrombin receptor signaling (via G_q/G_{13}-coupled PAR4) than RGS18. However, dual deletion of both RGS10 and RGS18 has a response nearly identical to RGS10 deletion alone, indicating that the effects of these two RGS proteins are not simply additive. Furthermore, responses to ADP (via G_q-coupled $P2Y_1$ and/or G_{i2}-coupled $P2Y_{12}$) and TxA_2 (via G_q/G_{13}-coupled TP) are similar between RGS10 deletion and dual deletion of both RGS10 and RGS18, while RGS18 deletion appears to a have a negligible impact. Since canonical RGS proteins, like RGS10 and RGS18, only have reported affinity for G_q and G_i α subunits,[31] we can reasonably assume that the observed differences are not due to RGS interactions with G_{13}. Considering this information, simple differences in affinity for G_q and/or $G_i\alpha$ subunits also fail to adequately explain the differential responses in our results, since RGS18 has a measurable impact on PAR4 signaling but not TP signaling (both G_q-coupled).

One potential model that might explain these results is that RGS18 has little to no GAP activity below a certain threshold of platelet activation (perhaps via post-translational modifications

such as phosphorylation, inhibition by scaffold proteins like spinophilin or both). This would explain why RGS18 deletion has a negligible impact on weaker platelet activation stimuli like ADP and TxA_2 but a moderate effect on stronger PAR4 signaling.

3.4.2 RGS10 and RGS18 restrain hemostatic platelet activation to prevent thrombosis

In prior studies, we have shown that penetrating injuries in the cremaster muscle microcirculation of mice bearing an RGS-insensitive G184S substitution in $G_{i2}\alpha$ causes increased platelet accumulation within the growing hemostatic mass.[119] Similar injuries in $RGS10^{-/-}$ mice also result in increased platelet accumulation as well as an increase in platelet activation.[102] Here we found that, when compared to controls, deleting both RGS10 and RGS18 has a more exaggerated effect than either $RGS10^{-/-}$ or $G_{i2}\alpha^{G184S/+}$. Platelet accumulation and activation in response to analogous injuries in $RGS10^{-/-}18^{-/-}$ mice occurred to a greater overall extent, so much so that there was an increased frequency of transient or stable occlusion at the site of injury. In contrast, there was no increase in fibrin deposition, from which we infer that there was no increase in thrombin generation, but rather an increase in thrombin receptor sensitivity. Taken together with the *in vitro* platelet function studies, this suggests that RGS proteins normally restrict platelet activation to prevent a response that exceeds that which is required to stem bleeding. Furthermore, although not directly tested, our results suggest that RGS proteins may have the beneficial effect of reducing the risk of thrombosis in the setting of vascular disease.

However, it is not yet clear why the results observed *in vivo* appear to be additive (and even possibly synergistic) while they do not appear this way *in vitro*. One obvious difference in our injury model is that platelets in a growing hemostatic plug experience a much more complex milieu of various agonists than can be replicated by single agonist experiments. As previously mentioned, RGS18 may not be activated until higher thresholds of platelet activation are achieved. Therefore, it is possible that RGS18 is normally activated under *in vivo* hemostatic conditions while RGS10 is constitutively active, which would explain the dramatic increase in platelet accumulation and activation and the increased incidence of thrombosis that we see in our injury model for $RGS10^{-/-}$

$18^{-/-}$ mice. Despite the gap in our mechanistic understanding of their individual roles, this nonetheless suggests that RGS10 and RGS18 are playing an even more prominent role in a hemostatic setting than we could realistically assess *in vitro*.

3.4.3 RGS18 promotes platelet production to maintain circulating platelet counts

RGS$18^{-/-}$ mice have a 15% reduction in platelet counts, which is consistent with what has been previously reported.[101] However, our data suggest that this may be explained by reduced platelet production and not reduced survival due to premature platelet activation. While numbers of Megs in the bone marrow, the capacity for Meg progenitors to differentiate to mature Megs, and Meg ploidy were all normal for RGS$18^{-/-}$ and RGS$10^{-/-}18^{-/-}$ mice, we observed a significant delay in platelet recovery after depletion and a trend towards a decrease in proplatelet formation from Megs *in vitro*. Furthermore, only RGS$10^{-/-}18^{-/-}$ platelets, and not RGS$18^{-/-}$ platelets, appear to have a reduced lifespan.

The role that GPCR signaling plays in thrombopoiesis remains poorly understood but there are a few examples that highlight its importance. Sphingosine 1-phosphate (S1P) is a bioactive sphingolipid that acts through sphingosine 1-phosphate GPCRs (S1pr) and is found at high concentrations in circulating blood.[120] Zhang *et al* have shown that G_i-coupled S1pr1 is expressed on megakaryocytes and plays a prominent role in thrombopoiesis, without impacting megakaryocyte differentiation or localization.[121] Similarly, the G_i-coupled ADP receptor $P2Y_{13}$, expressed in megakaryocytes but not in platelets, was shown to promote proplatelet formation.[122,123] Therefore, it seems likely that, generally speaking, G_i signaling in megakaryocytes promotes platelet production. However, the predicted effect of RGS18 GAP activity towards $G_i\alpha$ subunits would be to decrease platelet production (and therefore increase production when RGS18 is absent). It is therefore unlikely that RGS18 is significantly impacting these pathways via its canonical GAP function. The role that G_q signaling plays in thrombopoiesis remains largely unexplored. However, transforming growth factor β (TGFβ) reportedly upregulates calcium signaling in megakaryocytes and has been reported to inhibit proplatelet formation.[124,125] It is thus

possible that G_q signaling in megakaryocytes, which results in intracellular calcium flux as well, inhibits proplatelet formation, and that this effect is exaggerated in the absence of RGS18.

3.4.4 RGS10 and RGS18 cooperate to prevent preactivation and prolong platelet survival

In C57BL/6 mice, platelets normally circulate approximately 5 days before being cleared.[126] Here we found that, compared to matched controls, RGS10$^{-/-}$18$^{-/-}$ mice had approximately 40% fewer circulating platelets and those platelets had reduced survival in circulation as assessed by antibody labelling and clearance. Importantly, clearance studies using antibodies generally correlate well with those that rely upon covalent modification using NHS-biotin. In contrast, platelets from mice lacking either RGS10 or RGS18 exhibited no reduction in survival.

Several observations suggest that the decrease in survival of RGS10$^{-/-}$18$^{-/-}$ platelets is due to increased clearance via premature activation. First, the relative percentage of thiazole orange (TO) positive platelets was greater in RGS10$^{-/-}$18$^{-/-}$ mice than in WT controls. Since TO preferentially stains younger platelets,[108] increased turnover of older platelets would increase the relative proportion of newly-formed platelets. Second, RGS10$^{-/-}$18$^{-/-}$ platelets, and to a lesser extent RGS10$^{-/-}$ platelets, responded to epinephrine with an increase in Jon/A binding. Since epinephrine does not normally elicit a platelet activation response unless co-stimulated with a second agonist,[111,112] this suggests that RGS10$^{-/-}$18$^{-/-}$ platelets are already weakly activated. However, it is also possible that RGS10 deletion directly enhances G_z responses to epinephrine,[127] since we see no evidence of platelet preactivation in RGS10$^{-/-}$ mice. Third, resting platelets from RGS10$^{-/-}$18$^{-/-}$ mice have increased surface expression of TLT-1, which is thought to be a more sensitive marker for platelet activation than Jon/A or anti-P-selectin antibody binding,[109] again suggesting that RGS10$^{-/-}$18$^{-/-}$ platelets are partially activated. Finally, we found that treating RGS10$^{-/-}$18$^{-/-}$ mice with aspirin and prasugrel temporarily restored their platelet counts to levels comparable to RGS18$^{-/-}$, but not to WT or RGS10$^{-/-}$. Since dual therapy with aspirin and a $P2Y_{12}$ antagonist is standard of care for patients at risk for coronary and cerebral artery thrombosis, it raises questions about whether variability in RGS protein levels or availability could lead to variability in the response to these treatments.

Furthermore, we found no evidence for increased apoptosis, desialylation, spontaneous thrombosis or splenic sequestration of circulating RGS10$^{-/-}$18$^{-/-}$ platelets, suggesting an undetermined alternative mechanism of platelet clearance. Combined with the results of the *in vivo* hemostatic injury studies, these results suggest that RGS proteins normally help platelets avoid inappropriate activation and have a previously unappreciated role in maintaining platelet survival in the circulation.

While not previously recognized for RGS proteins, the phenomenon of shortened platelet survival is not unique to *Rgs10/18* dual deletion. Other examples that result in platelet hyperactivity and shortened platelet survival include deletion of the catalytic subunit for protein kinase A, thus ablating its ability to phosphorylate substrates,[128] and loss of RASA3 function , which leads to increased integrin activation due to an increase in the amount of activated RAP1B.[129] This supports the notion that platelets are basally stimulated in the circulation and that endogenous regulators of platelet activation extend platelet survival by protecting against unnecessary activation and premature clearance.

3.5 Supplemental Material

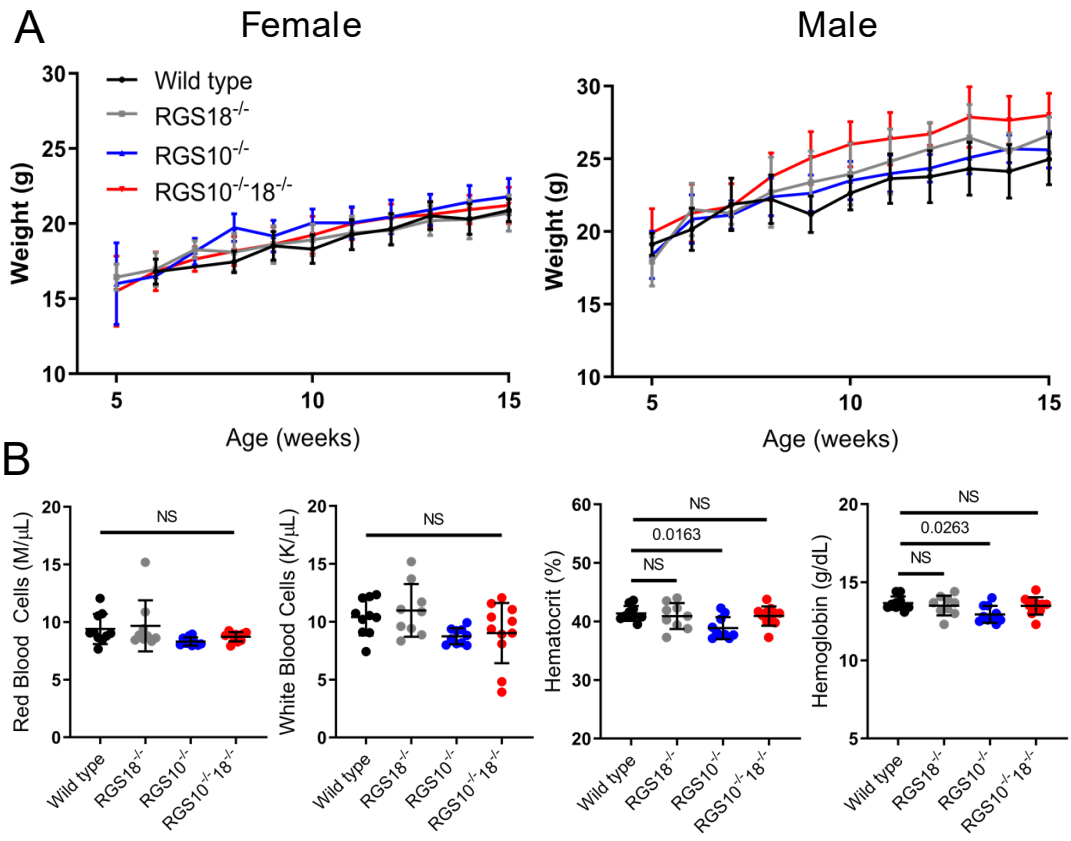

Figure S3-7. Characterization of mice. (A) Initial weight gains of female (left) and male (right) WT, RGS18$^{-/-}$, RGS10$^{-/-}$, and RGS10$^{-/-}$18$^{-/-}$ mice. At least 4 measurements were collected per genotype per day, mean ± SEM. (B) Blood counts, hematocrit and hemoglobin of 8-week-old WT, RGS18$^{-/-}$, RGS10$^{-/-}$, and RGS10$^{-/-}$18$^{-/-}$ mice. At least 9 measurements were collected per genotype. NS indicates P > 0.05, mean ± SEM.

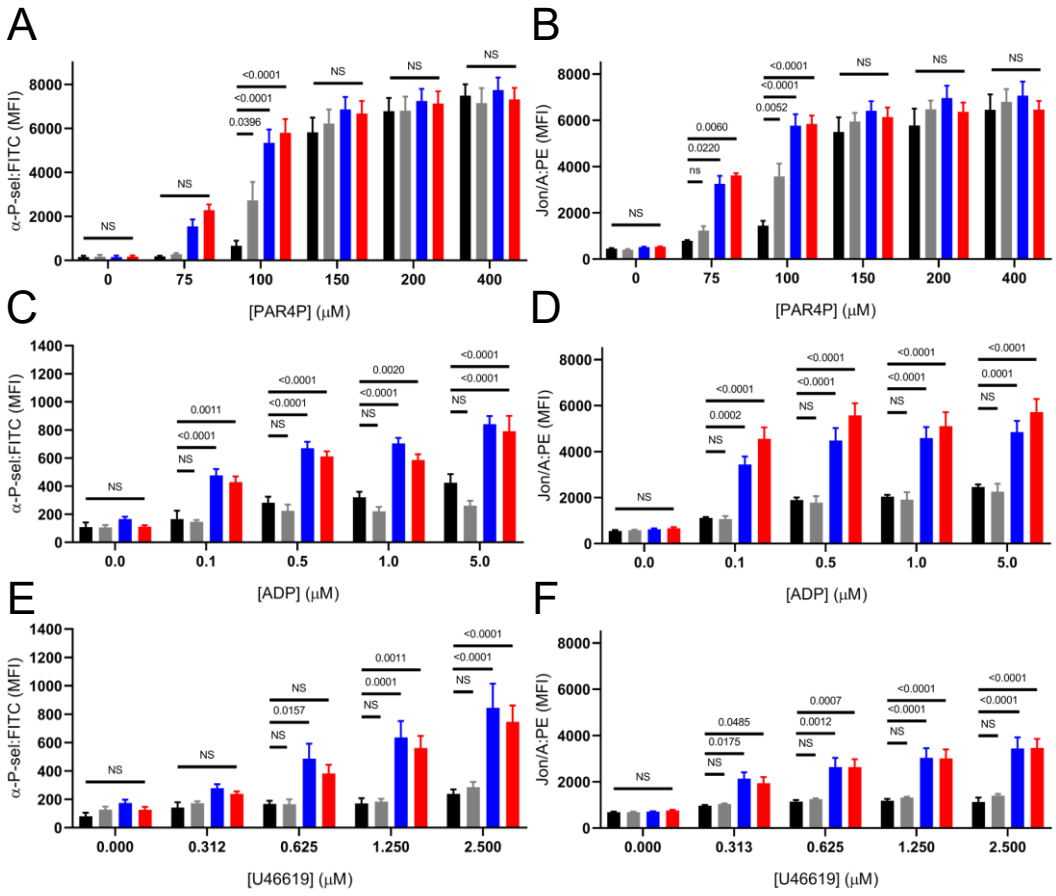

Figure S3-8. Pairwise comparisons for *in vitro* platelet activation. Statistical comparisons to WT controls for flow cytometric analysis of (A, C, E) P-selectin expression and (B, D, F) integrin $\alpha_{IIb}\beta_3$ activation of platelets from matched WT, RGS18$^{-/-}$, RGS10$^{-/-}$, and RGS10$^{-/-}$18$^{-/-}$ mice. Platelets were stimulated with increasing doses of: (A, B) PAR4 activating peptide (PAR4P, AYPGKF), (C, D) ADP and (E, F) TxA_2 analogue (U46619) and gated by FSC/SSC and CD41 positivity. At least 4 measurements were collected per genotype per condition. NS indicates $P > 0.05$, mean ± SEM.

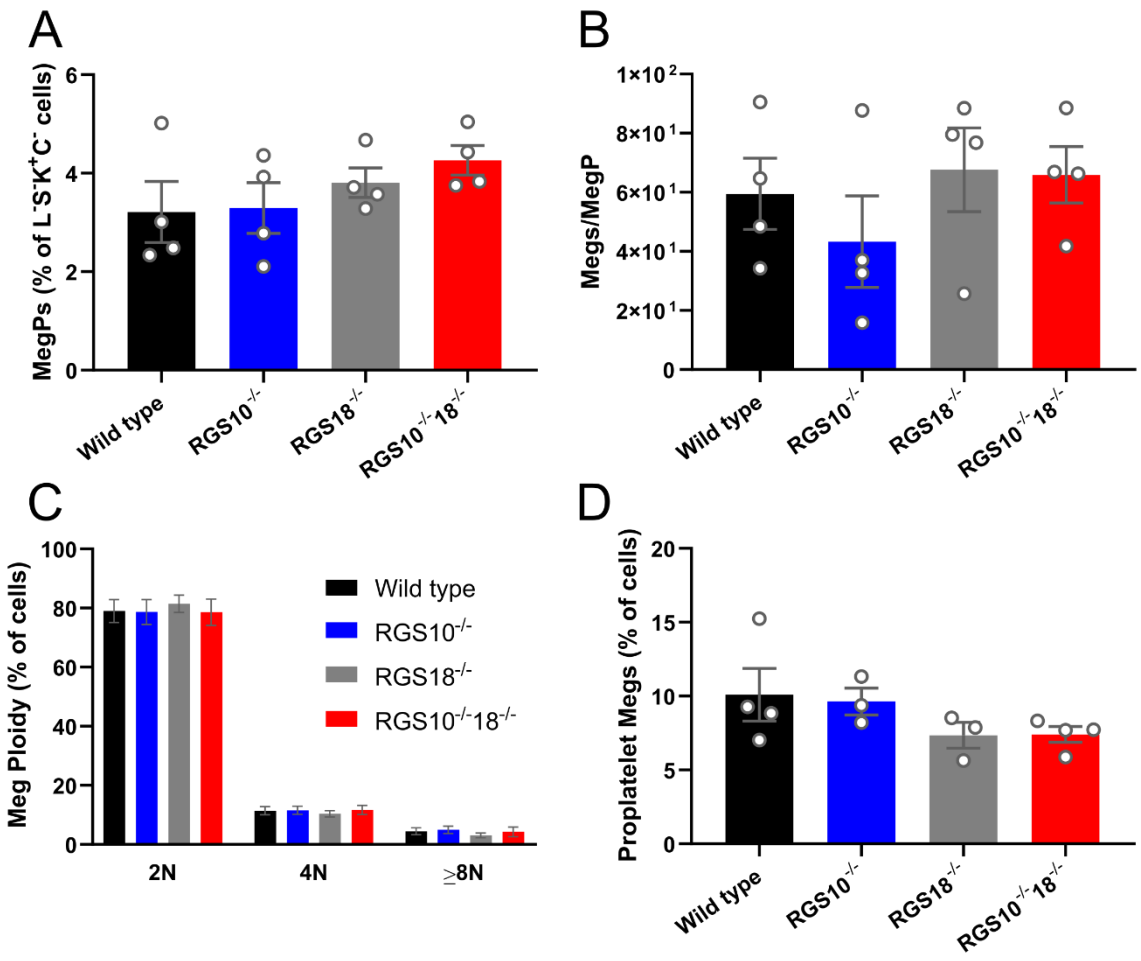

Figure S3-9. *In vitro* analysis of megakaryocytes. (A) Percentage of megakaryocyte progenitors (MegPs) in the lineage cocktail$^{(-)}$Sca-1$^{(-)}$c-Kit$^{(+)}$, CD16/32$^{(-)}$ ($L^-S^-K^+C^-$) subpopulation of bone marrow cells. MegPs were defined as CD150$^{(+)}$CD41$^{(+)}$ cells within the aforementioned subpopulation. (B) Number of megakaryocytes (Megs) per unit input of MegP after culturing for 5 days in the presence of thrombopoietin (TPO). Megs were defined as CD42d$^{(+)}$ and CD41$^{(+)}$ cells. (C) Percentage of TPO-cultured CD42d$^{(+)}$CD41$^{(+)}$ Megs that are diploid (2N), tetraploid (4N) or greater than or equal to octoploid (≥8N) as assessed via DNA dye. (D) Percentage of proplatelet-forming cells after BSA-gradient enrichment and culture on fibronectin-coated plates. Cells were defined as proplatelet-forming if they possessed visible membrane extensions or protrusions. N = 4. All results shown as mean ± SEM.

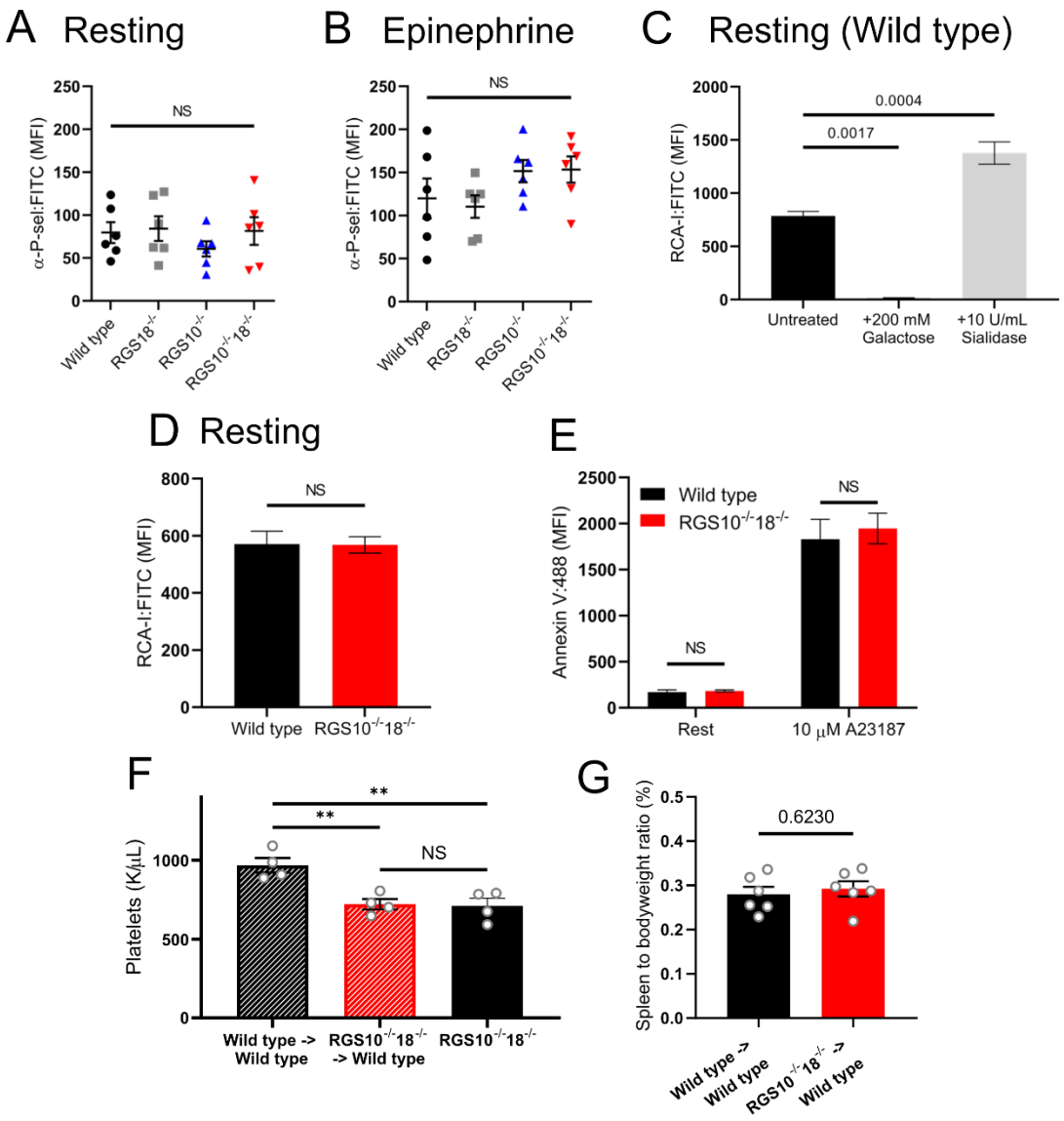

Figure S3-10. Exploring mechanisms of platelet clearance. Flow cytometric analysis of: (A, B) P-selectin on (A) resting or (B) epinephrine-stimulated platelets from WT, RGS18$^{-/-}$, RGS10$^{-/-}$, and RGS10$^{-/-}$18$^{-/-}$ mice; (C) RCA-I:FITC binding to untreated, galactose-blocked, or sialidase-treated WT platelets (N = 3); (D) RCA-I:FITC binding to WT and RGS10$^{-/-}$18$^{-/-}$ platelets (N = 6); and (E) Annexin-V:488 binding to resting or A23187 (calcium ionophore) treated WT and RGS10$^{-/-}$18$^{-/-}$ platelets (N = 3). (F) Platelet counts of lethally irradiated WT mice reconstituted with WT (WT -> WT) or RGS10$^{-/-}$18$^{-/-}$ (RGS10$^{-/-}$18$^{-/-}$ -> WT) bone marrow as compared to global RGS10$^{-/-}$18$^{-/-}$ mice (N = 4). (G) Spleen weight (in grams) to bodyweight ratio of chimeric WT and RGS10$^{-/-}$18$^{-/-}$ mice (N = 6). All results shown as mean ± SEM. NS = not significant. ** $p \leq 0.01$.

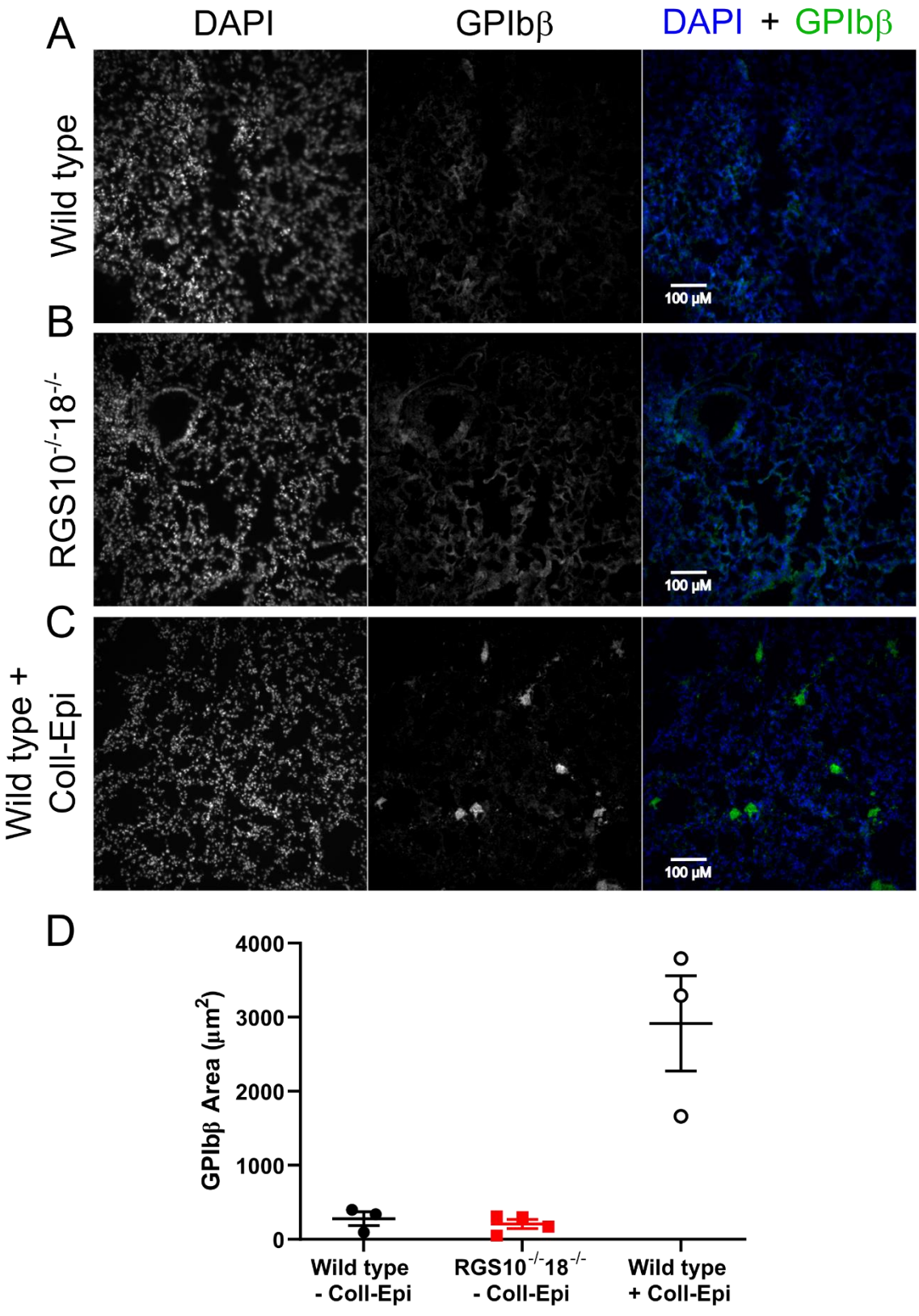
A
DAPI
GPIbβ
DAPI + GPIbβ
Wild type
100 μM
B
RGS10-/-18-/-
100 μM
C
Wild type + Coll-Epi
100 μM
D
GPIbβ Area (μm2)
4000
3000
2000
1000
0
Wild type - Coll-Epi
RGS10-/-18-/- - Coll-Epi
Wild type + Coll-Epi

Figure S3-11. Immunofluorescent analysis of pulmonary thrombosis. Mice were injected with DyLight488-labelled anti-GPIbβ antibody 24 hours prior to harvesting lung, fixation, sectioning and immunofluorescent staining for DAPI. Three minutes prior to euthanizing, mice were either injected with (A, B) vehicle control (saline) or (C) 18 µg/mL collagen and 150 µg/mL epinephrine to induce systemic thrombosis as a positive control. Images were acquired from at least three fields per sample using a Nikon Eclipse TE2000-U equipped with a blue (DAPI) and green (FITC) filters and analyzed with Slidebook6 software. (D) Quantification of total GPIbβ area for each condition.

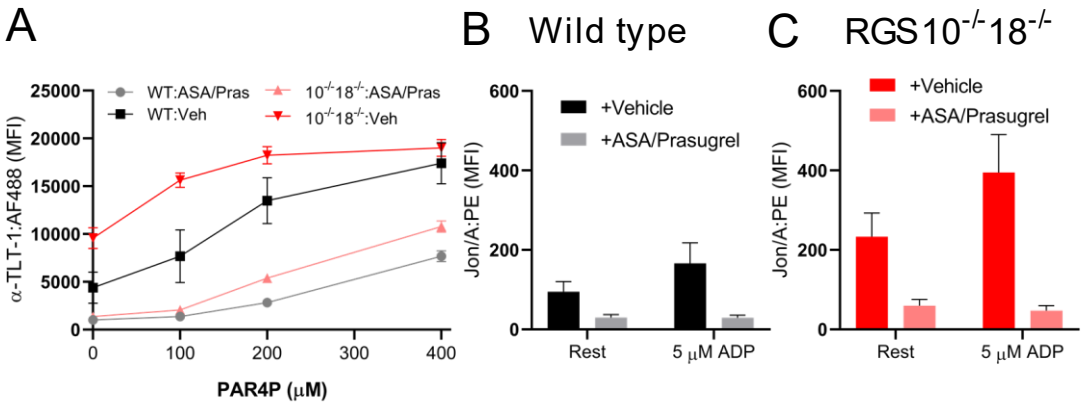

Figure S3-12. *Ex vivo* effects of aspirin and prasugrel administered *in vivo*. Flow cytometric analysis of from WT and RGS10$^{-/-}$18$^{-/-}$ platelets to measure: (A) TLT-1 exposure on the surface in response to increasing doses of PAR4P; (B, C) Jon/A binding in response to ADP. All the mice were given either aspirin plus prasugrel or vehicle (0.5% methylcellulose) daily by oral gavage for a total of 5 days prior to assessment. † indicates P ≤ 0.05 and * P ≤ 0.01. N = 4, mean ± SEM.

Table S3-1. Jon/A and P-selectin responses to PAR4 activating peptide. A weighted four parameter logistic regression was used to estimate the effective concentration of agonist that yields 50% of the maximal signal (EC50), the standard error of each measurement (SE), and the percent difference relative to the wild type controls (% Diff).

	Jon/A				P-selectin			
	Wild type	RGS18$^{-/-}$	RGS10$^{-/-}$	RGS10$^{-/-}$18$^{-/-}$	Wild type	RGS18$^{-/-}$	RGS10$^{-/-}$	RGS10$^{-/-}$18$^{-/-}$
EC50	129.5	103.6	89.2	83.19	126	99.62	78.5	73.75
SE (±)	11.96	4.435	7.013	4.405	7.228	4.001	2.794	2.024
% Diff	-	-20%	-31%	-36%	-	-21%	-38%	-41%

CHAPTER 4: RGS-Insensitive $G_q\alpha$ Disrupts Signaling in Platelets

4.1 Introduction

The most common method employed thus far to study individual effects of RGS proteins in various cell systems involve genetic deletion, either globally or cell specific. However, since most cells express several canonical RGS proteins (with described GAP activity towards $G_q\alpha$ and/or $G_i\alpha$ subunits),[31] delineating the net effects of *all* RGS proteins in a particular system would, more often than not, prove unreasonably cumbersome. One discovery that has helped circumvent this issue are RGS insensitivity mutations in α subunits. Because these mutations lie at the RGS interface, they impair interactions with all RGS proteins and thus inhibit RGS-mediated GAP activity.[65]

As outlined in 1.3, one such RGS insensitive mutation was a G184S substitution in the G_{i2} α subunit.[66] Using this model to probe the effects in platelets, our lab demonstrated hyperactivity downstream of G_{i2}-specific platelet activation pathways,[67] highlighting the importance of RGS proteins with respect to attenuating platelet activation. In an *in vivo* hemostatic model, penetrating injuries in the cremaster arterioles of $G_{i2}\alpha^{G184S/+}$ mice resulted in greater platelet accumulation at both the peak and the endpoints when compared to respective controls. In addition, aggregometry demonstrated enhanced aggregation of $G_{i2}\alpha^{G184S/+}$ platelets in response to GPCR-stimulating agonists ADP, PAR4 activating peptide (AYPGKF), and TxA_2 mimetic (U46619) as well as non-GPCR GPVI-stimulating agonists collagen and convulxin. However, the effects on GPVI agonists were no longer significant when secondary signaling via released ADP (and its effects on G_{i2}-coupled $P2Y_{12}$ signaling) were inhibited with the $P2Y_{12}$ antagonist, cangrelor. This serves to highlight not only the critical role that RGS regulation of ADP-mediated G_{i2} signaling plays in primary platelet activation, but also its importance in limiting secondary signaling that further enhances platelet activation. Finally, experiments probing intracellular signaling downstream of G_{i2} activation, including ADP-mediated cAMP depression and Akt phosphorylation, demonstrated enhanced responses for $G_{i2}\alpha^{G184S/+}$ platelets, while intracellular calcium mobilization (a G_q-driven process) was not significantly different, supporting the notion that the observed effects *in vivo* and

ex vivo were specific to G_{i2} signaling. Taken as a whole, these studies suggest that RGS/G_{i2} interactions are indeed important for regulating the hemostatic response via attenuation of platelet activation. Furthermore, these results likely underestimate the true impact, as only heterozygous mice were used, due to the poor survival of homozygous G184S mice.

The analogous mammalian RGS-insensitive glycine to serine substitution for $G_q\alpha$ (G188S) was first described by DiBello *et al*.[68] While the initial mutation was discovered in the homologous yeast gene via a large scale screen, the substitution was also made in human $G_q\alpha$. Furthermore, they demonstrated impaired RGS7-mediated regulation of 5-HT_{2C} receptor signaling in a co-transfected recombinant Chinese hamster ovary (CHO) cell model, without disrupting G_q-mediated calcium mobilization itself. Lastly, they modelled the effects of the analogous substitution in $G_{i1}\alpha$ (G183S) and its interactions with RGS4. Interestingly, their analysis suggests that this mutation creates unfavorable electrostatic and steric interactions for $G\alpha$:RGS but not $G\alpha$:$G\beta\gamma$.

To explore the impact of RGS-mediated regulation of G_q in platelet activation and hemostasis, our lab used CRISPR-Cas9 and homology directed repair to create the G188S substitution in mice. Unexpectedly, our phenotypic and biochemical analyses of this model suggest that the G188S mutation does indeed disrupt other downstream effectors, like PLCβ, as well as RGS proteins. Additionally, a structural analysis of Gqα interactions demonstrates the considerable overlap between RGS:Gqα and effector:Gqα interfaces, particularly at the position 188, indicating a potential reason for these unexpected findings. Finally, a predictive analysis was performed to determine if *any* substitutions within Gqα would selectively disrupt interactions RGS proteins but not effectors, and we propose several candidates for future studies.

4.2 Materials and Methods

4.2.1 $G_q\alpha^{G188S/G188S}$ mouse model

Generation of mutant mouse line using CRISPR-Cas9 genome-editing system was described in detail by Henao-Mejia et al.[130] Briefly, Cas9 mRNA was generated from pMJ920-Cas9

plasmid using mMESSAGE mMACHINE T7 Ultra Transcription Kit according to the manufacturer's instructions (Life Technologies, AM1345). The quality of the Cas9 mRNA was determined by analyzing Cas9 mRNA pre- and postpolyadenylation in a 2100 Bioanalyzer. sgRNA was designed by following the protocol described in Ran et al.[131] T7 promoter was added to the sgRNA template by PCR amplification. The PCR product was purified and then used as a template for in vitro transcription according to the manufacturer's specifications (MEGAshortscript T7 kit, Life Technologies). The sgRNA was then purified using the MEGAclear kit (Life Technologies). sgRNA's quality was verified on agarose gel. Single-stranded DNA (ssDNA) oligonucleotides that encode the desired G188S mutation was flanked on each side by ~100 bases homologous to the sequence surrounding the sgRNA-mediated double-strand break (DSB). The G188S missense mutation, encoded by a GGG→TCG change, also adds a diagnostic RsaI restriction digestion site. The CCCC, upstream of TCG change, was replaced with ACCA and introduced a silent mutation to prevent re-cutting by Cas9 after editing. Zygotes from C57BL/6 mice were injected with Cas9 mRNA (100 ng/μl), sgRNA (50 ng/μl), and 100 ng/μl donor ssDNA. Embryos were then transferred to pseudo-pregnant C57BL/6 females. After birth, 10-d-old mice were tail-snipped and genomic DNA was extracted for genotyping and sequencing. The two founder mice were each bred to the F1 generation using C57BL/6 mice for further analysis. All mouse protocols and procedures were approved by the Institutional Animal Care and Use Committee of the University of Pennsylvania.

4.2.2 Flow cytometric analysis of platelet activation

Platelet activation was detected as previously described.[80] Briefly, heparinized whole mouse blood was diluted 1:40 in modified Tyrode's buffer (137 mM NaCl, 20 mM HEPES, 5.6 mM glucose, 1 g/liter BSA, 1 mM MgCl2, 2.7 mM KCl, 3.3 mM, NaH2PO4, pH 7.4) and incubated with 1mM aspirin and 1U/ml apyrase for 30 mins at 37 ^{0}C. The blood was incubated with agonists in presence of saturating amounts of fluorophore-conjugated mAbs for 15 min at room temperature and analyzed on a FACSCanto II (BD Biosciences, San Jose, CA). The platelet population was

gated based on FSC/SSC and CD41 positivity. For activation studies with ADP, platelets were incubated with 1mM aspirin alone.

4.2.3 Light transmission aggregometry

Blood was drawn from the inferior vena cava of anesthetized mice (100:10:3 mg/kg of ketamine/xylazine/acepromazine) using a heparinized syringe (150 U/ml, 1:9 dilution with blood). Blood was diluted 1:1 with Tyrode's buffer, and spun at 129 x *g* for 7 min to prepare platelet-rich plasma (PRP). Platelet counts (Beckman-Coulter Z1) were adjusted to $2.5x10^8$/ml. Aggregation was observed in a dual-channel Chrono-log lumi-aggregometer. For experiments that focused on shape change, platelets were preincubated for 1 min with Integrilin (10 µM) prior to addition of the agonist.

4.2.4 Intracellular calcium mobilization

Calcium measurements were performed as described.[102] Briefly, isolated platelets were suspended in Tyrode's buffer without Ca^{2+} and loaded with fura-2/AM (5 µM) in the presence of Pluronic F-127 (0.2 µg/mL) for 20 minutes at 37 °C. The platelets were then washed and resuspended in Tyrode's buffer with no extracellular Ca^{2+}. Changes in fura-2 fluorescence were detected with an SLM/Aminco AB2 spectrophotometer, exciting at 340 and 380 nm, and measuring emission at 510 nm.

4.2.5 Hemostatic vascular injury model

Hemostatic thrombus formation was observed in the cremaster muscle microcirculation of male mice age 8-12 weeks as previously described.[132] Briefly, Alexa Fluor 568-labeled anti-CD41 antibody $F(ab)_2$ fragments and Alexa Fluor 647-labeled anti-P-selectin antibodies were administered via a catheter in the jugular vein. Arterioles 30–50 µm in diameter were studied. Vascular injury was induced using a pulsed nitrogen dye laser fired through the microscope objective. Thrombus formation was observed for 3 min at 1.9 frames/sec and analyzed using SlideBook 6 Software (Intelligent Imaging Innovations, Denver, CO).

4.2.6 Pull-down of Flag-tagged PLCβ

Flag-PLCβ fusion protein was harvested from Flag-PLCβ3 transfected HEK293 cells and then purified using ThermoFisher Scientific Pierce Anti-DYKDDDDK affinity resin kit (Thermo Fisher, Waltham, MA). Mouse platelets were lysed and then incubated with 100 μM GDP as a control or 100 μM GDP + AlF^{4-} (10 mM NaF and 30 μM $AlCl_3$). Lysates were incubated with activated Flag-PLCβ-bound resin beads overnight. After 3 washes with lysis buffer, bound proteins were subjected to SDS-PAGE and blotted with an anti-G_q, anti-G_{i2} or anti-Flag antibody.

4.2.7 Immunoblotting of platelet lysate

Platelets were lysed in NP-40 (50 mM Tris, 150 mM NaCl, 2mM EDTA, 1mM EGTA, 1% NP40, pH 7.4) or Triton X-100 lysis buffer (50 mM Tris-HCl, 100 mM NaCl, 5 mM EDTA, 1% Triton X-100, pH 7.4) in the presence of protease inhibitors. The lysates were boiled in sample buffer before sulfate-polyacrylamide gel electrophoresis (SDS PAGE) analysis. Binding of the primary antibodies was detected using HRP-conjugated secondary antibodies and the ECL-system (Amersham Biosciences). Individual bands were quantified by densitometry and analyzed using ImageJ software (NIH).

4.2.7 Structural and predictive mutation analysis

The interaction interface of G_q and its known in vivo binding partners (GRK2,[133] PLCβ-3,[134] Gβ1,[135] RGS18,[136] RGS2,[137] RGS10,[47] and RGS8[138]) was predicted using the Robetta Computational Interface Alanine Scanning Server[139] and existing structures available from the RCSB Protein Data Bank[140] (www.rcsb.org). An interface residue was defined as having at least one atom within a 4 Å radius from another atom in the binding partner and to be significantly buried upon complex formation[141]. Residues predicted to be critical to binding were identified as those with the greatest calculated change in binding free energy (ΔΔG) upon alanine mutation[141]. Structures were viewed and the interfaces manually mapped using PyMOL (The PyMOL Molecular Graphics System, Version 1.7 Schrödinger, LLC.). Because no structure of RGS18 or RGS10 in

complex with G_q exists, the structures were aligned with the analogous RGS8 protein (in complex with G_q) using PyMOL prior to performing calculations. To predict mutations that were likely to impair RGS interactions but not effector interactions, the aforementioned structures were analyzed using a systematic mutational scanning cutoff matrix (mSCM) method.[142] The average ΔΔG for effector proteins was subtracted from the average ΔΔG for RGS proteins to generate a relative "RGS specificity score". Scores above the arbitrary threshold of 0.4 were selected as candidates for RGS insensitive mutations.

4.3 Results

4.3.1 $G_q\alpha^{G188S/G188S}$ impairs survival and growth but not hematopoiesis

To understand how an RGS-insensitive mutation in G_q mutation affects platelet signaling and its function *in vitro* and *in vivo*, mice bearing the G188S mutation in exon 4 of G_q were generated using the CRISPR-Cas9 genome-editing approach (Figure 4-1A). Mice heterozygous for the mutation (G188S/+) were born in expected Mendelian ratios and developed normally. In contrast, only 7.2% of mice homozygous for the mutation (G188S/G188S) could survive after birth (Supplemental Figure 4-7). Furthermore, $G_q\alpha^{G188S/G188S}$ mice were drastically smaller at birth (Figure 4-1B) and exhibited markedly reduced weight gains (Figure 4-1C) as compared to their wild type (WT) control counterparts. Platelet counts, mean platelet volume and other hematological parameters were normal in $G_q\alpha^{G188S/G188S}$ mice, indicating that the mutation did not affect megakaryopoiesis or thrombopoiesis in these mice (data not shown).

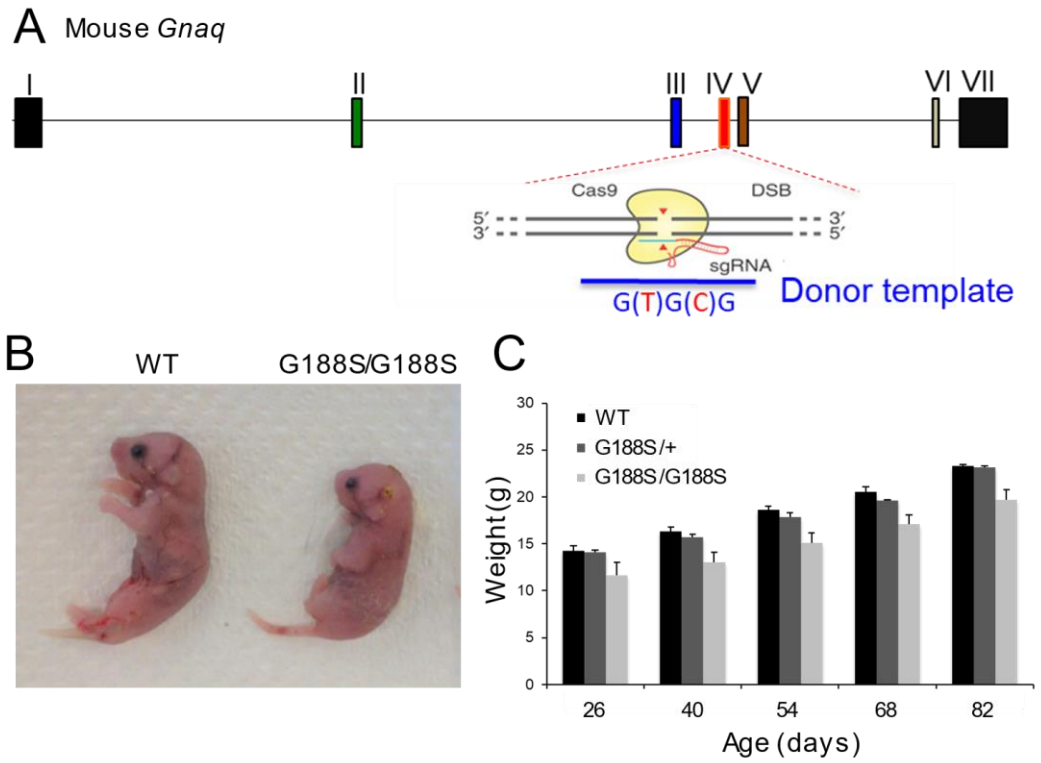

Figure 4-1. Generation and characterization of $G_q\alpha^{G188S/G188S}$ mice. (A) Strategy for introducing G188S substitution by CRISPR-Cas9 via homology-directed repair. (B) Representative images of WT and $G_q\alpha^{G188S/G188S}$ embryos. (C) Weight gains of WT, $G_q\alpha^{G188S/+}$ and viable $G_q\alpha^{G188S/G188S}$ mice. N = 6, represented as mean ± SEM.

4.3.2 $G_q\alpha^{G188S/G188S}$ platelet activation *ex vivo* is drastically attenuated

Next, to test the direct effects of the homozygous G188S substitution, flow cytometric analysis was performed on isolated platelets to measure activation markers, including integrin $\alpha_{IIb}\beta_3$ activation (Jon/A antibody) and P-selectin exposure (measure of α granule release). While integrin activation of $G_q\alpha^{G188S/G188S}$ platelets was normal in response to the non-GPCR glycoprotein VI (GPVI) agonist, convulxin, the response was significantly attenuated for all the GPCR-stimulating agonists: ADP, PAR4 agonist peptide (PAR4P; AYPGKF), and the stable thromboxane A2 analogue, U46619 (Figure 4-2A). The same pattern was also observed for P-selectin, although as a less sensitive measure of platelet activation, weaker stimuli like U46619 and ADP were not able to elicit a significant degranulation response and were thus not significantly different (Figure 4-2B).

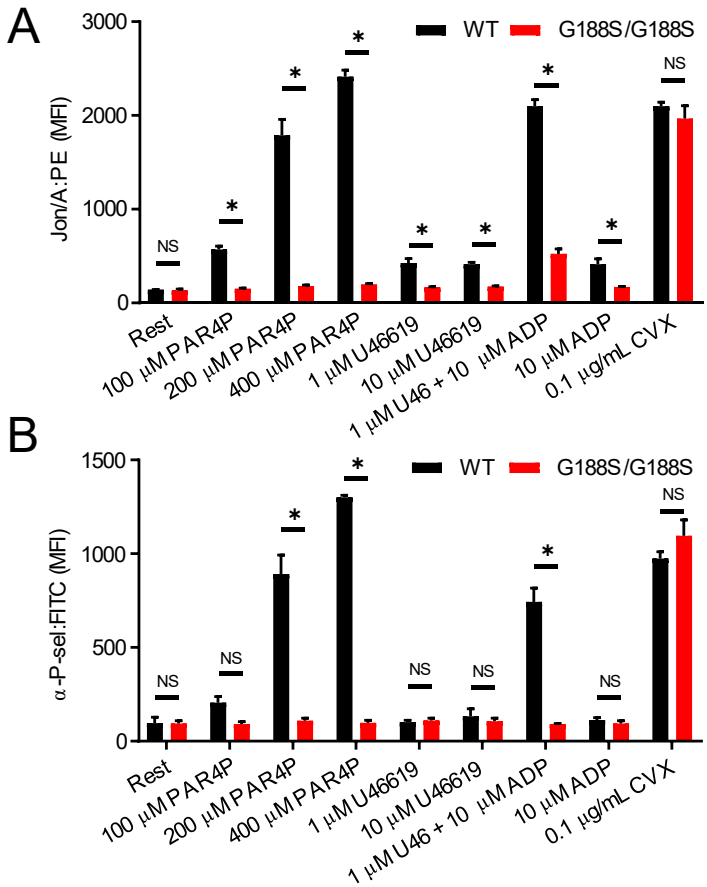

Figure 4-2. $G_q\alpha^{G188S/G188S}$ platelets are hyposensitive to GPCR agonists. (A, B) Platelets from $G_q\alpha^{G188S/G188S}$ mice and littermate controls (WT) were stained with fluorescently labelled antibodies specific to (A) activated $\alpha_{IIb}\beta_3$ integrin (Jon/A) or (B) P-selectin and stimulated with agonists as indicated. N = 4; *P < 0.05; mean ± SEM.

4.3.3 $G_q\alpha^{G188S/G188S}$ platelet aggregation and accumulation is reduced *ex vivo* and *in vivo*

Because our hypothesis was that the G188S substitution would impair RGS binding, and thus enhance G_q signaling and subsequent activation, our flow cytometry results were unexpected. To determine whether this apparent attenuated signaling via flow cytometry was anomalous, we next measured the functional consequences of the substitution with respect to aggregation *ex vivo* and platelet accumulation in response to injury *in vivo*. Consistent with the flow cytometric results, platelet aggregation in response to 100 μM PAR4P, 10 μM U46619, and 10 μM ADP was dramatically impaired for $G_q\alpha^{G188S/G188S}$ platelets (Figure 4-3A-C). In contrast, platelet aggregation was normal in response to 0.1 μg/mL convulxin (Figure 4-3D). Furthermore, platelet accumulation following a penetrating laser injury *in vivo* (assessed with fluorescently labelled anti-CD41/α_{IIb} antibody and intravital microscopy) was almost completely abolished for $G_q\alpha^{G188S/G188S}$ mice. Taken together, these results suggest that platelet activation and hemostatic function are drastically impaired by the G188S mutation.

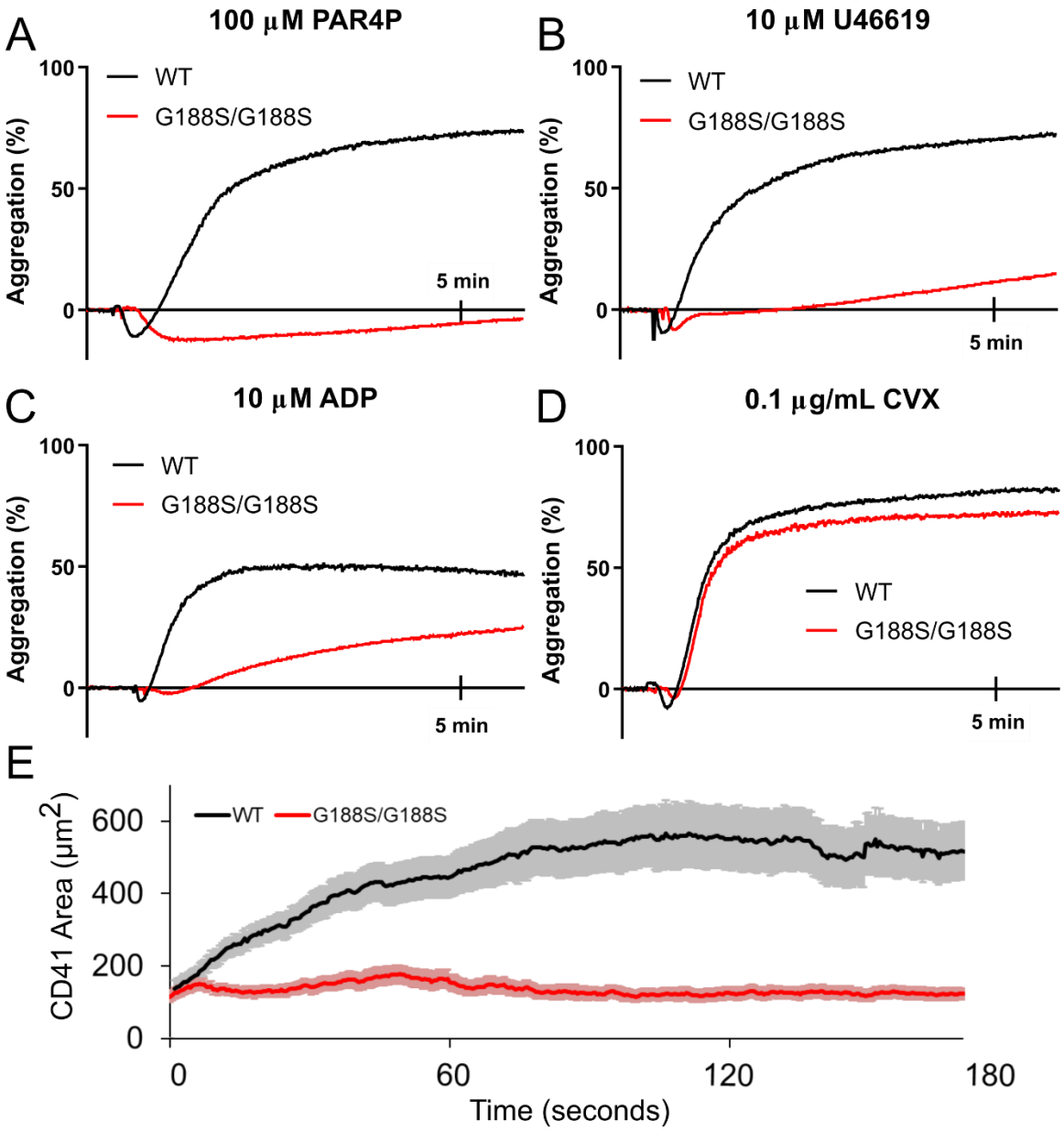

Figure 4-3. $G_q\alpha^{G188S/G188S}$ platelets have reduced function *ex vivo* and *in vitro*. (A-D) Platelet function was assessed via light transmission aggregometry in response to (A) 100 μM PAR4P, (B) 10 μM TxA_2 analogue (U46619), (C) 10 μM ADP and (D) 0.1 μg/mL convulxin (CVX); N = 3. (E) Mean CD41 (platelet) area in response to hemostatic penetrating laser injury as assessed by intravital confocal microscopy. At least 65 injuries performed in at least 7 mice per group; mean ± SEM.

4.3.4 $G_q\alpha^{G188S/G188S}$ calcium mobilization is significantly decreased *ex vivo*

From our previous results, the G188S substitution in $G_q\alpha$ appears to result in drastically impaired GPCR-mediated platelet activation. As mentioned in 1.2, stimulation of G_q-coupled receptors leads to activation of PLCβ, which in turn generates IP_3 and DAG from PIP_2. IP_3 stimulates the release of intracellular calcium from stores in the dense tubular system of platelets, where it acts as a potent secondary signaling molecule to mediate various platelet activation events. Therefore, to determine if the observed defect in GPCR signaling is a result of impaired G_q signaling specifically, we measured calcium mobilization in platelets with a cell-permeable ratiometric calcium-sensing dye, fura-2. In response to maximal concentrations of PAR4P, ADP and U46619, calcium mobilization was dramatically reduced in $G_q\alpha^{G188S/G188S}$ platelets (Figure 4-4A-D), confirming the notion that G_q signaling is impaired by the G188S substitution.

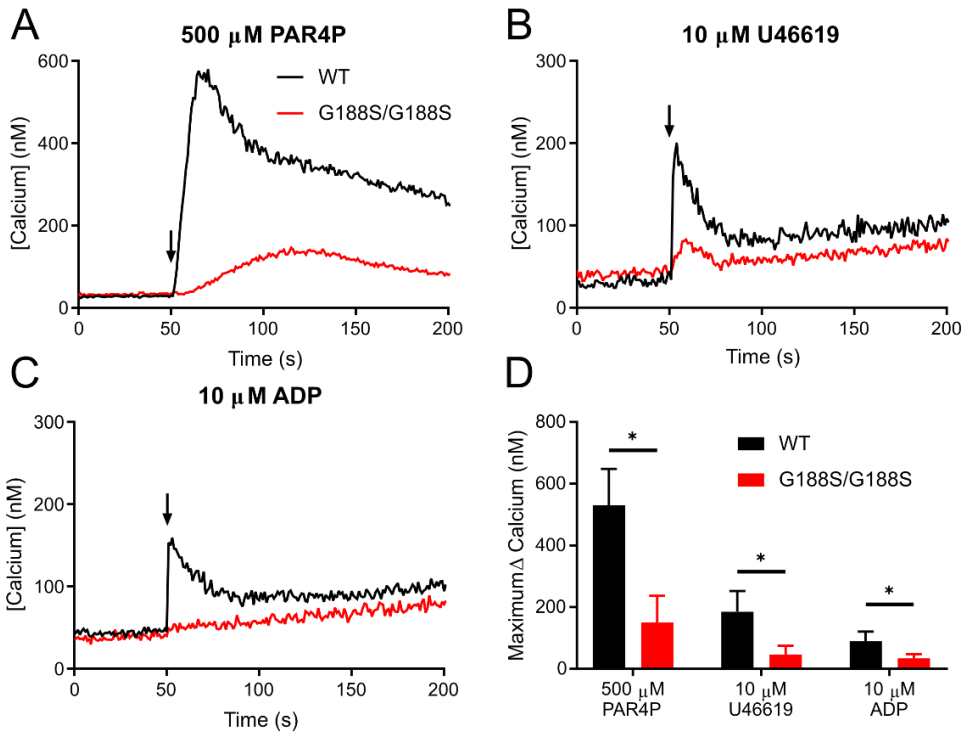

Figure 4-4. $G_q\alpha^{G188S/G188S}$ impairs calcium mobilization. Isolated platelets from $G_q\alpha^{G188S/G188S}$ and WT controls were loaded with fura-2AM and stimulated with agonist in the absence of extracellular calcium. Shown are representative traces in response to (A) 500 µM PAR4 agonist peptide (PAR4P), (B) 10 µM thromboxane A_2 analogue (U46619), and (C) 10 µM ADP. Arrows indicate addition of agonist. (D) Summary of maximum Ca^{2+} flux for 4 experiments; *P < 0.05; mean ± SEM.

4.3.5 $G_q\alpha^{G188S}$ disrupts RGS and PLC binding but doesn't impact protein expression

Because our body of evidence strongly suggests a defect in G_q signaling, we next asked whether protein expression was affected by the G188S substitution. Using an anti-$G_q\alpha$ antibody to immunoblot platelet lysate, we did not observe any obvious decrease in G_q protein expression, suggesting that the protein is being translated normally and that it is at least as stable as WT $G_q\alpha$ (Figure 4-5A). Another possible explanation for the defect in G_q signaling is that an off-target mutation has reduced expression of important signaling molecules downstream of G_q. Since PLCβ3 is highly expressed in mouse platelets and critical for G_q signaling,[143] we immunoblotted for this protein as well. Similarly, no defect in PLCβ3 expression was observed (Figure 4-5B), further indicating that decreased protein expression is not likely to explain the defect in G_q signaling. Next, we wanted to confirm that the G188S mutation does indeed impair (rather than enhance) binding of RGS proteins. To do this, a GST-RGS18 fusion protein was used as bait in a pull-down assay of platelet lysate from WT and $G_q\alpha^{G188S/G188S}$ mice in the presence of GDP and AlF^{4-} to mimic the high affinity α subunit transition state. As expected, wild type $G_q\alpha$, but not $G_q\alpha^{G188S}$, was precipitated by GST-RGS18 under these conditions (Figure 4-5C), confirming that RGS binding is indeed impaired by the G188S substitution. Finally, we sought determine whether PLCβ3 binding, required for G_q signaling, was impaired by the G188S substitution. Using flag-tagged recombinant PLCβ3 as bait, a pull-down assay was performed once more with platelet lysate. Only wild type $G_q\alpha$, but not $G_q\alpha^{G188S}$, was able to be precipitated by PLCβ3 (Figure 4-5D), suggesting that both RGS and PLC binding was disrupted by the G188S substitution. These results, in combination with those presented previously, indicate that $G_q\alpha^{G188S/G188S}$ mouse platelets are defective in G_q signaling because the downstream signaling molecule, PLCβ, cannot be activated via binding.

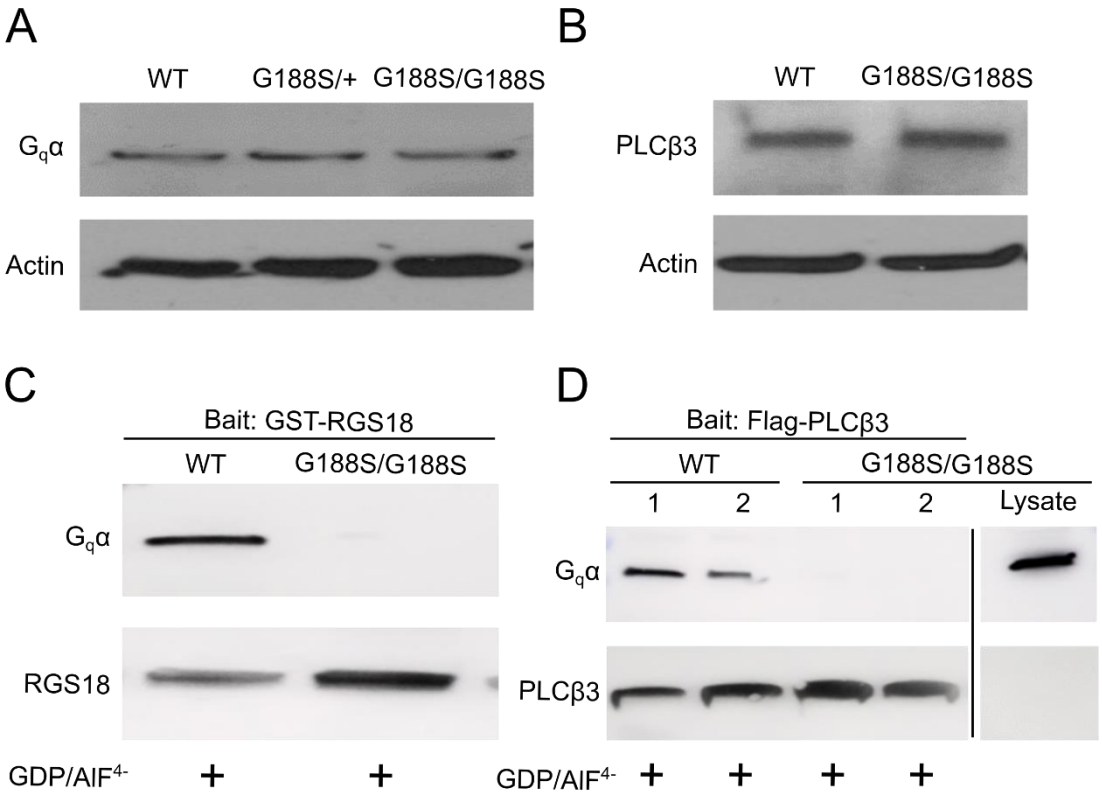

Figure 4-5. $G_q\alpha^{G188S/G188S}$ disrupts RGS and PLC binding. (A, B) Immunoblotting of WT, $G_q\alpha^{G188S/+}$, or $G_q\alpha^{G188S/G188S}$ mouse platelet lysate with antibodies directed to (A) $G_q\alpha$ and (B) PLCβ3 and reprobing for actin as a loading control. (C, D) Pull-down assays of WT or $G_q\alpha^{G188S/G188S}$ mouse platelet lysate, using as bait (C) GST-RGS18 or (D) Flag-PLCβ3. In addition to probing with antibodies against the bait protein, each blot was also probed with antibody against $G_q\alpha$ as the prey.

4.3.6 RGS and effector binding interfaces of $G_q\alpha$ overlap at G188S

Because the G188S substitution appears to impair binding of RGS proteins as well as effectors, primarily PLCβ, we next employed a structural analysis to understand why this might be the case. First, various crystal and solution structure models were collected from the RCSB Protein Data Bank.[140] (www.rcsb.org). For RGS proteins, we relied upon x-ray crystal structures of RGS2 and RGS8 in complex with $G_q\alpha$, RGS10 in complex with $G_{i3}\alpha$, and a solution NMR structure of RGS18. For effectors, we used x-ray structures of PLCβ3, Gβ1 and GRK2 all in complex with $G_q\alpha$. Since no native structures of RGS10 and RGS18 in complex with $G_q\alpha$ exist, both were aligned with RGS8 using PyMol prior to analysis (The PyMOL Molecular Graphics System, Version 1.7 Schrödinger, LLC.). Next, each $G_q\alpha$:protein-of-interest (POI) pair was analyzed using the Robetta Computational Interface Alanine Scanning Server to predict which residues, if mutated to alanine, would have the greatest impact on binding energetics. The residues with the greatest change in binding free energy (ΔΔG) and thus predicted to be most disruptive, were then mapped to the surface of $G_q\alpha$ using PyMol. As shown in Figure 4-6, the G188S substitution lies in a region where the binding interface of RGS proteins and PLCβ3 overlap considerably. This explains why the change in electrostatic and steric properties of this residue would disrupt not only RGS binding, but also PLCβ3 binding. Furthermore, this analysis indicates that the binding interface of RGS proteins is relatively small and overlaps almost entirely with other effectors, namely PLCβ3. Because of this overlap, identifying residues that would clearly disrupt RGS binding but not effector binding may be difficult. Nonetheless, we attempted to do so in a systematic, unbiased manner using a mutational scanning cutoff matrix (mSCM) method.[142] The analysis was performed for each of the $G_q\alpha$:POI pairs to substitute every possible residue at positions of $G_q\alpha$ predicted to be destabilizing for RGS interactions by alanine scanning. The predicted ΔΔG for each mutation was then averaged amongst RGS proteins and effectors before computing the difference between the two. The resulting “RGS specificity score” provided us with a metric for mutations that were more likely to

disrupt RGS binding while not impacting effector binding (Table 4-1). An arbitrary cutoff of 0.4 was used to propose viable candidate RGS insensitive mutations for future testing.

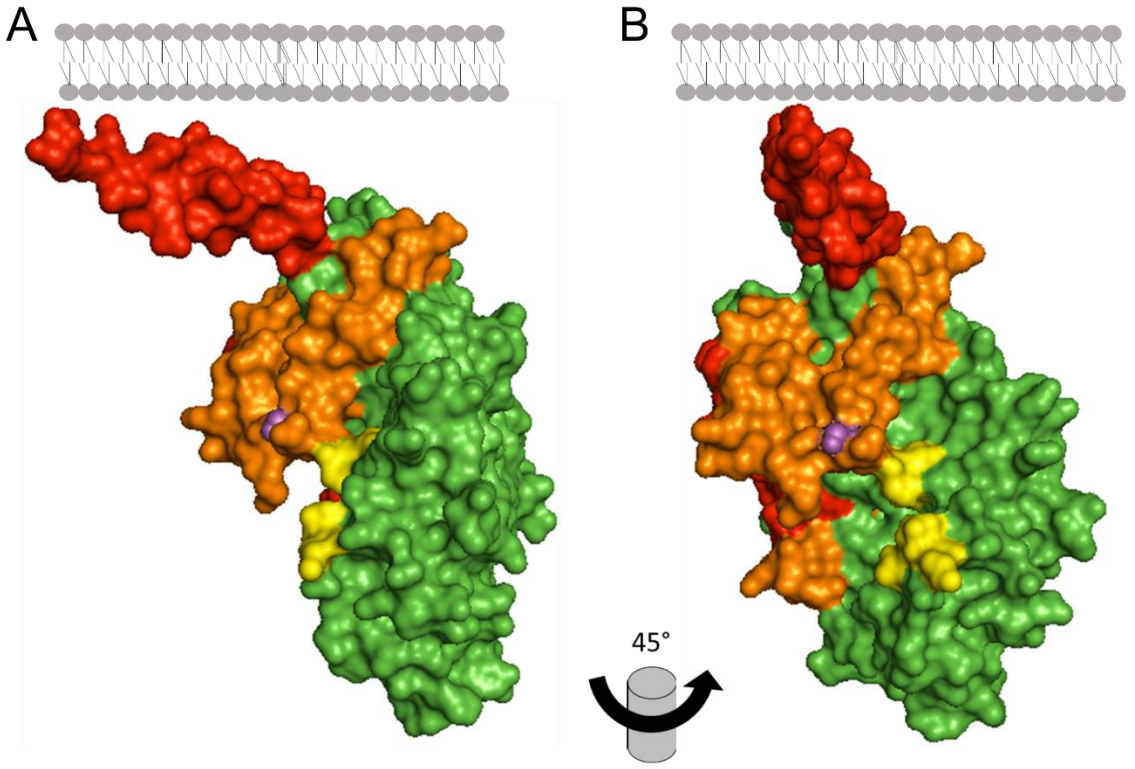

Figure 4-6. Predicted RGS and effector binding interfaces with $G_q\alpha$ overlap. (A, B) Structures of $G_q\alpha$ complexes were aligned to $G_q\alpha$ (3AH8) and subject to Robetta Computational Alanine Scanning to determine residues that are likely critical for intermolecular interactions. $G_q\alpha$ (green) binding partners were categorized as effectors [GRK2 (2BCJ), PLCβ3 (3OHM), and Gβ1 (3AH8)] and their interfaces displayed as red, or regulators of G protein signaling [RGS8 (5DO9), RGS2 (4EKC), RGS10 (2IHB) and RGS18 (2OWI)] and their interfaces displayed as yellow. The overlapping interfaces of RGS and effectors are shown in orange. The location of the G188S mutation is shown in purple and the predicted location of the plasma membrane shown in grey. The structure shown in (B) is the same as the (A) but rotated 45 degrees about the Y axis.

Table 4-1. Identification of candidate RGS insensitive $G_q\alpha$ mutations. Systematic cutoff scanning matrix was used to calculate the change in binding free energy (ΔΔG) between RGS (yellow) or effectors (red) and $G_q\alpha$ for various single amino acid substitutions at positions that were predicted by alanine scanning to impact RGS binding. The difference between the average ΔΔG for RGS and effectors was calculated to generate an "RGS specificity score". A larger differential (darker green) is indicative of a mutation that is more likely to impair RGS binding while minimally impacting effector binding. An arbitrary cutoff of 0.4 ΔΔG was used to select candidates for future testing.

			Change in binding free energy (ΔΔG)									
WT RES	RES #	MUT RES	RGS2	RGS8	RGS10	RGS18	Gβ1	PLCβ3	GRK2	RGS Avg	Effector Avg	Differential
K	77	H	-0.34	-0.076	-2.227	-0.275	0.186	0.158	0.146	-0.73	0.16	0.89
L	78	H	-0.954	-0.133	-1.022	-1.031	-0.154	-0.361	-0.055	-0.79	-0.19	0.60
Q	81	G	-0.361	-0.436	-1.786	-1.008	-0.289	-0.49	-0.122	-0.90	-0.30	0.60
Q	81	H	0.087	-0.085	-1.294	-0.547	0.274	-0.076	0.373	-0.46	0.19	0.65
Q	81	M	-0.224	-0.129	-1.736	-0.782	0.174	-0.423	-0.013	-0.72	-0.09	0.63
V	118	A	-0.599	-0.318	-0.709	-0.597	-0.152	-0.364	-0.488	-0.56	-0.33	0.22
V	118	G	-0.582	-0.239	-0.706	-0.571	-0.213	-0.262	-0.511	-0.52	-0.33	0.20
E	119	L	-0.081	-0.244	-0.524	-0.282	0.139	0.083	0.175	-0.28	0.13	0.42
E	119	P	-0.244	-0.433	-0.701	-0.435	-0.028	-0.082	0.03	-0.45	-0.03	0.43
E	119	I	-0.081	-0.244	-0.524	-0.282	0.139	0.083	0.175	-0.28	0.13	0.42
V	184	R	-0.506	-0.797	-0.516	-0.694	-0.313	-0.407	-0.481	-0.63	-0.40	0.23
T	186	C	-0.387	-0.262	-0.328	-0.212	0.119	-0.017	0.013	-0.30	0.04	0.34
T	186	F	-0.173	-0.135	-0.164	-0.182	0.2	0.187	0.205	-0.16	0.20	0.36
V	240	T	-0.211	-0.376	-0.029	-0.136	-0.107	-0.01	-0.08	-0.19	-0.07	0.12

4.4 Discussion

Studies employing RGS insensitive substitutions in $G_{i2}\alpha$ have proven useful in understanding how regulation of this G protein impacts platelet activation and function *in vitro* and *in vivo*. Since canonical RGS proteins, such as platelet RGS10 and RGS18, specifically interact with G_i and G_q α subunits, exploring the effects of an RGS insensitive substitution in $G_q\alpha$ was a logical step forward to expand our knowledge of RGS-mediated regulation of platelets. Furthermore, earlier studies by DiBello *et al* suggested that a mutation (G188S) analogous to the one we had previously studied for $G_{i2}\alpha$ (G184S) similarly impacted only RGS interactions without interrupting downstream signaling.[68] However, our results suggest that the G188S mutation in a mouse model does not phenocopy what was described in their recombinant cell-based system. Platelet activation responses as assessed by flow cytometry were dramatically impaired *ex vivo* for GPCR-stimulating agonists but not GPVI-stimulating convulxin. Functionally, this resulted in

dramatically reduced platelet aggregation in response to the same agonists and impaired platelet accumulation in response to *in vivo* hemostatic injuries. Interestingly, this very nearly phenocopies the $G_q\alpha^{-/-}$ mice described by Offermans *et al*.[144] Dramatically decreased calcium mobilization responses and decreased binding of PLCβ3 confirmed the notion that G_q signaling was indeed impaired by the G188S substitution. Taken together, this would suggest that the G188S mutation is not specific to RGS insensitivity and results in functionally deficient $G_q\alpha$.

Mouse and human $G_q\alpha$ proteins are nearly 100% identical, differing by only a single amino acid, so unexpected differences between the two proteins are unlikely to explain why our results differ from those described previously by DiBello *et al*. However, their experiments with human $G_q\alpha$ were performed in Chinese hamster ovary cells, relying upon endogenous PLCβ to generate DAG and IP_3. Mouse PLCβ3 differs considerably from Chinese hamster PLCβ3 (~40% identity). Thus, it is possible that Chinese hamster PLCβ can interact with $G_q\alpha^{G188S}$ normally while mouse PLCβ cannot.

Our structural analysis supports the conclusion that PLCβ3 (and possibly other PLCβ isoforms as well) is impaired by the G188S mutation. As we have shown, the substitution resides at an overlapping interface between RGS proteins and effectors, PLCβ3 in particular. The amino acid substitution from glycine to a serine not only creates the possibility of steric clash because serine is larger, but also electrostatic repulsion because its hydroxyl group has a partial negative charge. And although we have relied upon human PLCβ3 for this analysis, it is ~92% homologous to mouse PLCβ3, making it unlikely they would have drastically different intermolecular contacts with highly homologous $G_q\alpha$. Therefore, it seems quite likely that the mutation similarly disrupts both RGS and PLCβ interactions.

Because of the considerable overlap between the RGS and effector binding interfaces of $G_q\alpha$, identifying specific RGS insensitive residues has proven challenging. However, using a predictive systematic mutational cutoff scanning matrix method, we have identified mutations that

are more likely to specifically disrupt RGS interactions, without impacting effectors. Testing the functional consequences of these mutations should form the basis of future studies.

4.5 Supplemental Material

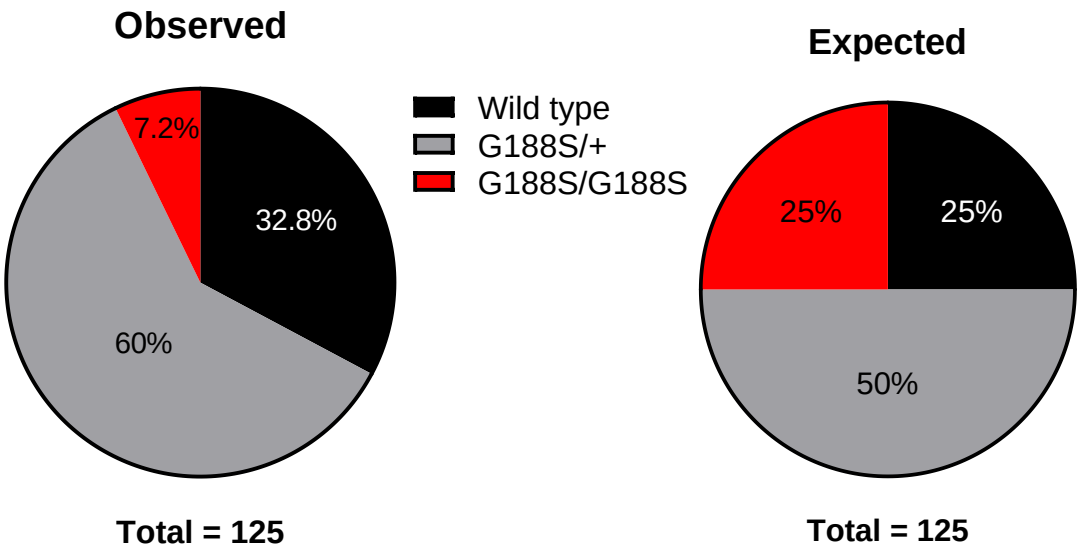

Figure S4-7. Chi square analysis of observed vs expected Gqα genotypes. A total of 125 mice that survived birth from hemizygous breeding pairs were genotyped for analysis. Of the total, 41 mice were homozygous wild type, 75 mice were hemizygous for the G188S allele and 9 were homozygous for the G188S allele. A Chi -square analysis of observed (left) vs expected (right) genotypes resulted in a P-value less than 0.0001, indicating that the observed results were significantly different than expected according to normal Mendelian inheritance patterns.

CHAPTER 5: Human RGS10 and RGS18 Variants and Platelet Function

5.1 Introduction

To date, our studies on RGS-mediated regulation of platelet function and physiology have been limited to mouse models. This is in large part due to a lack of suitable *in vitro* cell models (anucleate platelets cannot be cultured) and specific pharmacological inhibitors (while inhibitors have been identified, they are relatively non-specific or lack potency towards platelet RGS10 and RGS18).[145,146] Furthermore, routine scanning of public genomic databases indicate that loss of function mutations in RGS10 and RGS18, the two highest expressing RGS proteins in human platelets, are quite rare. This is possibly because mutations are not well tolerated due their relative physiological importance. Lastly, no genome wide association studies have yet identified any strong associations between RGS10 or RGS18 single nucleotide variants and disease phenotypes that we might expect from platelet hyperactivity, such as thrombosis. However, since these studies skew heavily towards common variants rather than rare variants, it is not surprising that rarer variants of RGS10 and RGS18 are typically below the threshold of statistical significance.

Despite the difficulties that have arisen in establishing humanized models for RGS function in platelets, it is nonetheless important to extend our understanding beyond the observations that have been made with mice. While RGS10 and RGS18 are the two highest expressed RGS proteins in both human and mouse platelets, predicted expression levels differ considerably between mice and humans. In mice, the estimated copy number per platelet for RGS10 is ~45,000, more than double that of RGS18 at ~20,000 (Figure 5-1A).[41] In stark contrast, the estimated copy number per platelet of RGS10 and RGS18 in human platelets are similar to one another, but much lower at ~4,500 (Figure 5-1B).[43] While it is possible that RGS proteins simply aren't as important for regulating human platelet function, it is equally likely that less is required because they are more potent or less subject to negative regulation. Thus, being able to probe the function of RGS proteins in human platelets would provide valuable insights into their relative importance.

The Penn Medicine Biobank (PMBB) has provided us with an opportunity to address these questions. The PMBB is a healthcare-based biorepository that recruits participants in a largely disease-agnostic manner from the entire Penn Medicine Health System, obtains biospecimens for research purposes, and consents participants for genomic analyses, permission to access electronic health record (EHR) data, and permission to recontact. Approximately 60,000 adult participants have been recruited as of November 2018. Of these approximately 67% are white/Caucasian, 25% are African-American, 3% are multiple races, 2% are Asian and 0.1% are native American. 50.4% are men. 25% are 18-40 years old, 34% are 41-60 years old, 23% are 61-70, and 17% are over 70. The PMBB continues recruiting approximately 15,000 participants annually, with plans for substantial expansion. Biospecimens include whole blood, serum, plasma, enriched cellular fractions, and selected tissues. To date, genome-wide genotype data has been generated on ~30,000 participants and whole exome sequencing has been completed on ~20,000. Using this genomic data, we have identified seven exonic variants in RGS10 and nine in RGS18 that are predicted to cause either a missense mutation, a frameshift, or a premature truncation. By recalling these patients to acquire blood samples, we hope to establish a correlation between RGS protein levels/function and platelet hemostatic reactivity.

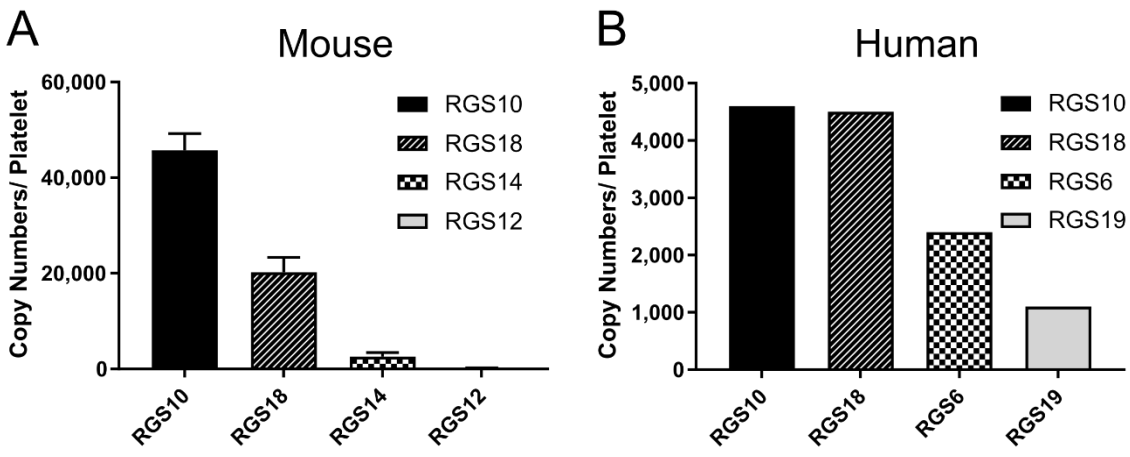

Figure 5-1. RGS10 and RGS18 are the highest expressed RGS in platelets. (A, B) Estimated copy numbers per platelet of RGS proteins identified in proteomics studies of (A) mouse and (B) human platelets.

5.2 Materials and Methods

5.2.1 Identification of exonic variants in RGS10 and RGS18

All whole exome sequenced patients in the Penn Medicine Biobank (PMBB) were queried to select potential exonic loss of function (LoF) mutations. Potential LoF variants were defined as: 1) nonsynonymous single nucleotide variants that cause a subsequent missense mutation (missense), 2) insertions or deletions that result in a frameshift introducing a premature stop codon (frameshift), or 3) single nucleotide variants that introduce a premature stop codon (stopgain).

5.2.2 Filtering predicted loss-of-function (pLoF) exonic variants in RGS10 and RGS18

To further predict in an unbiased manner which of these potential LoF mutations would be deleterious, each allowable variant was scored using the Rare Exome Variant Ensemble Learner (REVEL).[147] A REVEL score is between 0 and 1, with a higher score indicating an increased likelihood of pathogenicity. Notably, only nonsynonymous single nucleotide variants can be analyzed by REVEL, so by default frameshifts and stopgains, as defined in 5.2.1, were considered above the cutoff threshold. Graphics representing these variants were generated using the Illustrator for Biological Sequences.[148]

5.2.3 Structural analysis and predictions for missense mutations

Nonsynonymous single nucleotide variants resulting in missense mutations above the REVEL score threshold were mapped to the available structures of RGS18[136] and RGS10[47] and then analyzed via the DynaMut algorithm to predict effects on protein stability.[149] The results are presented as the change in folding free energy (kcal/mol) defined as $\Delta\Delta G = \Delta G_{WT} - \Delta G_{Mut}$, where WT is the native protein and Mut possesses the missense mutation. Next, because RGS18 is only available as a non-complexed solution structure, it was aligned with RGS10 in the RGS10:$G_{i3}\alpha$ complex structure for protein-protein analysis. The RGS:$G_{i3}\alpha$ complexes were then subject to analysis by mCSM-PPI2 to predict changes in protein-protein affinity.[150] The results are presented as the change in binding free energy defined as $\Delta\Delta G^{A} = \Delta G^{A}_{WT} - \Delta G^{A}_{Mut}$, where WT is the native

protein and Mut possesses the missense mutation. A negative change in Gibbs free energy (ΔΔG) suggests a destabilizing effect of the variant.

5.3 Results

5.3.1 Novel pLoF RGS10 and RGS18 variants in the Penn Medicine Biobank

A search of ~12,000 whole exomes in the Penn Medicine Biobank (PMBB) resulted in the identification of 21 unique exonic variants in RGS10 and 40 in RGS18. Of these, 12 for RGS10 and 30 for RGS18 were defined as potential loss of function (LoF) variants. Of note, all variants were present on only a single allele and there were no individuals with variants in both RGS10 and RGS18. To further predict which variants were likely to be deleterious to protein function, they were scored using REVEL, an ensemble method integrating multiple algorithms to predict the pathogenicity of rare missense variants. An arbitrary REVEL score threshold was set for RGS10 and RGS18. Because RGS10 had a narrower range and lower median REVEL score, mutations are predicted to be less tolerated. Therefore, a lower threshold was set at 0.1 to increase sensitivity (i.e. ability to detect true positives) at the cost of reducing specificity (i.e. ability to remove true negatives). For RGS18, with a wider range and higher median REVEL score indicative of being more tolerable to mutations, the threshold was set higher at 0.25, increasing specificity but sacrificing some sensitivity. Of the potential LoF variants, 7 for RGS10 and 9 for RGS18 were above the preset REVEL score threshold and considered predicted LoF variants (pLoF; Figure 5-2). Some of these variants were also detected in the Genome Aggregation Database (GnomAD; https://gnomad.broadinstitute.org), which is comprised of 141,546 individuals and contains data on 125,748 exomes and 15,708 genomes as of September 2019 (Table 5-1).[151]

Figure 5-2. pLoF RGS10 and RGS18 variants in Penn Medicine Biobank (on following page). Variants were identified based on predicted pathogenicity by REVEL scores >0.1 for RGS10 and >0.25 for RGS18. Variants are color coded as follows: yellow = missense mutation, red = premature stopgain, blue = frameshift insertion, and green = frameshift deletion. Circles indicate the direct effect of each variant. Squares indicate the indirect effects of frameshift insertions or deletions, for which red text indicates a novel premature stopgain. The canonical regulator of G protein signaling (RGS) domain, both sufficient and necessary for GTPase activity towards binding partner Gα subunits, is indicated in cyan.

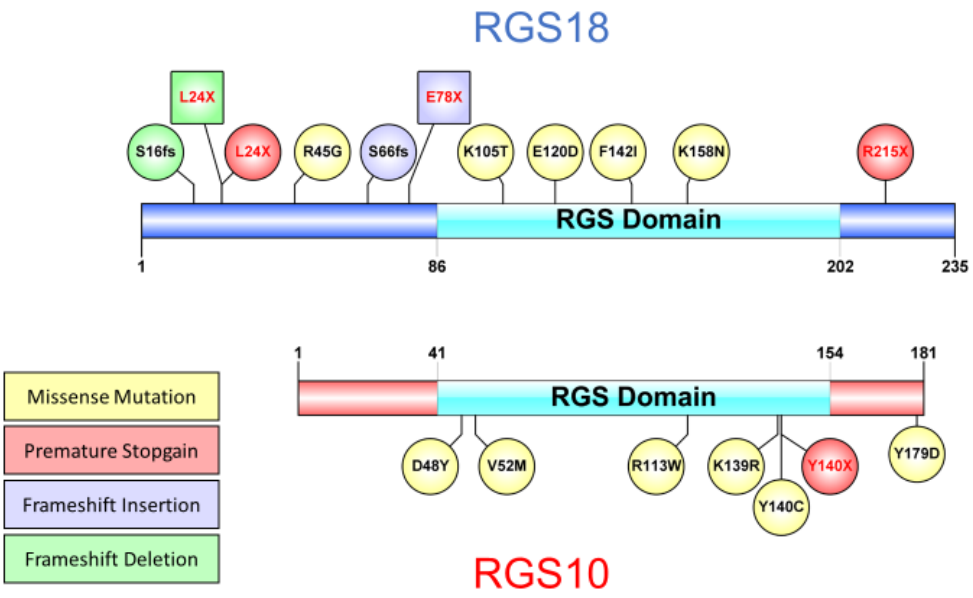

Table 5-1. pLoF RGS10 and RGS18 variants in the Penn Medicine Biobank. Variants were included if their REVEL (Rare Exome Variant Ensemble Learner) scores were >0.1 for RGS10 (red) and >0.25 for RGS18 (blue). REVEL is an ensemble method integrating multiple algorithms to predict the pathogenicity of rare missense variants. Scores range from 0 to 1 with higher scores predicted to be more pathogenic. 16 variants in 101 individuals were identified from a dataset of 11,451 exome-sequenced individuals. Frequencies are relative to the total Penn Medicine BioBank patient population. Allelic frequencies within the Genome Aggregation Database (GnomAD; 141,546 individuals comprising 125,748 exomes and 15,708 genomes as of September 2019, database is maintained online and publicly available by the Broad Institute) are also provided when available. Reference SNV identifiers (RSID): *rs117042762; **rs35623527.

Gene	Effect	Variant	#	PMBB Frequency	REVEL score	GnomAD Frequency
RGS10	Missense*	V52M	6	0.05240%	0.152	0.14000%
	Stopgain	Y140X	1	0.00873%	.	.
	Missense	D48Y	1	0.00873%	0.407	.
	Missense	K139R	1	0.00873%	0.271	0.00041%
	Missense	Y140C	1	0.00873%	0.243	.
	Missense	R113W	1	0.00873%	0.234	0.00041%
	Missense	Y179D	1	0.00873%	0.216	.
RGS18	Frameshift Deletion	S16fs	42	0.36678%	.	0.09000%
	Missense**	R45G	39	0.34058%	0.291	0.07000%
	Missense	K105T	2	0.01747%	0.322	0.00445%
	Stopgain	L24X	1	0.00873%	.	.
	Stopgain	R215X	1	0.00873%	.	0.00041%
	Frameshift Insertion	S66fs	1	0.00873%	.	.
	Missense	F142I	1	0.00873%	0.926	.
	Missense	E120D	1	0.00873%	0.63	.
	Missense	K158N	1	0.00873%	0.521	0.00041%

5.3.2 Common pLoF mutations in RGS10 and RGS18 are ethnically linked

A frameshift deletion at serine 16 of RGS18 (S16fs) is present in 42 PMBB patients, nearly half of the total number of RGS pLoF variant-harboring patients identified (101 individuals) and at a higher frequency than the total GnomAD population (0.36% in PMBB vs 0.09% in GnomAD; Table 5-1). Interestingly, this variant is observed at a much higher frequency in GnomAD for people of Ashkenazi Jewish ancestry (1.93% of Ashkenazi vs 0.09% of the total population). Similarly, an arginine to glycine missense mutation at position 45 of RGS18 (R45G) is present in 39 PMBB patients, more prevalent than in the total GnomAD population (0.34% in PMBB vs 0.07% in GnomAD), and preferentially effects individuals of African descent (0.96% of African vs 0.07% of the total population). The remaining non-unique variant is a valine to methionine missense mutation at position 52 (V52M) of RGS10 present in 6 PMBB patients (0.052%; Table 5-1). Its frequency is slightly lower in the total GnomAD population (0.14%) but considerably higher for individuals of East Asian descent (1.91%).

5.3.3 Missense mutations may disrupt RGS stability and/or RGS:Gα interactions

To further predict how these mutations might alter protein function, we first used DynaMut to estimate the change in folding free energy upon mutation of native RGS10 and RGS18 structures. DynaMut is a method of analyzing and visualizing protein dynamics and stability by sampling conformations and measuring vibrational entropy changes.[149] Each of the mutations for RGS18 was predicted to be destabilizing (-$\Delta\Delta$G) but to varying degrees (Table 5-2), suggesting a potential impact on protein functionality. Interestingly, the missense mutations for RGS10 were predicted to be either neutral ($\Delta\Delta$G ≈0) or stabilizing (+$\Delta\Delta$G; Table 5-2). Next, we estimated the change in binding free energy for a complex consisting of RGS10 or RGS18 and $G_{i3}\alpha$ using mCSM-PPI2. mCSM-PPI2 is a machine learning method that utilizes graph-based structural signatures to model the effects of mutations on protein-protein interactions.[150] Interestingly, all of the missense mutations analyzed were predicted to be destabilizing to various degrees except for the arginine to tryptophan mutation at position 113 (R113W) of RGS10 (Table 5-2).

		DynaMut	mCSM-PPI2
Gene	Mutation	ΔΔG	$\Delta\Delta G^A$
RGS18	F142I	-0.922	-0.673
RGS18	E120D	-0.348	-0.059
RGS18	K158N	-1.428	-0.697
RGS18	K105T	-0.221	-0.163
RGS10	D48Y	1.652	-0.245
RGS10	K139R	1.545	-0.181
RGS10	Y140C	1.866	-0.642
RGS10	R113W	0.090	0.422
RGS10	V52M	-0.086	-0.297

Table 5-2. RGS10 and RGS18 missense mutation predictions. DynaMut was used to predict changes in folding free energy as a measure of intrinsic protein stability using structures for RGS18 (PDB: 2OWI) and RGS10 in complex with $G_{i3}\alpha$ (PDB: 2IHB). $\Delta\Delta G = \Delta G_{WT} - \Delta G_{Mut}$, where WT is the wild type residue, Mut is the variant and units are kcal/mol. mCSM-PPI2 was used to predict changes in binding free energy as a measure of RGS affinity to $G_{i3}\alpha$. $\Delta\Delta G^A = \Delta G^A_{WT} - \Delta G^A_{Mut}$, where WT is the wild type residue, Mut is the variant and units are also kcal/mol. RGS18, available only as an apo solution structure, was aligned with RGS10 in PyMol prior to performing the analysis.

5.3.4 Structural analysis of mutant RGS stability and/or RGS:Gα interactions

Finally, we mapped these mutations the to their available structures to gain better insight into the potential effects of the observed mutations. Interestingly, the mutated residue predicted to be most destabilizing for RGS18, phenylalanine to isoleucine at position 142 (F142I), is partially buried within the protein structure. This suggests that changing the amino acid from a large hydrophobic residue to a smaller hydrophobic residue decreases stability, possibly by disrupting the proper fold of the native conformation (Figure 5-3A; Table 5-2). Additionally, the two mutations that are predicted to have the largest destabilizing effect on RGS18:$G_{i3}\alpha$ are at or near to protein-protein interface (Figure 5-3A; Table 5-2), suggesting direct or indirect impacts on intermolecular interactions. In contrast, the most stabilizing residue for native RGS10 is a tyrosine to cysteine mutation at position 140 (Y140C). Because this residue is solvent exposed, it suggests that mutation from a hydrophobic to nucleophilic residue is more energetically favorable in aqueous solution (Figure 5-3B). However, this same mutation is predicted to the most destabilizing for the RGS10:$G_{i3}\alpha$ complex (Table 5-2). This is likely because it also lies at the protein-protein interface and introduction of a partial negative charge creates electrostatic repulsion.

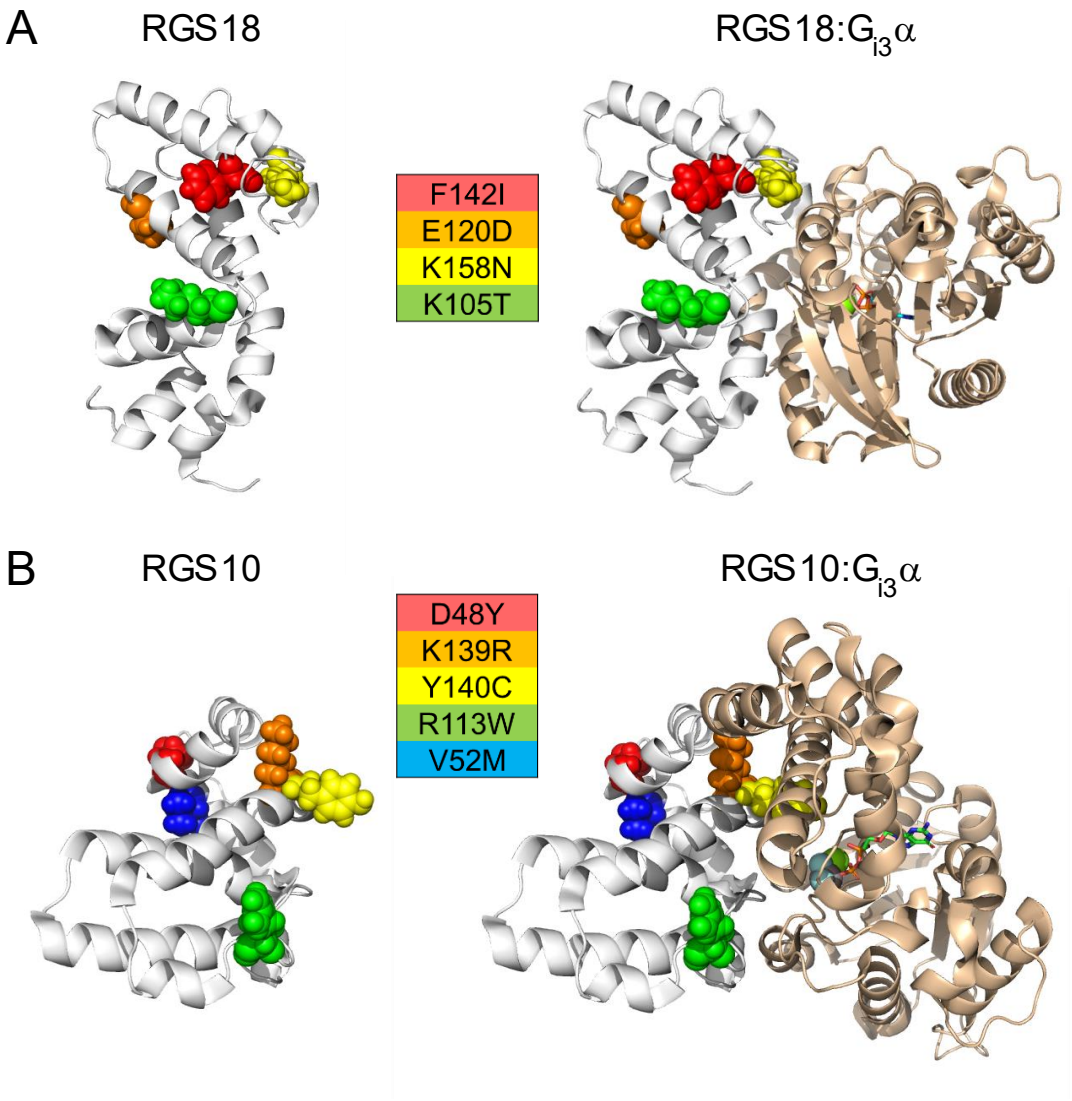

Figure 5-3. Structural analysis of RGS10 and RGS18 missense variants. Non-synonymous single nucleotide variants resulting in missense mutations were mapped to available structures of RGS10 and RGS18. RGS18 is a solution NMR structure not in complex with an α subunit. It was aligned with RGS10: $G_{i3}α$ using PyMol prior to amino acid mapping and analyses. RGS10 is an X-ray structure in complex with $G_{i3}α$. This native structure is missing a flexible region which is present in the solution NMR structure of RGS10 not in complex with any α subunits and is a site for one of the PMBB variants. This solution structure for RGS10 was aligned with RGS10: $G_{i3}α$ prior to amino acid mapping and analysis.

5.4 Discussion

The PMBB represents a valuable resource for studying relationships between genetics and phenotypic traits and the amount of available data continues to grow. Furthermore, the ability to recall patients provides additional benefits when studying freshly isolated biospecimens, like platelets, is an essential component of a functional analysis. Our search of the whole exome data available in the PMBB for RGS10 and RGS18, the two most abundant RGS proteins in human platelets,[43] resulted in the identification of ~200 unique variants. Of these, we identified 16 exonic variants in RGS10 (seven) and RGS18 (nine) in 101 total patients that were predicted to result in deleterious missense mutations, frameshifts, or premature stopgains. Additionally, many of these variants were identified in large-scale publicly available genetics databases, such as GnomAD, providing added information about ethnic prevalence of certain variants. For most missense mutations, we used predictive algorithms and available protein structures to provide further evidence of their purported functional consequences. Finally, we mapped these mutations to RGS:$G_{i3}\alpha$ complexes to better understand the effects on stability and protein-protein interactions.

The pLoF variant present in the most PMBB patients (42), a frameshift deletion at S16 of RGS18, is predicted to result in the introduction of a premature stop codon at lysine 24 (L24), thus truncating the protein (Figure 5-1). Importantly, this truncation would completely disrupt the RGS domain, which is both necessary and sufficient for GAP activity towards G α subunits. Because it is not a missense mutation, we could not employ our predictive algorithms to estimate stability changes. However, we can reasonably assume that loss of the RGS domain would either: a) result in protein degradation via improper folding or b) yield a non-functional truncated protein. Perhaps most interestingly, this variant is more heavily represented in individuals of Ashkenazi Jewish descent relative to the broader population available in GnomAD. While the PMBB does not provide population statistics for people of Ashkenazi Jewish ancestry, ~2/3 of patients are Caucasian and ~90% of the Jewish population of the United States is Ashkenazi in origin,[152] so it is reasonable to predict that a significant portion of these individuals are of Ashkenazi Jewish descent. Due to

distinct religious and cultural practices resulting in patterns of genetic isolation, the Ashkenazi Jewish population is one of several groups that have garnered interest from those studying rare homozygous mutations.[153] Notably, however, none of the individuals in the PMBB are homozygous for this variant, which could indicate more modern trends of increased genetic admixture.[154]

The second most prevalent pLoF variant that we identified in the PMBB database (39 patients) is a missense R45G mutation in RGS18. This mutation is more prevalent in individuals of African descent than the total GnomAD population and almost ¼ of the total PMBB patient population is designated as such. While data suggests that African populations are more genetically diverse than non-African populations,[155] heterozygous advantage is a well-documented phenomenon explaining the increased prevalence of certain deleterious mutations in African populations, particularly with respect to malarial resistance and sickle cell disease.[156] Similarly, a LoF mutation in RGS18 could reasonably provide a selective advantage with respect to malarial resistance, as it would be expected to enhance platelet reactivity and platelet granule release, a byproduct of platelet activation. Platelet granule release has been implicated as an important mechanistic step involved in the platelet-dependent destruction of Plasmodium parasites in malaria.[157,158] Therefore, it is not unreasonable to postulate that the R45G variant in RGS18 might be maintained in areas where malaria incidence is high, even if it could have a negative impact under settings of thrombosis. However, it is equally possible that this mutation doesn't impact function at all. R45G is spatially separated from the critical RGS domain and the REVEL score prediction of pathogenicity is the lowest of those identified for RGS18 (Table 5-1). Furthermore, we could not predict changes in stability because the residue is not present in the available structure. This is likely because the residue is not part of the rigid helical bundles that make up the core of the RGS protein, but rather resides in what we could predict is a more flexible N-terminal region.

Of the missense mutations that were present in the available structures, those predicted to be the most destabilizing in terms of protein-protein interactions were residues that lie at or near the protein-protein interface, as expected. The most destabilizing variant of RGS10, Y140C,

replaces a large hydrophobic residue with a polar residue. While this is predicted to disrupt the RGS:$G_{i3}\alpha$ interface, likely due to electrostatic repulsion, it surprisingly is predicted to stabilize the native structure of RGS10. This, however, is likely because the hydrophobic residue is exposed to aqueous solvent, an energetically unfavorable situation due to the hydrophobic effect, and replacing it with a hydrophilic residue relieves this energetic burden. The most destabilizing variant for RGS18, K158N, replaces a positively charged residue with a polar, but uncharged, residue. This is predicted to be destabilizing for RGS:$G_{i3}\alpha$ interactions, likely due to reduced electrostatic attraction, but also destabilizing for native RGS18, as folding free energy is minimized when exposed residues are more highly attracted to water molecules in the assumed aqueous solvent.

To translate our understanding of RGS-mediated regulation of platelet activation from mouse models to humans, we sought to identify variants in RGS10 and RGS18 from genetic data of patients enrolled in the Penn Medicine Biobank. After filtering for variants that were predicted to be loss of function according to our criteria, 16 variants in 101 patients remained. Finally, using computational and structural methods, we predicted the impacts of these variants on protein stability and protein-protein interactions where possible. While future studies are necessary (and pending) to establish the functional consequences of these mutations, we have laid the groundwork for the first studies concerning RGS regulation of human platelet activation.

CHAPTER 6: Conclusion

6.1 RGS-mediated regulation of murine and human platelet function

Much of what we know about RGS proteins and their role in regulating platelet GPCR signaling networks has come from mouse models. Fortunately, the two most abundant RGS proteins in both human and mouse platelets are the same: RGS10 and RGS18.[41,43] Therefore, our lab and others have been able to probe the individual impacts of these proteins in platelet activation and physiology by comparing their individual genetic knockouts to wild type controls. Additionally, we examined the combined contributions of both RGS10 and RGS18 to platelet activation and physiology by generating double knockouts and were able to perform direct comparisons of each individual knockout on the same genetic background. From our head to head comparisons, our data suggests that RGS10 plays a more prominent role in attenuating platelet GPCR signaling, while RGS18 is more important for platelet production from megakaryocytes. However, from our double knockout studies, we have shown that both proteins contribute to regulating platelet activation, as only the dual deletion mice have platelets that are hyperactive enough to be prematurely cleared from circulation and generate occlusive thrombi from hemostatic penetrating injuries.

While RGS10 and RGS18 are the most abundant RGS in human and mouse platelets as identified by transcriptomics and proteomics studies, we cannot rule out the possibility that other lower abundance RGS proteins are present and contribute to platelet activation. Indeed, prior studies have shown that RGS16 is expressed in both human and mouse platelets and contributes to regulating platelet GPCR signaling and hemostasis.[159,160] Interestingly, an earlier study had shown that RGS16 and RGS18 are both expressed in megakaryocytes but that only RGS16 specifically regulates stromal-cell-derived factor 1 (SDF-1)-mediated CXC chemokine receptor 4 (CXCR4) signaling.[161] SDF-1 has been shown to promote chemotaxis and migration of megakaryocyte progenitors to the junctions between sinusoidal bone marrow endothelial cells, thereby supporting the release of proplatelets into the circulation.[162] However, SDF-1-mediated

CXCR4 signaling and migratory potential decreases as megakaryocytes mature,[163] which negatively correlates with the increase in RGS16 expression,[161] thus suggesting that increasing RGS16 levels may serve to negatively regulate CXCR4 signaling during megakaryocyte development. While the difference does not reach the threshold of statistical significance, the slight increase in platelet counts for RGS16$^{-/-}$ mice supports the notion that RGS16 normally attenuates CXCR4 signaling to downregulate megakaryocyte proplatelet formation. Considering this data in light of our own, we propose a model in which RGS16 promotes proper localization of immature megakaryocytes, RGS18 promotes proplatelet formation, and RGS10 has the most prominent role in regulating platelet signaling. However, to reiterate, evidence suggests that RGS18 and RGS16 still contribute to regulating platelet GPCR signaling networks. Additionally, while mutations in RGS2 were reported to result in moderately decreased G_s-mediated signaling in human platelets via non-canonical interactions,[164] mouse knockout models did not suggest any functional consequences with respect to platelet function in hemostasis.[165] Finally, while reported at lower levels, RGS14 and RGS12 were detected by proteomics studies in mouse platelets,[41] while RGS6 and RGS9 were detected in human platelets.[43] Its thus possible that these RGS proteins may additionally contribute to regulating megakaryocyte development or platelet function.

Circumventing the issue of knocking out several RGS genes to probe global RGS regulation of specific cell types, RGS-insensitive mutants in Gα subunits have proven useful in some circumstances. Furthermore, the α subunits upon which RGS proteins are predicted to act in human platelets, $G_{i2}\alpha$ and $G_q\alpha$, are nearly identical to those in mouse platelets (98.3% and 99.7% sequence identity, respectively). We were previously able to elucidate the impact of RGS-mediated G_{i2} regulation in platelets using $G_{i2}\alpha$ G184S RGS-insensitive mice, and found that it significantly increased platelet accumulation in response to hemostatic injury primarily via expansion of the P-selectin$^{(-)}$ shell, but not the P-selectin$^{(+)}$ core.[67,78] However, we found that the analogous mutation in $G_q\alpha$ (G188S) dramatically *decreased* platelet function, due to drastically attenuated G_q signaling caused by disrupted interactions with PLCβ. Nonetheless, there are valuable lessons to be learned

from these studies. First, caution should be taken when attempting to translate results from contrived systems *in vitro* to *in vivo* models. Second, structural analysis of protein interactions can provide predictions to inform decisions regarding mutagenesis. Third, while $G_{i2}\alpha$ and $G_q\alpha$ are structurally very similar, our results suggest that their interactions with their respective effectors differ considerably. Finally, RGS and effector interfaces overlap considerably on the surface of $G_q\alpha$, meaning it may be difficult or even impossible to generate an RGS-insensitive but otherwise functional $G_q\alpha$ subunit. Using predictive algorithms, however, we have identified several viable RGS-insensitive candidates for future study.

Extending the observations made in mouse models to human platelet physiology has proven challenging. While we can reasonably predict that RGS10 and RGS18 play a role in human megakaryocyte development and/or platelet physiology due to their expression levels, we nonetheless have no conclusive evidence to substantiate our hypothesis. Furthermore, no RGS10 or RGS18 null human patients have been identified to date. To address the role of RGS10 and RGS18 in human platelet function we have, however, been able to identify 16 pLoF variants in human patients that have submitted samples to the PMBB. In addition, by using a structure-based predictive analysis, we have reason to believe that these mutations will indeed affect protein function. Our pending plans to recall patients and measure platelet functionality and protein levels are discussed in more detail in Chapter 7: Future Directions.

Our studies into the regulation of platelet GPCR activation have revealed a great deal about RGS proteins and their impact on platelet physiology. While evidence suggests that RGS10 regulates $G_{i2}\alpha$, $G_q\alpha$, and $G_z\alpha$ in platelets to have a more prominent impact on platelet activation and hemostatic potential, RGS18 plays a lesser role in this respect (with no apparent impact on $G_z\alpha$) but may be important in regulating proplatelet formation from mature megakaryocytes. Furthermore, the global impact of RGS-mediated regulation of $G_{i2}\alpha$ confirms the importance of these interactions with respect to regulating platelet function during hemostasis, while the impact of RGS-mediated regulation of $G_q\alpha$ remains to be determined. Finally, the identification of pLoF

RGS10 and RGS18 mutations in human patients has provided fertile ground for future studies concerning their contributions to human platelet function.

6.2 Negative regulators of platelet signaling preserve normal platelet function

Members of the RGS protein family belong to a broader class of negative regulators of platelet signaling that modulate many platelet-dependent processes, including hemostasis and thrombosis. Hemostasis and thrombosis are often considered two sides of the same coin; while hemostasis involves an appropriate and proportionate response to prevent bleeding via the coagulation cascade and platelet aggregation, thrombosis occurs when these processes (via acquired or hereditary means) are dysfunctional, often resulting in vascular occlusion. This then provides the basis for the prevailing theory as to why negative regulation of platelet activation is necessary: while rapid activation is required to prevent blood loss in response to injury, unwarranted or excessive platelet activation promotes thrombosis. Our own results with RGS10$^{-/-}$ 18$^{-/-}$ mice support this notion, as the response to hemostatic injury was surprisingly exaggerated to the extent that a large proportion of thrombi became occlusive. The fact that similar phenomenon is not observed in RGS10$^{-/-}$ mice suggests that a “multiple hit hypothesis”, much as has been described for cancer,[166] may apply to negative regulators of platelet activation. This would further help to explain why such a variety of negative regulators exist: redundancy at multiple levels prevents unnecessary activation even if one checkpoint fails. In the case of RGS proteins, RGS10 and RGS18 appear to be partially redundant with respect to limiting hemostatic platelet activation. Only loss of both results in a response dramatic enough to increase the risk of thrombosis. But how do other negative regulators compare in terms of their impacts on platelet biology?

The IP receptor, stimulated by PGI_2, couples to $G_s\alpha$ and represents an extrinsic regulator of platelet activation, as it activates AC to promote cAMP production and PKA activity, known to broadly inhibit platelet activation pathways.[26] IP receptor deletion in mice does not appear to affect hemostatic bleeding times, but it exacerbates thrombosis via a ferric chloride model.[167] This differs considerably from dual deletion of RGS10 and RGS18, as we do see enhanced effects on

hemostasis, and although not directly tested, would expect to see exacerbated thrombosis as well. One potential explanation for the difference in hemostatic effects is that $G_s\alpha$-mediated AC activation is readily overwhelmed by $G_{i2}\alpha$-mediated AC inhibition during the hemostatic response. Therefore, RGS-dependent $G_{i2}\alpha$ attenuation might be considered a more robust inhibitor of platelet activation than IP-coupled $G_s\alpha$ activation. But how, then, might we explain the impact on thrombosis? During a puncture-induced hemostatic injury, a pressure drop is created, and platelets accumulate where the endothelium is ruptured.[168] In contrast, in a ferric chloride model, endothelium may be damaged but not necessarily lost,[169] and there is no pressure drop. Therefore, soluble PGI_2 produced by the endothelium may be more protective under these settings because it is more closely localized to the site of platelet deposition and can't be flushed extravascularly via the pressure drop created by a physical hole.

Another extrinsic regulator with a role similar to PGI_2 is NO, also produced by endothelial cells via endothelial NO synthase (eNOS; NOSIII), that can diffuse across the cell membrane to activate soluble guanylyl cyclase (sGC), promoting cGMP production and PKG activity.[26] Like PKA, PKG is known to phosphorylate numerous targets that mediate inhibition of platelet activation. One report suggests that deletion of eNOS in mice, in contrast to IP receptor deletion, results in a reduced hemostatic bleeding time indicative of an enhanced platelet activation.[170] However, another report suggests that eNOS deletion results in a trend towards reduced hemostatic bleeding time, but this difference is not statistically significant.[171] It is important to note, however, that these were slightly different hemostatic models; whereas the former report was using a tail vein puncture injury model, the latter relied upon a tail transection model. It would thus seem likely that the impact of NO-mediated platelet inhibition depends upon the size and nature of the hemostatic injury; for a smaller injury, like a puncture, NO produced by adjacent endothelial cells is likely still able to diffuse into platelets accumulating at the site of injury. For a complete transection, however, there are no downstream endothelial cells to produce NO and it might be more readily carried away by higher

pressure, reducing its ability to inhibit platelet activation. This highlights the importance of interpreting results in light of their experimental context.

If we compare the results for $IP^{-/-}$ and $eNOS^{-/-}$ mice to our studies, some subtle but intriguing conclusions emerge. While not tested directly in our $RGS10^{-/-}18^{-/-}$ mice, we do see a dramatically enhanced hemostatic response that would more than likely correspond to a decreased bleeding time in a tail-bleeding model. Furthermore, both $RGS10^{-/-}$ and $RGS18^{-/-}$ mice individually have been previously shown to have reduced bleeding times in a tail-bleeding model.[62,63] While not definitive, RGS proteins seem to have a more dramatic impact on hemostatic platelet function than extrinsic regulators like PGI_2 and NO. However, it seems likely that these interpretations could differ in magnitude depending upon the context under which the hemostatic measurements are made. Nonetheless, this is not altogether surprising as the two groups of regulators are operating at very different stages of hemostatic platelet activation: while the extrinsic regulators are poised to prevent platelet activation under basal conditions, RGS proteins are positioned to limit the extent of activation once it is under way.

In addition to these extrinsic negative regulators, there are also additional intrinsic regulators. RASA3, a GTPase activating protein for the small GTPase RAP1, limits the extent of platelet aggregation by downregulating RAP1-GTP, which promotes activation of $\alpha_{IIb}\beta_3$ integrin. Stefanini *et al* present evidence that RASA3 is normally inhibited by $G_{i2}\alpha$-mediated PI3K activation and that a hypomorphic RASA3 variant with drastically reduced expression and GAP function has shortened platelet survival resulting in severe thrombocytopenia.[129] This further supports the notion that platelets encounter stimulating agonists, in this case ADP, under basal conditions and that there are negative regulatory mechanisms in place to prevent preactivation and clearance. The authors also present evidence that integrin activation in the hypomorph is enhanced in response to ADP, but they do not show the potential hemostatic effects *ex vivo* or *in vivo* for the hypomorph in isolation. Therefore, it is unclear how this mode of regulation alone impacts hemostatic platelet function. We can hypothesize, however, that it would not be as important as RGS proteins, because

it is further downstream in the signaling network. Furthermore, its function is downregulated during hemostasis, whereas we have no evidence that this is true for RGS proteins.

As a further confirmation of the importance of regulating ADP-mediated signaling under basal and hemostatic conditions, we can examine the ecto-apyrase, CD39. CD39 is expressed on the surface of endothelial cells and converts both ATP and ADP to AMP.[1] Peripheral platelet counts in $CD39^{-/-}$ mice are ~20% lower than controls, but the precise mechanisms of this decrease were not determined.[172] From our results and those presented previously, though, we can hypothesize that excessive ADP in circulation would lead to increased activation of platelets and subsequent clearance. However, the degree of thrombocytopenia is far more severe in the RASA3 hypomorph, which may suggest that sensitivity to ADP is more critical to regulating platelet survival than absolute quantities of ADP. Our own results support this, since platelet counts in the $RGS10^{-/-}18^{-/-}$ mice are reduced to a greater degree than $CD39^{-/-}$ mice, and RGS proteins modulate ADP sensitivity via regulation of G_q-coupled $P2Y_1$ and G_{i2}-coupled $P2Y_{12}$. Paradoxically, bleeding times and ferric chloride-induced thrombosis were prolonged in $CD39^{-/-}$ mice, rather than shortened. However, the authors present evidence suggesting that this is due to desensitization of P2Y receptors in response to constant stimulation, thus effectively reducing ADP-mediated signaling.[172] Therefore, it is readily apparent that careful regulation of ADP-mediated signaling, both intrinsically and extrinsically, is important for maintaining normal basal and hemostatic platelet function.

Clearly, platelets possess numerous negative regulatory mechanisms, operating at various stages of platelet activation and having varied impacts on platelet survival, hemostatic potential, thrombotic risk. This lends further support to the idea that platelet signaling networks, under normal circumstances, are in a delicate balance between activating and inhibitory pathways and that perturbing this balance can have dramatic effects. We can only speculate as to why this exquisitely sensitive system has evolved, but it is likely due the specific nature of the primary hemostatic role of platelets. Under basal conditions, platelets need to constantly patrol the circulation for insults. In doing so, they are likely encountering numerous mechanical and biochemical stimuli. Without a

variety of negative regulators in place to prevent it, these stimuli would presumably result in platelet preactivation and premature clearance. On the other hand, platelets need to be ready to spring into action at a moment's notice to prevent excessive bleeding in response to injury. As such, they need to be extremely sensitive to the appropriate stimuli under the proper circumstances to be maximally effective. However, in the absence of negative regulators, such as RGS proteins, an excessive hemostatic response could quickly turn into pathological thrombosis. Therefore, negative regulators of platelet signaling preserve an optimal balance between activation and inhibition, both under basal and hemostatic settings, to prevent preactivation and hyperactivation, respectively.

CHAPTER 7: Future Directions

7.1 Phosphorylation of RGS10 and effects on GPCR-mediated platelet function

Our results suggest that RGS10 is phosphorylated in response to agonist stimulation in human platelets and that this phosphorylation may impact interactions with Gα subunits (see Chapter 2). However, we have yet to determine the precise site(s) of phosphorylation or the functional impact of these phosphorylation events with respect to platelet function. Efforts to isolate substantial quantities of endogenous RGS10 from human platelets using either immunoprecipitation or Halo-$G_{i2}\alpha$ pull down have not proven viable. Furthermore, we have not had success detecting agonist-mediated phosphorylation of recombinantly overexpressed RGS10 in cultured cell lines. However, we do have evidence to suggest that the kinases responsible for phosphorylation may be novel and/or conventional isoforms of protein kinase C. Therefore, it may be possible to perform *in vitro* phosphorylation studies using purified Halo-RGS10 (which we have already generated) and one or more of the six PKC isoforms reportedly expressed in human platelets.[173] However, the main pitfall of this approach is that in the absence of cellular trafficking, localization, and inhibition mechanisms, phosphorylation may occur indiscriminately and at sites that bear no physiological relevance.

A more complicated, although arguably more robust approach, would involve using CRISPR-Cas9 to introduce a purification tag into endogenous RGS10 in human inducible pluripotent stem cells (iPSCs).[174,175] A tag like SpyTag, engineered by splitting a bacterial fibronectin-binding protein, would be ideal since its small size (13 amino acids) is unlikely to perturb protein function and easier to insert via genome-editing techniques, and it covalently binds to its bait (133 amino acid SpyCatcher) to allow robust capture and high purity.[176] Furthermore, a cleavable linker, such as the tobacco etch virus (TEV) protease recognition sequence consisting of an additional 7 amino acids, could be appended for elution while minimally increasing the size of the tag.[177] The iPSCs can then be differentiated into megakaryocytes, induced to generate functional platelets, and assessed for agonist-mediated RGS10 phosphorylation as described for

patient-isolated platelets.[178] Finally, the protein could be isolated using a SpyCatcher-coupled substrate, such as magnetic beads, and eluted using TEV protease for mass spectrometry analysis to identify the sites of phosphorylation.[179] The main limitation of this approach would likely be low yields of functional platelets. However, mass spectrometry can be extremely sensitive, requiring only femtomolar quantities of protein if sufficiently enriched.[180]

Once the phosphorylation sites have been identified, we could similarly employee CRISPR-Cas9 to mutate phosphorylated residues to either phosphoresistant (such as alanine) or phosphomimetic (serine to aspartic acid, for example) residues. Lastly, following generation of platelets, we could assess the impact of these mutations on the hemostatic function using flow cytometry. An increase in the GPCR-mediated activation response of a phosphoresistant mutant would suggest that phosphorylation of that residue inhibits RGS10 function. Conversely, a decrease in response would indicate that phosphorylation enhances RGS10 function. Using these methods, the nature of RGS10 phosphorylation and the functional consequences could be systematically assessed in human platelets.

7.2 Mechanisms of RGS10$^{-/-}$RGS18$^{-/-}$ platelet clearance

While we have evidence to suggest that platelet clearance in RGS10$^{-/-}$18$^{-/-}$ mice is a result of premature platelet activation in circulation (see Chapter 3), the mechanisms that mediate this clearance remain elusive. Annexin V staining was normal for RGS10$^{-/-}$18$^{-/-}$ mice, suggesting normal phosphatidylserine (PS) exposure. During apoptosis, platelets, like many other cells, undergo membrane redistribution, whereby PS translocates from the inner to outer membrane.[181] Exposed PS is a molecular signal for phagocytosis and clearance by macrophages.[182] However, annexin V may not be the most sensitive marker for smaller changes in PS exposure. Studies suggest that lactadherin, a PS-binding protein produced by macrophages, can detect apoptotic cells earlier and with more sensitivity than annexin V.[183,184] Thus, additional studies to stain RGS10$^{-/-}$18$^{-/-}$ platelets with fluorescently labelled lactadherin may provide evidence of increased apoptosis. Alternatively, it is possible that PS$^{(+)}$ platelets are cleared so rapidly that we are only able to detect the PS$^{(-)}$

RGS10$^{-/-}$18$^{-/-}$ platelets that remain. To address these concerns, one could specifically deplete macrophages *in vivo* using clodronate liposomes. Clodronate is a hydrophilic bisphosphonate toxic to cells in high concentrations and liposomes allow for encapsulation of this molecule for drug delivery, where it is subsequently phagocytosed by macrophages.[185] Several reports have shown improved platelet counts in mice bearing clearance-enhancing mutations,[186-188] so it is quite possible that this would hold true for RGS10$^{-/-}$18$^{-/-}$ mice as well. How, though, might these two seemingly disparate pathways, platelet activation and apoptosis, be interconnected? One report indicates that PKA activity is negatively correlated with apoptosis in platelets.[189] Since both G_q signaling, via phosphodiesterase activation,[190] and G_{i2} signaling, via adenylate cyclase inhibition,[191] are both involved in reducing cAMP levels, enhanced signaling in the absence of RGS proteins could therefore theoretically reduce PKA activity and promote apoptosis.

We have also presented evidence indicating that desialylation, as assessed by the binding of RCA-I lectin, was normal in RGS10$^{-/-}$18$^{-/-}$ mice, suggesting recognition of desialylated platelets by hepatic Ashwell-Morell receptors is not likely to explain the reduced survival.[192] However, desialylated glycans expose β-galactose, which can then be removed via β-galactosidases to expose β-N-acetylglucosamine (βGlcNAc).[193] βGlcNAc is recognized by integrin $\alpha_M\beta_2$ on the surface of liver macrophages and leads to phagocytosis and clearance of chilled platelets.[194] Furthermore, β-galactosidases are reportedly stored in platelet granules and mobilized to the surface of aged platelets.[195] Thus, it is possible that RGS deletion results in enhanced granule release, β-galactosidase surface expression, βGlcNAc exposure and $\alpha_M\beta_2$-mediated macrophage phagocytosis. This would not necessarily be inconsistent with our results, since RCA-I binds preferentially to β-galactose, but not sialic acid or βGlcNAc. Therefore, using a lectin specific to βGlcNAc could reveal differences between RGS10$^{-/-}$18$^{-/-}$ and control platelets. And as above, if the platelets are being cleared too quickly to detect, clodronate liposomes could be employed *in vivo*, since both processes are similarly macrophage dependent.

7.3 Candidate RGS-insensitive $G_q\alpha$ mutations

Our results suggest that the G188S RGS-insensitive mutation in $G_q\alpha$ impacts not only RGS interactions and function, but also PLCβ, the primary $G_q\alpha$ effector. We have also shown, using structural and computational methods, that the overlap between the binding interfaces of RGS proteins and effectors on the surface of $G_q\alpha$ is considerable, raising concerns about the viability of an RGS-insensitive mutation that maintains primary $G_q\alpha$ signaling functionality. However, using a systematic predictive approach, we have identified several candidate mutations that are reasonably likely to impact RGS interactions without affecting PLCβ and other effectors (see Chapter 4). How, then, might one evaluate these mutations to overcome the limitations of the original recombinant CHO-cell based method?

First, careful consideration should be given to the cell type being used. While CHO cells are easily transfected for overexpression of recombinant proteins,[196] the expression profile of endogenous proteins as well as their exact composition may differ considerably from human (or mouse) platelets. Furthermore, the use of cell lines or primary platelets is limited because platelets are anucleate and therefore cannot be expanded in cell culture or easily manipulated genetically. However, the use of induced pluripotent stem cell (iPSC)-derived megakaryocytes provides a promising approach for studying the effects of candidate RGS-insensitive mutations in subsequently derived human platelets.[178]

The second consideration involves endogenous protein expression. While overexpressing proteins is simple and straightforward, it may not accurately reflect the effects of mutation within a physiological context. To overcome this, targeting and genetic modification of specific endogenous genes can be employed, using techniques such as CRISPR-Cas9 genome-editing.[98] Fortunately, this technique has been used within the context of iPSCs for genome-editing and is routinely employed by the Children's Hospital of Pennsylvania Human Pluripotent Stem Cell core.[197] By precisely editing individual nucleotides within the $G_q\alpha$ gene, one can induce specific candidate RGS-insensitive mutations that would be present at endogenous levels in the resultant platelets.

Finally, care should be taken when deciding appropriate methods to be used to assess the functional consequences of mutation in platelets. While generating platelets from iPSC-derived megakaryocytes is useful, yields are generally quite low. Thus, traditional methods, such as aggregometry, may not be viable without the use of large-scale culturing resources. However, single cell methods, such as flow cytometry, can overcome these challenges since relatively few cells are required for analysis. In the case of RGS-resistant mutations in $G_q\alpha$, measuring P-selectin exposure or $\alpha_{IIb}\beta_3$ integrin activation would be a useful measurement of function, since these are largely G_q-driven processes. Furthermore, inhibitors of G_i signaling, such as Pertussis toxin, could be employed to minimize RGS:G_i effects as a confounding factor.[198] A successful RGS-insensitive mutation in $G_q\alpha$ would be expected to enhance the measurable responses outlined above, much as we have seen in our RGS knockout mouse models. An unsuccessful RGS-insensitive mutation would have no effect on response (neutral mutation) or a decreased response (likely due to disrupted PLCβ interactions). To further confirm the findings of these experiments, immunoprecipitation for WT or mutant $G_q\alpha$ could be performed to measure effects on protein interactions.

7.4 Function and RGS expression of RGS10 and RGS18 variant platelets

To improve our understanding of RGS-mediated platelet regulation in humans, we have identified 16 predicted loss-of-function variants in RGS10 and RGS18 within 101 individuals who have submitted samples to the Penn Medicine Biobank (see Chapter 5). Our goal is to determine how these mutations functionally impact platelet activation, RGS expression and platelet hemostatic potential.

To determine impacts on platelet activation from patients, we will isolate platelets from whole blood and measure activation in response to GPCR-activating agonists via flow cytometry (as outlined in 7.2). We will also perform similar studies on controls that have been matched by age, gender, ethnicity and, if possible, use of medications expected to impact platelet activation (such as aspirin).

RGS expression levels will be determined using commercially available enzyme-linked immunosorbent assays (ELISA) for human RGS10 and RGS18. Use of standard curves with recombinant protein and the sensitivity of ELISA allows for the precise quantification of low levels of endogenous protein. While missense mutations would not necessarily be expected to alter expression levels, frameshifts and stopgains might and we predict that total RGS levels will negatively correlate with platelet activating potential.

Finally, since we do not yet have a way of assessing human platelet function *in vivo*, we will use CRISPR-Cas9 to induce candidate mutations in iPSCs (as outlined in 7.2) for the generation of RGS variant megakaryocytes. These megakaryocytes will then be injected into immunocompromised NOD-*scid*-IL-2Rγ^{null} (NSG) mice[199] that also express a von Willebrand factor variant (R1326H or VWF$^{RH/RH}$) that can bind to human GPIbα on human platelets, but not mouse GPIbα.[200,201] The double transgenic mice were developed by Morty Poncz at Children's Hospital of Philadelphia using CRISPR/Cas9 to induce the VWF R1326H mutation in NSG mice.[202] Megakaryocytes produced in this manner lodge in the lungs after intravenous injection, releasing sufficient platelets to account for 5-10% of the circulating platelet pool in the mice.[203] Even though human platelets are a minority in this model, they have a competitive advantage over the mouse platelets, which are unable to bind to VWF^{RH}. Therefore, this method provides us with a novel way to study the *in vivo* hemostatic effects of mutations in human megakaryocytes and their derived platelets following a mouse cremaster laser injury, as first described in Chapter 2.

BIBLIOGRAPHY

1. Marcus AJ, Broekman MJ, Drosopoulos JH, et al. The endothelial cell ecto-ADPase responsible for inhibition of platelet function is CD39. *Journal of Clinical Investigation*. 1997;99(6):1351-1360.

2. Wang G-R, Zhu Y, Halushka PV, Lincoln TM, Mendelsohn ME. Mechanism of platelet inhibition by nitric oxide: In vivo phosphorylation of thromboxane receptor by cyclic GMP-dependent protein kinase. *Proceedings of the National Academy of Sciences*. 1998;95:4888-4893.

3. Weiss HJ, Turitto VT. Prostacyclin (prostaglandin I2, PGI2) inhibits platelet adhesion and thrombus formation on subendothelium. *Blood*. 1979;53(2):244-250.

4. Yip J, Shen Y, Berndt MC, Andrews RK. Primary Platelet Adhesion Receptors. *IUBMB Life*. 2005;57(1):103-108.

5. Grüner S, Prostredna M, Schulte V, et al. Multiple integrin-ligand interactions synergize in shear-resistant platelet adhesion at sites of arterial injury in vivo. *Blood*. 2003;102(12):4021-4027.

6. Stalker TJ, Newman DK, Ma P, Wannemacher KM, Brass LF. Platelet Signaling. In: Gresela P, Born GVR, Patrono C, Page CP, eds. Handbook of Experimental Pharmacology: Antiplatelet Agents. Vol. 210: Springer; 2010:60-80.

7. Brass LF. Thrombin and Platelet Activation. *Chest*. 2003;124(3):18S-25S.

8. Smith SA, Travers RJ, Morrissey JH. How it all starts: Initiation of the clotting cascade. *Crit Rev Biochem Mol Biol*. 2015;50(4):326-336.

9. Bolton-Maggs PHB, Pasi KJ. Haemophilias A and B. *Lancet*. 2003;361:1801-1809.

10. Nurden AT. Platelet Membrane Glycoproteins: A Historical Review. *Seminars in Thrombosis and Hemostasis*. 2014;40:577-584.

11. Nigel M. Triggers, targets and treatments for thrombosis. *Nature*. 2008;451:914-918.

12. Badimon L, Vilahur G. Thrombosis formation on atherosclerotic lesions and plaque rupture. *Journal of Internal Medicine*. 2014;276:618-632.

13. Vilahur G, Badimon JJ, Bugiardini R, Badimon L. Perspectives: The burden of cardiovascular risk factors and coronary heart disease in Europe and worldwide. *European Heart Journal Supplements*. 2014;16:A7-A11.

14. Gibbins JM, Okuma M, Farndale R, Barnes M, Watson SP. Glycoprotein VI is the collagen receptor in platelets which underlies tyrosine phosphorylation of the Fc receptor γ-chain. *FEBS Lett*. 1997;413(2):255-259.

15. Watson SP, Asazuma N, Atkinson B, et al. The role of ITAM- and ITIM-coupled receptors in platelet activation by collagen. *Thrombosis and haemostasis*. 2001;86(1):276-288.

16. Siess W. Molecular mechanisms of platelet activation. *Physiol Rev*. 1989;69(1):58-178.

17. Heemskerk J, Harper MT, Cosemans J, Poole AW. Unravelling the different functions of protein kinase C isoforms in platelets. *FEBS Lett*. 2011;585(12):1711-1716.

18. Varga-Szabo D, Braun A, Nieswandt B. Calcium signaling in platelets. *Journal of Thrombosis and Haemostasis*. 2009;7(7):1057-1066.

19. Hilger D, Masureel M, Kobilka BK. Structure and dynamics of GPCR signaling complexes. *Nat Struct Mol Biol*. 2018;25(1):4-12.

20. Hamm HE. The Many Faces of G Protein Signaling. *Journal of Biological Chemistry*. 1998;273(2):669-672.

21. Angiolillo DJ, Fernandez-Ortiz A, Bernardo E, et al. Variability in Individual Responsiveness to Clopidogrel Clinical Implications, Management, and Future Perspectives. *J Am Coll Cardiol*. 2007;49(14):1505-1516.

22. Kamato D, Mitra P, Davis F, et al. Gaq proteins: molecular pharmacology and therapeutic potential. *Cell Mol Life Sci*. 2016;74(8):1379-1390.

23. Siehler S. Regulation of RhoGEF proteins by G12/13-coupled receptors. *Br J Pharmacol*. 2009;158(1):41-49.

24. Klages B, Brandt U, Simon MI, Schultz G, Offermanns S. Activation of G12/G13 Results in Shape Change and Rho/Rho-Kinase–mediated Myosin Light Chain Phosphorylation in Mouse Platelets. *The Journal of Cell Biology*. 1999;144(4):745-754.

25. Procter NEK, Hurst NL, Nooney VB, et al. New Developments in Platelet Cyclic Nucleotide Signalling: Therapeutic Implications. *Cardiovascular Drugs and Therapy*. 2016;30(5):505-513.

26. Smolenski A. Novel roles of cAMP/cGMP-dependent signaling in platelets. *Journal of Thrombosis and Haemostasis*. 2012;10(2):167-176.

27. Koelle MR. A new family of G-protein regulators — the RGS proteins. *Curr Opin Cell Biol*. 1997;9(2):143-147.

28. He W, Cowan CW, Wensel TG. RGS9, a GTPase accelerator for phototransduction. *Neuron*. 1998;20(1):95-102.

29. Tesmer JJ, Berman DM, Gilman AG, Sprang SR. Structure of RGS4 bound to AlF4--activated G(i alpha1): stabilization of the transition state for GTP hydrolysis. *Cell*. 1997;89(2):251-261.

30. Gamblin SJ, Smerdon SJ. GTPase-activating proteins and their complexes. *Curr Opin Struct Biol*. 1998;8(2):195-201.

31. Stewart A, Fisher RA. Progress in Molecular Biology and Translational Science. *Progress in molecular biology and translational science*. 2015;133:1-11.

32. Siderovski DP, Willard FS. The GAPs, GEFs, and GDIs of heterotrimeric G-protein alpha subunits. *International journal of biological sciences*. 2005;1(2):51-66.

33. Jones TLZ. Role of Palmitoylation in RGS Protein Function. *Methods Enzymol*. 2004;389:33-55.

34. Cornell RB, Taneva SG. Current Protein and Peptide Science. Vol. 7 (ed 6); 2006.

35. Snow BE, Krumins AM, Brothers GM, et al. A G protein gamma subunit-like domain shared between RGS11 and other RGS proteins specifies binding to Gbeta5 subunits. *Proceedings of the National Academy of Sciences of the United States of America*. 1998;95(22):13307-13312.

36. Consonni SV, Maurice MM, Bos JL. DEP domains: structurally similar but functionally different. *Nature Reviews Molecular Cell Biology*. 2014;15(5):357-362.

37. Kimple RJ, Vries LD, Tronchère H, et al. RGS12 and RGS14 GoLoco Motifs Are GαiInteraction Sites with Guanine Nucleotide Dissociation Inhibitor Activity. *Journal of Biological Chemistry*. 2001;276(31):29275-29281.

38. Willard MD, Willard FS, Li X, Cappell SD, Snider WD, Siderovski DP. Selective role for RGS12 as a Ras/Raf/MEK scaffold in nerve growth factor-mediated differentiation. *The EMBO Journal*. 2007;26(8):2029-2040.

39. Schiff ML, Siderovski DP, Jordan JD, et al. Tyrosine-kinase-dependent recruitment of RGS12 to the N-type calcium channel. *Nature*. 2000;408(6813):723-727.

40. Snow BE, Hall RA, Krumins AM, et al. GTPase Activating Specificity of RGS12 and Binding Specificity of an Alternatively Spliced PDZ (PSD-95/Dlg/ZO-1) Domain. *Journal of Biological Chemistry*. 1998;273(28):17749-17755.

41. Zeiler M, Moser M, Mann M. Copy Number Analysis of the Murine Platelet Proteome Spanning the Complete Abundance Range. *Mol Cell Proteomics*. 2014;13(12):3435-3445.

42. Rowley JW, Oler AJ, Tolley ND, et al. Genome-wide RNA-seq analysis of human and mouse platelet transcriptomes. *Blood*. 2011;118(14):e101-e111.

43. Burkhart JM, Vaudel M, Gambaryan S, et al. The first comprehensive and quantitative analysis of human platelet protein composition allows the comparative analysis of structural and functional pathways. *Blood*. 2012;120(15):e73-e82.

44. Iwai K, Koike M, Ohshima S, et al. RGS18 Acts as a Negative Regulator of Osteoclastogenesis by Modulating the Acid-Sensing OGR1/NFAT Signaling Pathway. *J Bone Miner Res*. 2007;22(10):1612-1620.

45. Yowe D, Weich N, Prabhudas M, et al. RGS18 is a myeloerythroid lineage-specific regulator of G-protein-signalling molecule highly expressed in megakaryocytes. *Biochemical Journal*. 2001;359(1):109-118.

46. Gagnon AW, Murray DL, Leadley RJ. Cloning and characterization of a novel regulator of G protein signalling in human platelets. *Cellular Signalling*. 2002;14(7):595-606.

47. Soundararajan M, Willard FS, Kimple AJ, et al. Structural diversity in the RGS domain and its interaction with heterotrimeric G protein alpha-subunits. *Proceedings of the National Academy of Sciences of the United States of America*. 2008;105(17):6457-6462.

48. Yang S, Li Y-PP. RGS10-null mutation impairs osteoclast differentiation resulting from the loss of [Ca2+]i oscillation regulation. *Genes Dev*. 2007;21(14):1803-1816.

49. Hooks SB, Callihan P, Altman MK, Hurst JH, Ali MW, Murph MM. Regulators of G-Protein signaling RGS10 and RGS17 regulate chemoresistance in ovarian cancer cells. *Mol Cancer*. 2010;9:289.

50. García-Bernal D, Dios-Esponera A, Sotillo-Mallo E, García-Verdugo R, Arellano-Sánchez N, Teixidó J. RGS10 restricts upregulation by chemokines of T cell adhesion mediated by α4β1 and αLβ2 integrins. *J Immunol*. 2011;187(3):1264-1272.

51. Alqinyah M, Maganti N, Ali MW, et al. Regulator of G-protein Signaling 10 (RGS10) expression is transcriptionally silenced in activated microglia by histone deacetylase activity. *Mol Pharmacol*. 2016;91(3):197-207.

52. Miao R, Lu Y, Xing X, et al. Regulator of G-Protein Signaling 10 Negatively Regulates Cardiac Remodeling by Blocking Mitogen-Activated Protein Kinase–Extracellular Signal-Regulated Protein Kinase 1/2 Signaling. *Hypertension*. 2018;67(1):86-98.

53. Lee J-KK, Tansey MGG. Physiology of RGS10 in Neurons and Immune Cells. *Progress in molecular biology and translational science*. 2015;133:153-167.

54. Hunt TW, Fields TA, Casey PJ, Peralta EG. RGS10 is a selective activator of G alpha i GTPase activity. *Nature*. 1996;383(6596):175-177.

55. Tu Y, Popov S, Slaughter C, Ross EM. Palmitoylation of a conserved cysteine in the regulator of G protein signaling (RGS) domain modulates the GTPase-activating activity of RGS4 and RGS10. *The Journal of biological chemistry*. 1999;274(53):38260-38267.

56. Burgon PG, Lee WL, Nixon AB, Peralta EG, Casey PJ. Phosphorylation and Nuclear Translocation of a Regulator of G Protein Signaling (RGS10). *Journal of Biological Chemistry*. 2001;276(35):32828-32834.

57. Altman MK, Alshamrani AA, Jia W, et al. Suppression of the GTPase-activating protein RGS10 increases Rheb-GTP and mTOR signaling in ovarian cancer cells. *Cancer Lett*. 2015;369(1):175-183.

58. Alqinyah M, Maganti N, Ali MW, et al. Regulator of G-protein Signaling 10 (RGS10) expression is transcriptionally silenced in activated microglia by histone deacetylase activity. *Molecular Pharmacology*. 2016;91(3):mol.116.106963.

59. Alqinyah M, Almutairi F, Wendimu MY, Hooks S. RGS10 regulates the expression of Cyclooxygenase-2 and Tumor Necrosis Factor alpha through a G-protein-independent mechanism. *Molecular Pharmacology*. 2018;94(4):mol.118.111674.

60. Morse HC. Building a Better Mouse: One Hundred Years of Genetics and Biology. The Mouse in Biomedical Research. Vol. 1; 2007:1-11.

61. Delesque-Touchard N, Pendaries C, Volle-Challier C, et al. Regulator of G-Protein Signaling 18 Controls Both Platelet Generation and Function. *PLoS ONE*. 2014;9(11):e113215.

62. Alshbool FZ, Karim ZA, Vemana H, Conlon C, Lin OA, Khasawneh FT. The regulator of G-protein signaling 18 regulates platelet aggregation, hemostasis and thrombosis. *Biochemical and Biophysical Research Communications*. 2015;462(4):378-382.

63. Hensch NR, Karim ZA, Druey KM, Tansey MGG, Khasawneh FT. RGS10 Negatively Regulates Platelet Activation and Thrombogenesis. *PloS one*. 2016;11(11):e0165984.

64. Ma P, Gupta S, Sampietro S, et al. RGS10 shapes the hemostatic response to injury through its differential effects on intracellular signaling by platelet agonists. *Blood Advances*. 2018;2(16):2145-2155.

65. Kaur K, Kehrl JM, Charbeneau RA, Neubig RR. RGS-insensitive Gα subunits: probes of Gα subtype-selective signaling and physiological functions of RGS proteins. *Methods in molecular biology (Clifton, NJ)*. 2011;756:75-98.

66. Huang X, Fu Y, Charbeneau RA, et al. Pleiotropic Phenotype of a Genomic Knock-In of an RGS-Insensitive G184S Gnai2 Allele. *Mol Cell Biol*. 2006;26(18):6870-6879.

67. Signarvic RS, Cierniewska A, Stalker TJ, et al. RGS/Gi2alpha interactions modulate platelet accumulation and thrombus formation at sites of vascular injury. *Blood*. 2010;116(26):6092-6100.

68. DiBello PR, Garrison T, Apanovitch DM, et al. Selective Uncoupling of RGS Action by a Single Point Mutation in the G Protein α-Subunit. *Journal of Biological Chemistry*. 1998;273(10):5780-5784.

69. García A, Prabhakar S, Hughan S, et al. Differential proteome analysis of TRAP-activated platelets: involvement of DOK-2 and phosphorylation of RGS proteins. *Blood*. 2004;103(6):2088-2095.

70. Gegenbauer K, Elia G, Blanco-Fernandez A, Smolenski A. Regulator of G-protein signaling 18 integrates activating and inhibitory signaling in platelets. *Blood*. 2012;119(16):3799-3807.

71. Gegenbauer K, Nagy Z, Smolenski A. Cyclic nucleotide dependent dephosphorylation of regulator of G-protein signaling 18 in human platelets. *PloS one*. 2013;8(11):e80251.

72. Allen PB, Ouimet CC, Greengard P. Spinophilin, a novel protein phosphatase 1 binding protein localized to dendritic spines. *Proceedings of the National Academy of Sciences of the United States of America*. 1997;94(18):9956-9961.

73. Wang X, Zeng W, Soyombo AA, et al. Spinophilin regulates Ca2+ signalling by binding the N-terminal domain of RGS2 and the third intracellular loop of G-protein-coupled receptors. *Nature Cell Biology*. 2005;7(4):405-411.

74. Ma P, Cierniewska A, Signarvic R, et al. A newly identified complex of spinophilin and the tyrosine phosphatase, SHP-1, modulates platelet activation by regulating G protein-dependent signaling. *Blood*. 2012;119(8):1935-1945.

75. Ma P, Ou K, Sinnamon AJ, Jiang H, Siderovski DP, Brass LF. Modulating platelet reactivity through control of RGS18 availability. *Blood*. 2015;126(24):2611-2620.

76. Zambrowicz BP, Friedrich GA, Buxton EC, Lilleberg SL, Person C, Sands AT. Disruption and sequence identification of 2,000 genes in mouse embryonic stem cells. *Nature*. 1998;392(6676):608-611.

77. Lee J-K, McCoy MK, Harms AS, Ruhn KA, Gold SJ, Tansey MG. Regulator of G-Protein Signaling 10 Promotes Dopaminergic Neuron Survival via Regulation of the Microglial Inflammatory Response. *The Journal of Neuroscience*. 2008;28(34):8517-8528.

78. Stalker TJ, Traxler EA, Wu J, Blood W-KM. Hierarchical organization in the hemostatic response and its relationship to the platelet-signaling network. *Blood*. 2013;121(10):1875-1885.

79. Tutwiler V, Litvinov RI, Lozhkin AP, et al. Kinetics and mechanics of clot contraction are governed by the molecular and cellular composition of the blood. *Blood*. 2016;127(1):149-159.

80. Ramanathan G, Gupta S, Thielmann I, et al. Defective diacylglycerol-induced Ca2+entry but normal agonist-induced activation responses in TRPC6-deficient mouse platelets. *J Thromb Haemost*. 2012;10(3):419-429.

81. Gupta S, Braun A, Morowski M, et al. CLP36 is a negative regulator of glycoprotein VI signaling in platelets. *Circ Res*. 2012;111(11):1410-1420.

82. Shen J, Sampietro S, Wu J, et al. Coordination of platelet agonist signaling during the hemostatic response in vivo. *Blood Advances*. 2017;1(27):2767-2775.

83. Welsh JD, Colace TV, Muthard RW, Stalker TJ, Brass LF, Diamond SL. Platelet-targeting sensor reveals thrombin gradients within blood clots forming in microfluidic assays and in mouse. *Journal of Thrombosis and Haemostasis*. 2012;10(11):2344-2353.

84. Law DA, DeGuzman FR, Heiser P, Ministri-Madrid K, Killeen N, Phillips DR. Integrin cytoplasmic tyrosine motif is required for outside-in alphaIIbbeta3 signalling and platelet function. *Nature*. 1999;401(6755):808-811.

85. Stalker TJ, Welsh JD, Tomaiuolo M, et al. A systems approach to hemostasis: 3. Thrombus consolidation regulates intrathrombus solute transport and local thrombin activity. *Blood*. 2014;124(11):1824-1831.

86. Hathaway DR, Adelstein RS. Human platelet myosin light chain kinase requires the calcium-binding protein calmodulin for activity. *Proceedings of the National Academy of Sciences*. 1979;76(4):1653-1657.

87. Garcia A, Kim S, Bhavaraju K, Schoenwaelder SM, Kunapuli SP. Role of phosphoinositide 3-kinase β in platelet aggregation and thromboxane A2 generation mediated by Gi signalling pathways. *Biochemical Journal*. 2010;429(2):369-377.

88. Kim S, Jin J, Kunapuli SP. Akt Activation in Platelets Depends on Gi Signaling Pathways. *Journal of Biological Chemistry*. 2004;279(6):4186-4195.

89. Abrams CS, Zhang J, Downes CP, Tang X-w, Zhao W, Rittenhouse SE. Phosphopleckstrin Inhibits Gβγ-activable Platelet Phosphatidylinositol-4,5-bisphosphate 3-Kinase. *Journal of Biological Chemistry*. 1996;271(41):25192-25197.

90. Lee JK, Chung J, Druey KM, Tansey MG. RGS10 exerts a neuroprotective role through the PKA/c-AMP response-element (CREB) pathway in dopaminergic neuron-like cells. *J Neurochem*. 2012;122(2):333-343.

91. Pomel V, Klicic J, Covini D, et al. Furan-2-ylmethylene Thiazolidinediones as Novel, Potent, and Selective Inhibitors of Phosphoinositide 3-Kinase γ. *J Med Chem*. 2006;49(13):3857-3871.

92. Kase H, Iwahashi K, Nakanishi S, et al. K-252 compounds, novel and potent inhibitors of protein kinase C and cyclic nucleotide-dependent protein kinases. *Biochemical and Biophysical Research Communications*. 1987;142(2):436-440.

93. Hennequin LF, Allen J, Breed J, et al. N -(5-Chloro-1,3-benzodioxol-4-yl)-7-[2-(4-methylpiperazin-1-yl)ethoxy]-5- (tetrahydro-2 H -pyran-4-yloxy)quinazolin-4-amine, a Novel, Highly Selective, Orally Available, Dual-Specific c-Src/Abl Kinase Inhibitor †. *J Med Chem*. 2006;49(22):6465-6488.

94. Toullec D, Pianetti P, Coste H, et al. The bisindolylmaleimide GF 109203X is a potent and selective inhibitor of protein kinase C. *The Journal of biological chemistry*. 1991;266(24):15771-15781.

95. Ryves WJ, Evans AT, Olivier AR, Parker PJ, Evans FJ. Activation of the PKC-isotypes α, β 1 , γ, δ, and ε by phorbol esters of different biological activities. *FEBS Lett*. 1991;288(1-2):5-9.

96. Mellor H, Parker PJ. The extended protein kinase C superfamily. *Biochemical Journal*. 1998;332(2):281-292.

97. Henao-Mejia J, Williams A, Rongvaux A, Stein J, Hughes C, Flavell RA. Generation of Genetically Modified Mice Using the CRISPR-Cas9 Genome-Editing System. *Cold Spring Harb Protoc*. 2016:doi:10.1101/pdb.prot090704.

98. Ran FA, Hsu PD, Wright J, Agarwala V, Scott DA, Zhang F. Genome engineering using the CRISPR-Cas9 system. *Nature Protocols*. 2013;8:2281.

99. Capitano M, Zhao L, Cooper S, et al. Phosphatidylinositol transfer proteins regulate megakaryocyte TGF-β1 secretion and hematopoiesis in mice. *Blood*. 2018;132(10):1027-1038-1038.

100. Alshbool FZ, Karim ZA, Vemana HP, Conlon C, Lin OA, Khasawneh FT. The regulator of G-protein signaling 18 regulates platelet aggregation, hemostasis and thrombosis. *Biochem Biophys Res Commun*. 2015;462(4):378-382.

101. Delesque-Touchard N, Pendaries C, Volle-Challier C, et al. Regulator of G-protein signaling 18 controls both platelet generation and function. *PLoS One*. 2014;9(11):e113215.

102. Ma P, Gupta S, Sampietro S, et al. RGS10 shapes the hemostatic response to injury through its differential effects on intracellular signaling by platelet agonists. *Blood Adv*. 2018;2(16):2145-2155.

103. Berman CL, Yeo EL, Wencel-Drake JD, Furie BC, Ginsberg MH, Furie B. A platelet alpha granule membrane protein that is associated with the plasma membrane after activation. Characterization and subcellular localization of platelet activation-dependent granule-external membrane protein. *J Clin Invest*. 1986;78(1):130-137.

104. Hsu-Lin S, Berman CL, Furie BC, August D, Furie B. A platelet membrane protein expressed during platelet activation and secretion. Studies using a monoclonal antibody specific for thrombin-activated platelets. *J Biol Chem*. 1984;259(14):9121-9126.

105. Bertoni A, Tadokoro S, Eto K, of Biological … P-N. Relationships between Rap1b, affinity modulation of integrin αIIbβ3, and the actin cytoskeleton. *J Biol Chem*. 2002;277(28):25715–25721.

106. Shen J, Sampietro S, Wu J, et al. Coordination of platelet agonist signaling during the hemostatic response in vivo. *Blood Adv*. 2017;1(27):2767-2775.

107. Da Q, Derry PJ, Lam FW, Rumbaut RE. Fluorescent labeling of endogenous platelets for intravital microscopy: Effects on platelet function. *Microcirculation*. 2018;25(6):e12457.

108. Lee LG, Chen CH, Chiu LA. Thiazole orange: A new dye for reticulocyte analysis. *Cytometry*. 1986;7(6):508-517.

109. Smith CW, Raslan Z, Parfitt L, et al. TREM-like transcript 1: a more sensitive marker of platelet activation than P-selectin in humans and mice. *Blood Adv*. 2018;2(16):2072-2078.

110. Washington VA, Schubert RL, Quigley L, et al. A TREM family member, TLT-1, is found exclusively in the α-granules of megakaryocytes and platelets. *Blood*. 2004;104(4):1042-1047.

111. Yang J, Wu J, Kowalska AM, et al. Loss of signaling through the G protein, Gz, results in abnormal platelet activation and altered responses to psychoactive drugs. *Proc Natl Acad Sci*. 2000;97(18):9984-9989.

112. Lanza F, Beretz A, Stierlé A, Hanau D, Kubina M, Cazenave JP. Epinephrine potentiates human platelet activation but is not an aggregating agent. *Am J Physiol*. 1988;255(6 Pt 2):1276-1288.

113. Grozovsky R, Begonja A, Liu K, et al. The Ashwell-Morell receptor regulates hepatic thrombopoietin production via JAK2-STAT3 signaling. *Nat Med*. 2014;21:47-54.

114. Green ED, Brodbeck RM, Baenziger JU. Lectin affinity high-performance liquid chromatography. Interactions of N-glycanase-released oligosaccharides with Ricinus communis agglutinin I and Ricinus communis agglutinin II. *J Biol Chem*. 1987;262(25):12030-12039.

115. Koopman G, Reutelingsperger CP, Kuijten GA, Keehnen RM, Pals ST, Oers MHv. Annexin V for flow cytometric detection of phosphatidylserine expression on B cells undergoing apoptosis. *Blood*. 1994;84(5):1415-1420.

116. Zhang H, Nimmer PM, Tahir SK, et al. Bcl-2 family proteins are essential for platelet survival. *Cell Death and Differ*. 2007;14(5):943-951.

117. Greenberg EM. Thrombocytopenia. *Journal of Infusion Nursing*. 2017;40(1):41-50.

118. Wada H, Matsumoto T, Suzuki K, et al. Differences and similarities between disseminated intravascular coagulation and thrombotic microangiopathy. *Thrombosis Journal*. 2018;16(1):14.

119. Signarvic RS, Cierniewska A, Stalker TJ, et al. RGS/Gi2alpha interactions modulate platelet accumulation and thrombus formation at sites of vascular injury. *Blood*. 2010;116(26):6092-6100.

120. Yatomi Y, Igarashi Y, Yang L, et al. Sphingosine 1-Phosphate, a Bioactive Sphingolipid Abundantly Stored in Platelets, Is a Normal Constituent of Human Plasma and Serum. *The Journal of Biochemistry*. 1997;121(5):969-973.

121. Zhang L, Orban M, Lorenz M, et al. A novel role of sphingosine 1-phosphate receptor S1pr1 in mouse thrombopoiesisS1pr1 controls bone marrow thrombopoiesis. *The Journal of Experimental Medicine*. 2012;209(12):2165-2181.

122. Ortega F, Pérez-Sen R, Miras-Portugal MT. Gi-coupled P2Y-ADP receptor mediates GSK-3 phosphorylation and β-catenin nuclear translocation in granule neurons. *J Neurochem*. 2008;104(1):62-73.

123. Balduini A, Buduo CAD, Malara A, et al. Constitutively released adenosine diphosphate regulates proplatelet formation by human megakaryocytes. *Haematologica*. 2012;97(11):1657-1665.

124. Yan J, Schmid E, Almilaji A, et al. Effect of TGFβ on calcium signaling in megakaryocytes. *Biochemical and Biophysical Research Communications*. 2015;461(1):8-13.

125. Kuroda H, Matsunaga T, Terui T, et al. Decrease of Smad4 gene expression in patients with essential thrombocythaemia may cause an escape from suppression of megakaryopoiesis by transforming growth factor-beta1. *Br J Haematol*. 2004;124(2):211-220.

126. Josefsson EC, James C, Henley KJ, et al. Megakaryocytes possess a functional intrinsic apoptosis pathway that must be restrained to survive and produce platelets. *J Exp Med*. 2011;208(10):2017-2031.

127. Popov S, Yu K, Kozasa T, Wilkie TM. The Regulators of G Protein Signaling (RGS) Domains of RGS4, RGS10, and GAIP Retain GTPase Activating Protein Activity in vitro. *JSTOR*. 1997;94(14):7216-7220.

128. Zhao L, Liu J, He C, et al. Protein kinase A determines platelet life span and survival by regulating apoptosis. *J Clin Invest*. 2017;127(12):4338-4351.

129. Stefanini L, Paul DS, Robledo RF, et al. RASA3 is a critical inhibitor of RAP1-dependent platelet activation. *J Clin Invest*. 2015;125(4):1419-1432.

130. Henao-Mejia J, Williams A, Rongvaux A, Stein J, Hughes C, Flavell RA. Generation of Genetically Modified Mice Using the CRISPR-Cas9 Genome-Editing System. *Cold Spring Harb Protoc*. 2016;2016(2):pdb prot090704.

131. Ran FA, Hsu PD, Wright J, Agarwala V, Scott DA, Zhang F. Genome engineering using the CRISPR-Cas9 system. *Nat Protoc*. 2013;8(11):2281-2308.

132. Stalker TJ, Traxler EA, Wu J, et al. Hierarchical organization in the hemostatic response and its relationship to the platelet-signaling network. *Blood*. 2013;121(10):1875-1885.

133. Tesmer VM, Kawano T, Shankaranarayanan A, Kozasa T, Tesmer JJ. Snapshot of activated G proteins at the membrane: the Galphaq-GRK2-Gbetagamma complex. *Science*. 2005;310(5754):1686-1690.

134. Waldo GL, Ricks TK, Hicks SN, et al. Kinetic scaffolding mediated by a phospholipase C-beta and Gq signaling complex. *Science*. 2010;330(6006):974-980.

135. Nishimura A, Kitano K, Takasaki J, et al. Structural basis for the specific inhibition of heterotrimeric Gq protein by a small molecule. *Proceedings of the National Academy of Sciences of the United States of America*. 2010;107(31):13666-13671.

136. Soundararajan M, Willard FS, Kimple AJ, et al. Structural diversity in the RGS domain and its interaction with heterotrimeric G protein alpha-subunits. *Proc Natl Acad Sci U S A*. 2008;105(17):6457-6462.

137. Nance MR, Kreutz B, Tesmer VM, Sterne-Marr R, Kozasa T, Tesmer J. Structural and Functional Analysis of the Regulator of G Protein Signaling 2-Gαq Complex. *Structure*. 2013;21(3):438-448.

138. Taylor VG, Bommarito PA, Tesmer JJG. Structure of the Regulator of G Protein Signaling 8 (RGS8)-Gαq Complex: MOLECULAR BASIS FOR Gα SELECTIVITY. *The Journal of biological chemistry*. 2016;291(10):5138-5145.

139. Kortemme T, Kim DE, Baker D. Computational alanine scanning of protein-protein interfaces. *Sci STKE*. 2004;2004(219):pl2.

140. Berman HM, Westbrook J, Feng Z, et al. The Protein Data Bank. *Nucleic Acids Res*. 2000;28(1):235-242.

141. Kortemme T, Baker D. A simple physical model for binding energy hot spots in protein-protein complexes. *Proc Natl Acad Sci U S A*. 2002;99(22):14116-14121.

142. Pires DEV, Ascher DB, Blundell TL. mCSM: predicting the effects of mutations in proteins using graph-based signatures. *Bioinformatics*. 2014;30(3):335-342.

143. Lian L, Wang Y, Draznin J, et al. The relative role of PLCβ and PI3Kγ in platelet activation. *Blood*. 2005;106(1):110-117.

144. Offermanns S, Toombs CF, Hu Y-H, Simon MI. Defective platelet activation in Gαq-deficient mice. *Nature*. 1997;389(6647):183-186.

145. Blazer LL, Zhang H, Casey EM, Husbands SM, Neubig RR. A nanomolar-potency small molecule inhibitor of regulator of G-protein signaling proteins. *Biochemistry*. 2011;50(15):3181-3192.

146. Hayes MP, Bodle CR, Roman DL. Evaluation of the Selectivity and Cysteine-Dependence of Inhibitors Across the Regulator of G Protein Signaling Family. *Molecular Pharmacology*. 2017;93(1):mol.117.109843.

147. Ioannidis NM, Rothstein JH, Pejaver V, et al. REVEL: An Ensemble Method for Predicting the Pathogenicity of Rare Missense Variants. *Am J Hum Genet*. 2016;99(4):877-885.

148. Liu W, Xie Y, Ma J, et al. IBS: an illustrator for the presentation and visualization of biological sequences. *Bioinformatics*. 2015;31(20):3359-3361.

149. Rodrigues CH, Pires DE, Ascher DB. DynaMut: predicting the impact of mutations on protein conformation, flexibility and stability. *Nucleic Acids Research*. 2018;46(W1):W350-W355.

150. Rodrigues CH, Myung Y, Pires DE, Ascher DB. mCSM-PPI2: predicting the effects of mutations on protein–protein interactions. *Nucleic Acids Research*. 2019;47(W1):W338-W344.

151. Karczewski KJ, Francioli LC, Tiao G, et al. Variation across 141,456 human exomes and genomes reveals the spectrum of loss-of-function intolerance across human protein-coding genes. *bioRxiv*. 2019:531210.

152. Ostrer H. A genetic profile of contemporary Jewish populations. *Nature Reviews Genetics*. 2001;2(11):891-898.

153. Arcos-Burgos M, Muenke M. Genetics of population isolates. *Clin Genet*. 2002;61(4):233-247.

154. Bray SM, Mulle JG, Dodd AF, Pulver AE, Wooding S, Warren ST. Signatures of founder effects, admixture, and selection in the Ashkenazi Jewish population. *Proceedings of the National Academy of Sciences*. 2010;107(37):16222-16227.

155. Campbell MC, Tishkoff SA. The Evolution of Human Genetic and Phenotypic Variation in Africa. *Curr Biol*. 2010;20(4):R166-R173.

156. Campbell MC, Tishkoff SA. African Genetic Diversity: Implications for Human Demographic History, Modern Human Origins, and Complex Disease Mapping. *Annual Review of Genomics and Human Genetics*. 2008;9(1):403-433.

157. McMorran BJ, Wieczorski L, Drysdale KE, et al. Platelet Factor 4 and Duffy Antigen Required for Platelet Killing of Plasmodium falciparum. *Science*. 2012;338(6112):1348-1351.

158. Kho S, Barber BE, Johar E, et al. Platelets kill circulating parasites of all major Plasmodium species in human malaria. *Blood*. 2018;132(12):1332-1344.

159. Karim ZA, Alshbool FZ, Vemana HP, Conlon C, Druey KM, Khasawneh FT. CXCL12 regulates platelet activation via the regulator of G-protein signaling 16. *Biochimica et biophysica acta*. 2016;1863(2):314-321.

160. Hernandez KR, Karim ZA, Qasim H, Druey KM, Alshbool FZ, Khasawneh FT. Regulator of G-Protein Signaling 16 Is a Negative Modulator of Platelet Function and Thrombosis. *Journal of the American Heart Association*. 2019;8(5):e011273.

161. Berthebaud M, Rivière C, Jarrier P, et al. RGS16 is a negative regulator of SDF-1–CXCR4 signaling in megakaryocytes. *Blood*. 2005;106(9):2962-2968.

162. Avecilla ST, Hattori K, Heissig B, et al. Chemokine-mediated interaction of hematopoietic progenitors with the bone marrow vascular niche is required for thrombopoiesis. *Nature Medicine*. 2003;10(1):64-71.

163. Mathur A, Hong Y, Martin JF, Erusalimsky JD. Megakaryocytic differentiation is accompanied by a reduction in cell migratory potential. *Br J Haematol*. 2001;112(2):459-465.

164. NoÉ L, Michele MD, Giets E, et al. Platelet Gs hypofunction and abnormal morphology resulting from a heterozygous RGS2 mutation. *Journal of Thrombosis and Haemostasis*. 2010;8(7):1594-1603.

165. Banno F, Nojiri T, Matsumoto S, Kamide K, Miyata T. RGS2 deficiency in mice does not affect platelet thrombus formation at sites of vascular injury. *Journal of Thrombosis and Haemostasis*. 2012;10(2):309-311.

166. Knudson AG. Two genetic hits (more or less) to cancer. *Nature Reviews Cancer*. 2001;1(2):157-162.

167. Murata T, Ushikubi F, Matsuoka T, et al. Altered pain perception and inflammatory response in mice lacking prostacyclin receptor. *Nature*. 1997;388(6643):678-682.

168. Tomaiuolo M, Matzko CN, Poventud-Fuentes I, Weisel JW, Brass LF, Stalker TJ. Interrelationships between structure and function during the hemostatic response to injury. *Proceedings of the National Academy of Sciences*. 2019;116(6):201813642.

169. Ciciliano JC, Sakurai Y, Myers DR, et al. Resolving the multifaceted mechanisms of the ferric chloride thrombosis model using an interdisciplinary microfluidic approach. *Blood*. 2015;126(6):817-824.

170. Freedman JE, Sauter R, Battinelli EM, et al. Deficient Platelet-Derived Nitric Oxide and Enhanced Hemostasis in Mice Lacking the NOSIII Gene. *Circul Res*. 1999;84(12):1416-1421.

171. Özüyaman B, Gödecke A, Küsters S, Kirchhoff E, Scharf R, Schrader J. Endothelial nitric oxide synthase plays a minor role in inhibition of arterial thrombus formation. *Thrombosis and Haemostasis*. 2005;93(06):1161-1167.

172. Enjyoji K, Sévigny J, Lin Y, et al. Targeted disruption of cd39/ATP diphosphohydrolase results in disordered hemostasis and thromboregulation. *Nature Medicine*. 1999;5(9):1010-1017.

173. Walton GM, Bertics PJ, Hudson LG, Vedvick TS, Gill GN. A three-step purification procedure for protein kinase C: Characterization of the purified enzyme. *Anal Biochem*. 1987;161(2):425-437.

174. Haupt A, Grancharova T, Arakaki J, Fuqua MA, Roberts B, Gunawardane RN. Endogenous Protein Tagging in Human Induced Pluripotent Stem Cells Using CRISPR/Cas9. *Journal of Visualized Experiments*. 2018(138).

175. Hayashi K, Yamashita R, Takami R, et al. Strategy for Identification of Phosphorylation Levels of Low Abundance Proteins in Vivo for Which Antibodies Are not Available. *Journal of Cardiovascular Development and Disease*. 2017;4(4):17.

176. Pessino V, Citron YR, Feng S, Huang B. Covalent Protein Labeling by SpyTag–SpyCatcher in Fixed Cells for Super-Resolution Microscopy. *ChemBioChem*. 2017;18(15):1492-1495.

177. Kapust RB, Tözsér J, Copeland TD, Waugh DS. The P1′ specificity of tobacco etch virus protease. *Biochemical and Biophysical Research Communications*. 2002;294(5):949-955.

178. Borst S, Sim X, Poncz M, French DL, Gadue P. Induced Pluripotent Stem Cell–Derived Megakaryocytes and Platelets for Disease Modeling and Future Clinical Applications. *Atertio Thromb Vasc Biol*. 2017;37(11):2007-2013.

179. Dephoure N, Gould KL, Gygi SP, Kellogg DR. Mapping and analysis of phosphorylation sites: a quick guide for cell biologists. *Molecular Biology of the Cell*. 2013;24(5):535-542.

180. Han X, Aslanian A, Yates JR. Mass spectrometry for proteomics. *Curr Opin Chem Biol*. 2008;12(5):483-490.

181. Pereira J, Palomo I, Ocqueteau M, Soto M, Aranda E, Mezzano D. Platelet aging in vivo is associated with loss of membrane phospholipid asymmetry. *Thrombosis and haemostasis*. 1999;82(4):1318-1321.

182. Badlou BA, Wu YP, Smid WM, Akkerman JWN. Platelet binding and phagocytosis by macrophages. *Transfusion*. 2006;46(8):1432-1443.

183. Albanyan A-M, Murphy MF, Rasmussen JT, Heegaard CW, Harrison P. Measurement of phosphatidylserine exposure during storage of platelet concentrates using the novel probe lactadherin: a comparison study with annexin V. *Transfusion*. 2009;49(1):99-107.

184. Shi J, Shi Y, Waehrens LN, Rasmussen JT, Heegaard CW, Gilbert GE. Lactadherin detects early phosphatidylserine exposure on immortalized leukemia cells undergoing programmed cell death. *Cytometry Part A*. 2006;69A(12):1193-1201.

185. Rooijen Nv, Hendrikx E. Liposomes, Methods and Protocols, Volume 1: Pharmaceutical Nanocarriers. 2009:189-203.

186. Bender M, Stritt S, Nurden P, Nature … JMM. Megakaryocyte-specific Profilin1-deficiency alters microtubule stability and causes a Wiskott–Aldrich syndrome-like platelet defect. 2014.

187. Stritt S, Beck S, Becker IC, Vögtle T, Blood HM. Twinfilin 2a is a regulator of platelet reactivity and turnover in mice. 2017.

188. Paul DS, Casari C, Wu C, et al. Deletion of the Arp2/3 complex in megakaryocytes leads to microthrombocytopenia in mice. *Blood Advances*. 2017;1(18):1398-1408.

189. Zhao L, Liu J, He C, et al. Protein kinase A determines platelet life span and survival by regulating apoptosis. *Journal of Clinical Investigation*. 2017.

190. Zhang W, Colman RW. Thrombin regulates intracellular cyclic AMP concentration in human platelets through phosphorylation/activation of phosphodiesterase 3A. *Blood*. 2007;110(5):1475-1482.

191. Yang J, Wu J, Jiang H, et al. Signaling through Gi family members in platelets. Redundancy and specificity in the regulation of adenylyl cyclase and other effectors. *The Journal of biological chemistry*. 2002;277(48):46035-46042.

192. Hoffmeister KM, Falet H. Platelet clearance by the hepatic Ashwell-Morrell receptor: mechanisms and biological significance. *Thrombosis Research*. 2016;141:S68-S72.

193. Grozovsky R, Hoffmeister KM, Falet H. Novel clearance mechanisms of platelets. *Current Opinion in Hematology*. 2010;17(6):585.

194. Hoffmeister KM, Felbinger TW, Falet H, et al. The Clearance Mechanism of Chilled Blood Platelets. *Cell*. 2003;112(1):87-97.

195. Jansen GAJ, Josefsson EC, Rumjantseva V, et al. Desialylation accelerates platelet clearance after refrigeration and initiates GPIbα metalloproteinase-mediated cleavage in mice. *Blood*. 2012;119(5):1263-1273.

196. Kim JY, Kim Y-G, Lee GM. CHO cells in biotechnology for production of recombinant proteins: current state and further potential. *Appl Microbiol Biotechnol*. 2012;93(3):917-930.

197. Maguire JA, Cardenas-Diaz FL, Gadue P, French DL. Highly Efficient CRISPR-Cas9-Mediated Genome Editing in Human Pluripotent Stem Cells. *Current Protocols in Stem Cell Biology*. 2018;48(1):e64.

198. Mangmool S, Kurose H. Gi/o Protein-Dependent and -Independent Actions of Pertussis Toxin (PTX). *Toxins*. 2011;3(7):884-899.

199. Shultz LD, Lyons BL, Burzenski LM, et al. Human lymphoid and myeloid cell development in NOD/LtSz-scid IL2R gamma null mice engrafted with mobilized human hemopoietic stem cells. *J Immunol*. 2005;174(10):6477-6489.

200. Magallon J, Egalka M, Diacovo TG. Humanizing thrombi in mice. *Trends Cardiovasc Med*. 2011;21(1):33-36.

201. Magallon J, Chen J, Rabbani L, et al. Humanized mouse model of thrombosis is predictive of the clinical efficacy of antiplatelet agents. *Circulation*. 2011;123(3):319-326.

202. Adair BD, Alonso JL, Agthoven Jv, et al. Structure-guided design of pure orthosteric inhibitors of αIIbβ3 that prevent thrombosis but preserve hemostasis. *Nature Communications*. 2020;11(1):398.

203. Fuentes R, Wang Y, Hirsch J, et al. Infusion of mature megakaryocytes into mice yields functional platelets. *Journal of Clinical Investigation*. 2010;120(11):3917-3922.